DEVELOPMENTS IN THE FIELD OF ENGINEERING 2023

Editors:

Assoc. Prof. Dr. Asaf Tolga ÜLGEN

Assoc. Prof. Dr. Mehmet HASKUL

yaz
yayınları

DEVELOPMENTS IN THE FIELD OF ENGINEERING 2023

Editors

Assoc. Prof. Dr. Asaf Tolga ÜLGEN

Assoc. Prof. Dr. Mehmet HASKUL

yaz yayınları

2023

yaz yayınları

DEVELOPMENTS IN THE FIELD OF ENGINEERING 2023

Editor: Assoc. Prof. Dr. Asaf Tolga ÜLGEN

ORCID NO: 0000-0002-7112-5607

Editor: Assoc. Prof. Dr. Mehmet HASKUL

ORCID NO: 0000-0001-8671-4597

E_ISBN 978-625-6524-70-5

Aralık 2023 – Afyonkarahisar

Dizgi/Mizanpaj: YAZ Yayınları

Kapak Tasarım: YAZ Yayınları

YAZ Yayınları. Yayıncı Sertifika No: 73086

M.İhtisas OSB Mah. 4A Cad. No:3/3
İscehisar/AFYONKARAHİSAR

www.yazyayinlari.com

yazyayinlari@gmail.com

info@yazyayinlari.com

CONTENTS

RECOMMENDATION SYSTEMS

Rasım ÇEKİK[1]

1. INTRODUCTION

The rapid development of web technology has given a major boost to human-computer interaction. This development has penetrated almost all areas of people's lives and has led to a differentiation in their preferences. For example, instead of watching TV, people now watch movies on digital platforms such as Netflix, Amazon Prime Video, Exxen. When listening to music, applications such as Fizy Sportify are used instead of the radio, while e-commerce websites are preferred to shopping in stores. A huge amount of dirty data has been generated by this intensive use of web technologies. This not only costs people, companies or organizations time and money, but also has negative effects on human psychology. So, when people access information, they often want to focus on topics that interest them. Therefore, in information aggregation and dissemination centers, classification and indexing play an important role to manage content more effectively. This process allows users to access the information they want more quickly and easily. Recommender systems are undoubtedly one of the most important systems that

[1] Assist. Prof. Dr., Şırnak University, Faculty of Engineering, Department of Computer Engineering, rasimcekik@sirnak.edu.tr, ORCID: 0000-0002-7820-413X.

enable people to quickly access what they want in the digital world.

Recommender systems are structures that contain algorithms that recommend specific content or products to users by analyzing their past behavior or learning from the behavior of similar users. These systems are often used to personalize the user experience, drive sales or increase user interest. They are also used to achieve business goals such as improving the user experience, increasing customer loyalty and driving sales in a wide range of settings, from e-commerce platforms to media publications. Recommender systems differ according to their purpose of operation, such as identifying related products, identifying personal preferences, and analyzing user similarity. In identifying relevant products, the user's shopping, click, or review history is analyzed to identify relevant products or content. Based on this data, the user's interests are identified. In personal preference identification, products or content with similar features or categories are recommended based on the user's previous preferences. This provides personalized recommendations based on the user's previous interests. User similarity analysis examines the behavior of similar users to make recommendations for products or content that may be of interest to a user. The analysis supports community-based models of recommender systems.

The operating principles of recommendation systems consist of a few basic steps. These are the processes of data collection, pre-processing, user profiling, content and attribute generation, similarity calculation, recommendation, and feedback. Among these processes, pre-processing, feature extraction, similarity calculation and prediction (recommendation) are crucial for the success of the recommendation model. Different computational methods and technologies are used in these processes. Ultimately, algorithms follow these steps to understand user preferences, identify similar users and provide personalized recommendations. As a result, the need for these systems is increasing and research in this area is developing rapidly. The aim of this paper is to introduce recommendation systems and to provide some preliminary information on their understanding.

2. WHAT ARE RECOMMENDATION SYSTEMS?

Recommender systems are artificial intelligence-based systems that recommend specific content to users. These systems typically analyze data such as a user's past preferences, behavior, or profile information to recommend interesting or relevant content. Recommender systems often use complex algorithms and artificial intelligence techniques. They are designed to personalize the user experience and engage users. Today, such systems are used in many different application areas. For example, e-commerce sites, media and entertainment platforms, social media, online news sites, educational platforms, etc. The underlying reasons for their use in such a wide range of areas can be listed as follows:

- *Providing Personalized User Experience*: Recommendation systems personalize users' experiences by recommending content that matches their personal preferences. This allows users to access relevant content more quickly and effectively.

- *Driving Sales and Revenue Growth:* Recommendation systems for e-commerce sites and online retailers recommend products based on users' past shopping behavior. This can increase sales and strengthen customer loyalty.
- *Enabling Content Discovery:* Recommendation systems on media and entertainment platforms help users discover content that matches their viewing, listening, or reading tastes. This contributes to users using the platform more actively.
- *Increasing User Engagement and Loyalty:* Recommending content to users that may be of interest to them can increase user engagement and create long-term customer loyalty.
- *Enhancing Community Experience:* Collaboration-based recommendation systems can strengthen the community experience by bringing together users with similar interests. This can increase user engagement on platforms such as social media platforms or forums.
- *Providing Information Enrichment:* Recommendation systems can help users learn more in areas of interest. For example, recommendation systems on education platforms can recommend content that will enrich users' learning experiences.
- Save time: Reduce the time users spend searching for and finding what they want by suggesting content that speaks directly to their interests.

For these reasons, recommendation systems can help companies provide a more effective and personalized service by increasing user satisfaction. At the same time, they can increase engagement across different platforms by enabling users to access content that is more relevant to their interests.

3. RECOMMENDATION SYSTEMS METHODS

In the widely used recommendation systems, the methods used to make recommendations vary according to their purpose. Some recommendation systems use similarities between users to make predictions, while others work on the basis of content analysis or content similarity (Özgöbek & Erdur, 2015). Recommendation systems can be grouped under four main headings according to how they work: collaborative filtering, content-based filtering, popularity-based filtering and hybrid filtering. Figure 1 shows the grouping of recommender system methods.

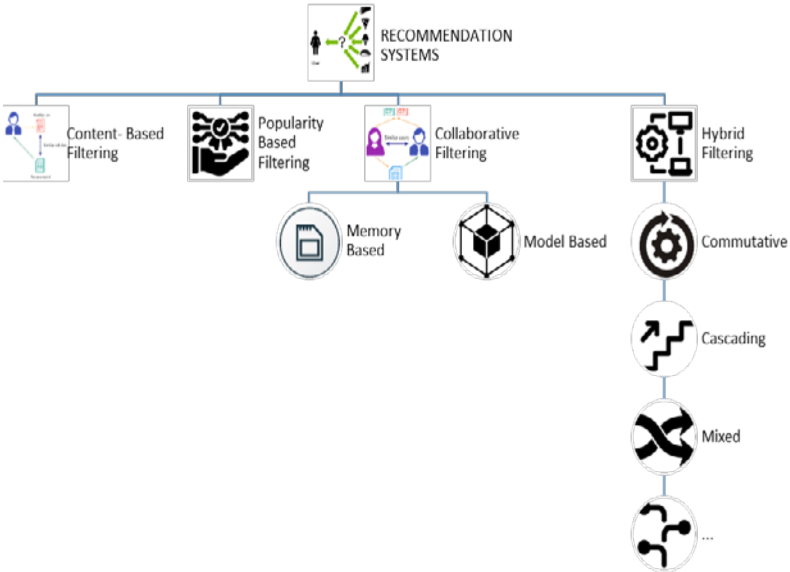

Figure 1. Classification of recommendation systems methods according to their working mechanisms

3.1. Collaborative filtering

Collaborative Filtering (CF) is a technique for predicting a user's preferences or interests by aggregating (collaborating) the preferences of multiple users. The basic operating principle is that users who have previously agreed will tend to agree in the future (SU & Khoshgoftaar, 2009). Collaborative Filtering systems are widely used in a variety of applications such as movie, music, book, or product recommendations. Figure 2 depicts a simplified version of the working mechanism.

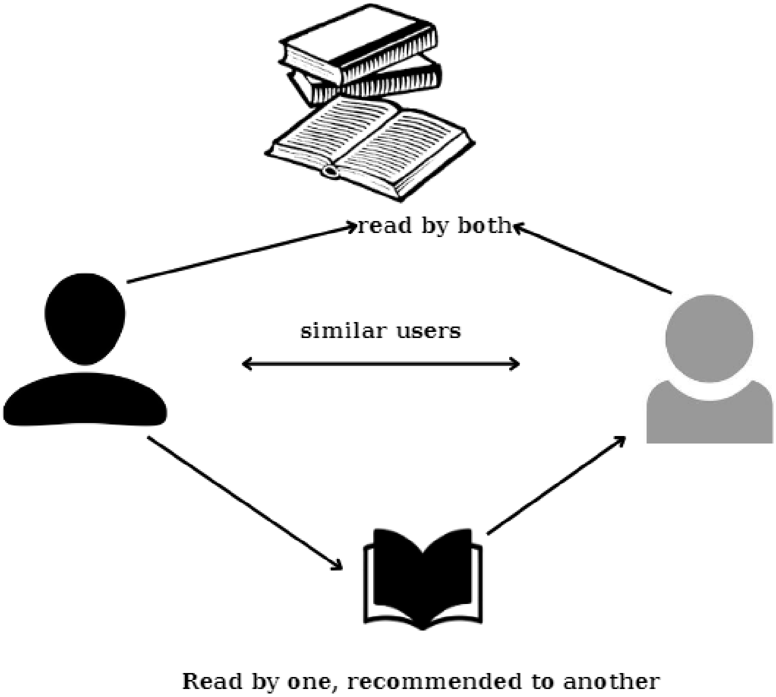

Figure 2. Collaborative filtering systems

In the current collaborative filtering algorithm, a user is typically defined as an M-dimensional vector of elements. The algorithm compares these vectors to bring similar users together as neighbors, eliminates users with different behaviors, and recommends items to the target user based on the behavior of the neighbors.

In the literature, there are generally two main types of collaborative filtering techniques. *Memory-Based* techniques (Herlocker, Konstan, Borchers, & al., 1999) compute the similarity between users or items using user rating data and provide predictions or recommendations based on a K-nearest neighbor algorithm. These techniques are advantageous in that they are easy to implement and generally provide efficient results. However, there are some limitations to these techniques. Because similarity values are frequently based on common elements, their reliability may suffer when data is sparse and common elements are scarce. The *Model-Based* (Aggarwal & Aggarwal, 2016) collaborative recommendation technique has emerged to address these shortcomings and provide more efficient recommendations. The goal of this technique is to predict or learn a model from pure rating data and then apply that model to an online system. The model used is usually a data mining or machine learning algorithm. There are well-known model-based collaborative filtering techniques such as factor models, Bayesian classifier models, clustering models, and graph-based models. However, model-based techniques often require a costly model-building process, making them difficult to use online and introducing the need to strike a balance between predictive performance and scalability (Shen & Yang, 2013).

3.2. Content-based filtering

The Content-Based Filtering (Pazzani & Billsus, 2007) method employs data obtained from the user, either explicitly through voting or implicitly (for example, by clicking on a link...). This data is used to create a user profile, which is then used to provide better recommendations to the user. The system becomes more precise as the user provides more information or interacts based on suggestions. Based on the similarity between a user's characteristics and an item's characteristics, the user's past interactions, and given information (e.g., the user's age, the category of a restaurant's cuisine, the average review for a movie, etc.), this approach models the likelihood that a new item will be of interest to the user. For instance, if a content filtering recommender notices that you enjoyed the movies.

Content-based recommendation systems are used for information retrieval. In the first stage, terms are manually assigned, i.e., these terms are manually determined to be compared with the information in the customer's profile. Then, a technique to evaluate these terms is selected and a learning algorithm to apply these techniques displays the relevant results based on the information in the customer's profile (Sieg & Burke, 2007). Figure 3 shows the general working mechanism of Content Based Filtering.

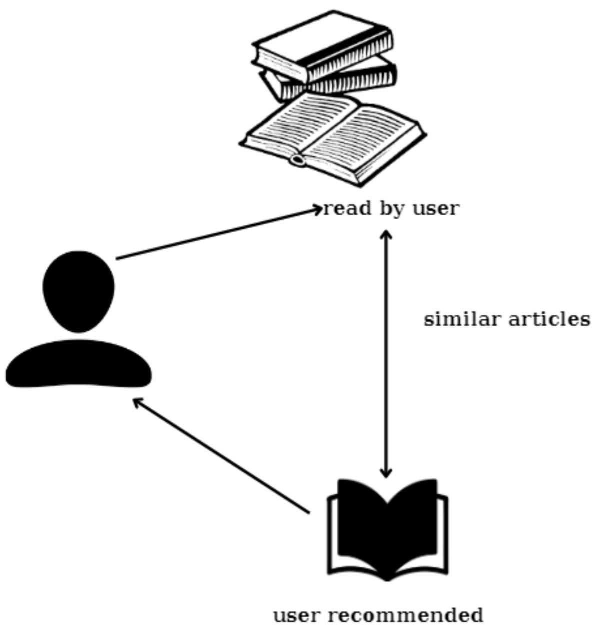

Figure 3. Content-based filtering

The advantages of Content Based Systems can be listed as follows:

- The ability to make a recommendation to a specific user without needing data from other users allows the system to easily scale to large numbers of customers.
- Since recommendations are based on the user's daily activities, preferences and parameters can be fine-tuned to the user's individual preferences. In this way, the model can successfully recommend certain niche products that other users may not be interested in.
- Features are available from the start, so the newest items can be quickly recommended as they become available. This ensures users are immediately aware of current and interesting content.

There are some difficulties encountered when applying such methods. These:

- Building a content-based recommendation engine requires extensive domain knowledge as feature selection of items is mostly hard-coded by the system. Therefore, the model depends only on the level of knowledge of the person who created it.
- The model can recommend new items based on the user's current interest. In this case, it may not be possible to explore and expand new topics that may be of interest to the user.
- Due to not having enough information about a new user, the system may have difficulty making recommendations that suit a new user's preferences.

- It can be difficult to make new and interesting suggestions to users who are not very active. This may cause difficulty in updating or varying the user's preferences.

3.3. Hybrid filtering

Hybrid Filtering methods are systems that combine the best features of both Content-Based and Collaborative Filtering methods. During the implementation phase, Content-Based and Collaborative systems face some challenges. In Collaborative Filters, for example, there is an obligation to find similar users in the dataset to provide suggestions. However, there may be no similar users in the data set, and thus no recommendation can be made. Content-Based filtering can be used to overcome this situation. Similarly, in cases where it is difficult to create user or product profiles in content-based filtering, recommendations can be generated by using the advantages of collaborative filtering recommendation systems with neighbourhood calculations (Terzi, 2017). In this way, a more efficient recommendation system can be created. Such systems are also defined as hybrid filtering. Therefore, hybrid systems that combine content-based and collaborative systems can provide stronger recommendations by using the advantages of both approaches. This enables more comprehensive results by combining recommendations based on both content-based features and user similarities.

Hybrid Filtering is frequently used in conjunction with other techniques such as genetic algorithms, neural networks, Bayesian networks, and clustering techniques (Aygün & Yildiz, 2016). There are several ways to combine Content-Based Filtering and Collaborative Filtering methods (Seyrek, 2020) (Manouselis, Drachsler, Vuorikari, Hummel, & Koper, 2011) :

Separate implementation and combining: Collaborative and content-based filtering methods are implemented separately, and then the results are combined. This method focuses on combining the advantages of both filtering approaches.

Incorporating content-based features into the collaborative approach: By integrating collaborative features into content-based methods, one can leverage the advantages of collaborative filtering to better understand user preferences and those of similar users.

Incorporating collaborative features into content-based approach: By incorporating collaborative features into content-based filtering methods, more influence of content can be integrated into the recommendation system.

Creating a general unifying model: Creating a general unifying model that combines both content-based and collaborative features. This model represents a more complex and comprehensive recommendation system that includes the advantages of both approaches.

The general structure of Hybrid systems is given in Figure 4.

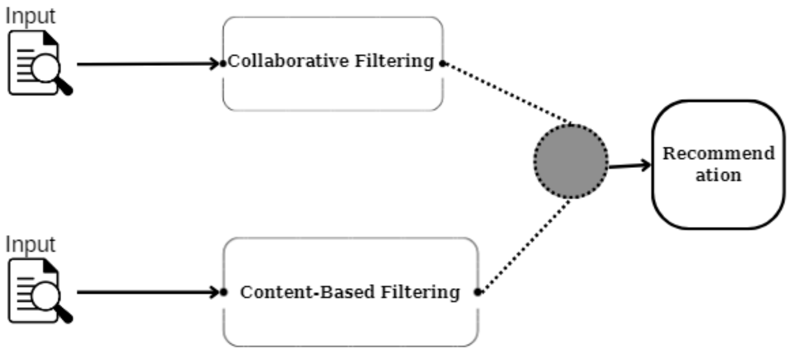

Figure 4. Hybrid filtering

3.4. Popularity Based Filtering

A system that recommends popular, trending, or highly consumed products without analyzing user behavior is known as popularity-based filtering (Kwan & Jasser, 2020). Such systems are based on general demand and popularity and present users with products that are in high demand. They also do not consider the user's previous behavior or preferences. Instead, it suggests items based on how many times they have been viewed, liked, or shared. On an e-commerce site, for example, a recommendation system that uses popularity-based filtering may recommend the best-selling or most-viewed products. This can be useful for users who want to learn about a new product or service or who are looking for products that are similar to their current interests. As a result, these systems can make recommendations.

- Best-selling books
- Best-selling clothing products
- Best-selling electronic products
- Best-selling games

The absence of a requirement to collect data in order to analyze user behavior in Popularity-Based systems can lower the cost of development and operation. It can also be beneficial for users who want to learn about new products or services. It does not, however, take into account the user's personal preferences. This could result in recommendations that aren't relevant to the user's interests. Furthermore, popular items are not always the best. This may lead to users purchasing low-quality goods or services.

Popularity-based recommender systems work by recommending the most frequently purchased products to customers. This open-ended idea can be set to certain limits with at least two concrete applications:

General popular product recommendations: Determine which products are most frequently purchased by all customers. Provide these well-known products as a general recommendation to all customers. Create a list of popular products on an e-commerce site, for example, and recommend these products to customers throughout the site.

Personalized popular product recommendations: Identify the most frequently purchased products per customer. Offer each customer a personalized, popular product recommendation based on their previous shopping history. For example, analyses a customer's previous purchases and recommend similar products that other customers prefer.

These applications use general and personalized popularity analysis to make various recommendations to customers.

Customers can thus be offered products that are in high demand while also receiving recommendations tailored to their specific preferences.

4. RECOMMENDATION SYSTEMS' PROBLEMS DURING THE IMPLEMENTATION PHASE

There are some challenges due to the structure of the data used in recommendation systems, a lack of data, and reliance on user history. These issues and their solutions are detailed below.

4.1. Cold start

The cold start problem is related to the difficulty of making the right recommendations to a new user. Since there is no data about the user yet, it is not possible to provide recommendations that match the user's preferences. This is a problem where, when a new user or item is added, recommendations cannot be calculated because there is no stored information about this user or item in the system. This problem occurs especially in the collaborative filtering method. In the collaborative filtering method, recommendations are made based on similarities between users. In this method, the past behavior and preferences of the user are important. However, since past behavior and preferences are not known to a new user, recommendations cannot be calculated. The reasons for the problem can be listed as follows:

- When a new user is added to the system
- When a new item is introduced into the system.
- When the behavior or preferences of an existing user change

The issue has the potential to reduce the effectiveness of recommender systems. To address the issue, various approaches have been developed. Here are a few examples:

Pre-promotion: Introducing new users or items ahead of time can encourage users to explore and interact with them. This can aid in learning about previous user behavior and preferences.

Content-based filtering: Recommendations are made based on the features and attributes of the items in content-based filtering. This method can aid in the creation of better recommendations for new users or items.

Social networks: Social networks can help users find other users with similar interests. This can enable users to learn about items with similar interests and receive recommendations.

The cold start problem degrades the effectiveness of recommender systems. The methods developed, however, can reduce the impact of this problem.

4.2. Sparsity

Sparsity occurs when users fail to provide feedback on the products they use, making user and product analysis difficult. As a result of this situation, a large portion of the user-product information matrices used in recommendation systems are empty, and the data set becomes sparse. This sparsity makes it more difficult to understand user preferences and recommend similar users or products. There are some solutions to this problem in the literature. The first is the process of completing the missing data. This procedure is based on the use of methods to fill in blanks or missing data in order to complete missing information. The matrix-decomposition technique is the second method. The technique aims to reduce data sparsity by decomposing the user and product matrices into a smaller matrix. The value method is a sophisticated model. The negative impact of sparse data on recommendation systems is reduced by using advanced learning models such as deep learning.

4.3. Confidentiality

To function properly, recommendation systems frequently require large amounts of data. This data may contain personal information about the user. Users may be concerned about their privacy and security as a result of this. Data collection, storage, and processing of personal preferences, purchasing habits, and other behaviors of users may violate their privacy. Users may be concerned about safeguarding such information and preventing unauthorized access. To address these privacy concerns, the following steps can be taken:

- *Anonymization* is the process of protecting users' true identities by removing personal information from user data.
- *Data encryption:* To protect against unauthorized access, user data is encrypted.
- *Opt-in and opt-out options*: Providing users with the option to opt-in or opt-out of data sharing.
- *Transparent policies*: Communicate with users in a clear and understandable manner about data collection, storage, and use policies.
- *Consent request*: Collecting and using personal data with prior consent from users.

These safeguards are intended to ensure that recommendation systems function properly while also protecting user privacy.

5. DISCUSSION AND CONCLUSION

Recommender systems are artificial intelligence applications that extract meaningful information from large amounts of data in order to select products that may be useful to users. These applications use various methods and approaches to provide the best recommendation. Four methods are commonly used in this context: collaborative, content-based, popularity-based, and hybrid. Each method has its own set of benefits and drawbacks. In real-world applications, recommendations are made by analyzing the user-product relationship. A user profile is formed as a result of a user's browsing, movements, actions, and feedback about products in the web environment. These profiles are used by recommendation systems to return recommendations to users. The demand for and interest in recommendation systems is growing by the day. Furthermore, recommendation systems have emerged as the most important artificial intelligence application and are a critical component of new web technologies. This demonstrates the significance of recommender systems and the need for them in the future.

This study explains what suggestion systems are and what benefits they provide. Furthermore, the methods used in recommendation systems are examined, and general explanations of the methods used are provided. The problems encountered by the methods used in recommendation systems are discussed, as well as the methods' working mechanisms.

REFERENCES

Aggarwal, C. C., & Aggarwal, C. C. (2016). Model-based collaborative filtering. Recommender systems:. *the textbook* (s. 71-138.).

Aygün, C., & Yildiz, O. (2016). (2016). Genetik Algoritma Kullanılarak İçerik Tabanlı Kitap Tavsiye Sistemi Geliştirilmesi Development Of Content Based Book Recommendation System Using Genetic Algorithm. *Fen Bilimleri Enstitüsü, Yüksek Lisans Tezi, Ankara,*, 43s.

Herlocker, J. L., Konstan, J. A., Borchers, A., & al., e. (1999). An algorithmic framework for performing collaborative filtering. *Proceedings of the 22nd Annual International ACM SIGIR Conference on Research and Development in Information Retrieval.*

Kwan, C. K., & Jasser, M. (2020). A Comparison Study Between Content-Based and Popularity-Based Filtering via Implementing a Book Recommendation System. *IJARET* (s. 11(12), 1121-1135.).

Manouselis, N., Drachsler, H., Vuorikari, R., Hummel, H., & Koper, R. (2011). Recommender systems in technology enhanced learning. . *Recommender systems handbook,* (s. 387-415.).

Özgöbek, Ö., & Erdur, R. C. (2015). Öneri sistemleri ve bir uygulama alanı olarak haber öneri sistemleri. *Akademik Bilişim Konferansları*, (s. 31).

Pazzani, M. J., & Billsus, D. (2007). Content-based recommendation systems. *In The adaptive web: methods and strategies of web personalization* (s. pp. 325-341). Berlin, Heidelberg: : Springer Berlin Heidelberg.

Seyrek, H. (2020). Genetik algoritma ile ağırlıklandırılmış hibrit bir film öneri sistemi/A hybrid film recommendation system weighted with genetic algorithm. *Doctoral dissertation*.

Shen, J. W., & Yang, Y. (2013). Collaborative filtering recommendation algorithm based on two stages of similarity learning and its optimization. *IFAC Proceedings Volumes,* , (s. 46(13), 335-340.).

Sieg, A. M., & Burke, R. D. (2007). Learning ontology-based user profiles: A semantic approach to personalized web search. *IEEE Intell. Informatics Bull.*, 8(1), 7-18.

SU, X., & Khoshgoftaar, T. M. (2009). A survey of collaborative filtering techniques. *Advances in artificial intelligence.*

Terzi, İ. (2017). (2017). Kullanıcı/ürün çiftleri için en iyi öneri algoritmalarının tespit edilmesi . *Master's thesis, Anadolu Üniversitesi.*

CHANGE OF MICROSTRUCTURAL, CRYSTALLINE QUALITY, AND SURFACE MORPHOLOGICAL FEATURES OF $Bi_{2.1}Sr_{2.0}Ca_{2.1}Cu_{3.0}O_y$ CERAMIC MATERIALS WITH THE CdO ADDITION

Yahya ALTUNPAK[1] and Asaf Tolga ÜLGEN [2]

1. INTRODUCTION

As well known, the material sciences have possessed very large studying areas from chemical material productions to numerical studies (Li, et al. 2023, Wang, 2023, Bilge, et al. 2019). Lately the scientists have been working on the improvement of the mechanical strengths and electrical properties to increase the application fields (Bilge, et al. 2019, Bilge & Morgül, 2023). Especially studies on superconductors are extremely interesting in terms of energy management. Accordingly, the first superconductor (metallic mercury) was discovered in 1911 by observing no resistance under the applied current in the temperature-dependent electrical resistance test. Immediately

[1] Prof. Dr., Abant Izzet Baysal University, Department of Mechanical Engineering, Bolu–Turkey, 14280, e-mail: altunpak_y@ibu.edu.tr, ORCID: 0000-0001-8676-4789.

[2] Assoc. Prof. Dr., Şırnak University, Department of Electric-Electonic Engineering, Sirnak–Turkey, 73000. e-mail: asaftolgaulgen@gmail.com ORCID: 0000-0002-7112-5607.

after, the superconducting phenomenon was described by two important physical quantities: (I) exhibition of resistance after the critical transition temperature for material, and (II) disappearance of magnetic flux fields before the critical transition temperature (Onnes, 1911). Over time, it has been observed that many materials including the elements, semi-metals, semi-metal-containing compounds, metals, sulfides, carbides, alloys, rare earth borocarbides, organic materials, fullerenes, nitrides, heavy fermions, chevrel phase, A-15 inorganic samples, magnesium diboride, ruteno-cuprate samples, metal-based samples, carbon-containing compounds, chalcogens, silicon-based samples, iron-based materials, pyrochlorine oxides, and oxygen deficit perovskite-based cuprate type-II materials have shown superconductivity until today (Kleiner, 2016, Erdem, et al. 2017, Ozturk, et al. 2017, Taylan, et al. 2016, Savaşkan, et al. 2015, Güner, et al. 2019).

In the year of 1986, the first type-II superconductor, $La_{2-x}Ba_xCuO_4$, was discovered with a transition temperature of nearly 35 K Bednorz & Müller, 1986, Ford & Saunders, 2004). After the breaking point for the superconductivity, yttrium has been replaced by lanthanum in the $La_{2-x}Ba_xCuO_4$ system, and hence $YBa_2Cu_3O_{7-y}$ compound was the first material discovered material exhibiting a transition temperature greater than the liquid nitrogen Bordet, et al.1988, Marsh, et al. 1988, Guner, et al. 2017, Çakır, et al. 2019, Abdioglu, et al. 2019, Savaskan, et al. 2020). Thus, the discovery of perovskite-based cuprates with short-range ordered antiferromagnetic Cu-O chains and layers has opened new potential application areas for superconductors

[Bednorz & Müller, 1986, Ford & Saunders, 2004). Additionally, the cuprate parents have widely been preferred to use in the industrial power systems and energy-related sectors due to their intrinsic superior characteristic properties, viz. higher thermodynamic stability, optical and electronic characteristics, and resistance to the humidity environments, as well as the easy access to starting chemicals, simple chemical (light, abundant, low cost, and nonpoisonous) compositions, easy access to cooling refrigerant, easily deforming/shaping/rolling for long cables, wires (≈ higher than one-kilometer length) and tape-casting constructions, easily accessible of nitrogen for the cooling system, and stability to compositions and oxygen contents Saritekin, et al., 2016, Wu, et al. 1987, Takayama-Muromachi, 1998, Yamauchi & Karppinen, 2000, Sheahen, 2022, Saxena, 2012).

However, the cuprate parents such as the Bi-containing ceramic parents have possessed some problematic issues including the intergranular boundary, mechanical stabilization, different oriented micro-crystals, brittleness and various phase compositions in the crystal system. Besides, structural characteristic issues, large penetration depth, weak-links interaction problems, low charge carrier densities, short coherence length, relatively lower operating temperatures, high responsibility to applied magnetic fields and applied current have damaged the usage of Bi-based ceramics in the application fields (Salama, et al. 1989, Ulgen, 2021, Akdemir, et al., 2016, Autret-Lambert, et al., 2006, Guner, et al., 2019). The systematic faults achieved are overcome by several preparation conditions such as dopant type, ambient conditions, and chemical addition

(Sarıtekin, et al., 2016, Roa, et al., 2010, Dadras, et al., 2017, Sarıtekin, et al., 2016, Parinov, 2013, Lian, et al., 1990, Jin, et al., 1988).

In the present work, we have tried to examine the change of fundamental microstructural, crystalline quality, and surface morphological features of $Bi_{2.1}Sr_{2.0}Ca_{2.1}Cu_{3.0}O_y$ ceramic materials with the CdO addition in the crystal lattice by using the standard scanning electron microscope measurements at 20 kV high voltage with the magnification of 10000X. Similarly, the influence of CdO impurity addition on the reaction kinetics of the nucleation and crystal growth mechanisms has extensively been inspected with the variation in the activation energy, nucleation stability, nucleation transition, and crystallization temperatures in this paper for the first time.

Moreover, the local elemental distributions for the Cd, Cu, Sr, Ca, Bi, and O elements have been determined with the aid of electron dispersive X-ray findings. It has been observed form the EDX findings that the bulk $Bi_{2.1}Sr_{2.0}Ca_{2.1}Cu_{3.0}O_y(CdO)_x$ ceramic matrices have been produced as required. Both the SEM and reaction kinetics have clearly shown that with the enhancement in the cadmium oxide impurity addition, all the fundamental microstructural, crystalline quality, and surface morphological features have been recorded to decrease seriously.

2. EXPERIMENTAL DETAILS FOR BULK $Bi_{2.1}Sr_{2.0}Ca_{2.1}Cu_{3.0}O_y(CdO)_x$ CERAMIC STRUCTURES

In this work, we have prepared the bulk $Bi_{2.1}Sr_{2.0}Ca_{2.1}Cu_{3.0}O_y(CdO)_x$ ceramic structures within the different cadmium oxide impurity additions intervals 0.00-0.10 by using the conventional ceramic process. All the heating treatments have been conducted under the atmospheric air conditions. Throughout the preparation conditions, the high-purity powders of chemicals such as CdO, CuO, Bi_2O_3, $SrCO_3$, and $CaCO_3$ chemicals have been used to synthesize the $Bi_{2.1}Sr_{2.0}Ca_{2.1}Cu_{3.0}O_y(CdO)_x$ ceramic materials. The purity levels have been higher than the value of 99.99%. All the components have been mixed by weighing 2 grams of the chemical powders within the stoichiometric ratios of $Bi_{2.1}Sr_{2.0}Ca_{2.1}Cu_{3.0}O_y(CdO)_x$.

The weighing has been performed by an electronic balance under atmospheric air ambient. After that, the chemicals of powders have been placed in the porcelain crucibles and have been exposed to the mixing process in a grinding machine in the air medium for the duration of 9 hours so as to decrease the particle sizes of chemicals and also prepare a homogeneous mixture. After, the homogenous mixed powders have been mixed in an agate mortar for 40 minutes without solvents both to diminish the particle size of chemicals and form new atomic bonds between the atoms placed in the crystal structure. All the compounds have been exposed to the calcination process in the porcelain crucibles placed into a programmable furnace at 800°C for 36 hours at atmospheric air conditions. Through the calcination, not only cooling but also heating rates have been adjusted as 5°C/m. Correspondingly, with the help of calcination process, we have removed the impurity phases from the bulk $Bi_{2.1}Sr_{2.0}Ca_{2.1}Cu_{3.0}O_y(CdO)_x$ ceramic structures. Thus, the homogenous structured materials have been ready for palletization in the rectangular bar volume of 2.0*x*0.5*x*0.2 cm^3 in the atmospheric air conditions. The palletization process has enabled us to produce new bonds between the atoms and enhance the grain boundary coupling strength between the stacked planes in the Bi-2223 crystal lattice. As for the main heating process, all the bars pelletized have been sintered at t 850°C for 36 h under medium of air in the furnace. Henceforward, new ceramic $Bi_{2.1}Sr_{2.0}Ca_{2.1}Cu_{3.0}O_y(CdO)_x$ materials prepared at various cadmium oxide additions as regards x=0.000, 0.005, 0.010, 0.050, 0.070, and 0.100 have been presented as pure, CdO/1, CdO/2, CdO/3, CdO/4, and CdO/5, respectively.

As for the characterization methods, the scanning electron microscopy (SEM) inspections taken 10000X magnification have been conducted by an FEI Quanta FE-SEM electron microscope under 20 kV external under secondary electron image to discuss the main microstructural, crystalline quality, and surface morphological features of $Bi_{2.1}Sr_{2.0}Ca_{2.1}Cu_{3.0}O_y$ ceramic materials with the CdO addition in the crystal lattice. The role of cadmium oxide impurity addition on the partial melting sites, texturing, cracks, voids, micropores, microcrystal coalescence orientations, grain alignment distribution, boundary coupling problems, surface appearance, flaky layered structure, and grain size distribution has extensively been revealed through the main text.

Furthermore, local elemental distributions for the Cd, Cu, Sr, Ca, Bi, and O elements on the surface of $Bi_{2.1}Sr_{2.0}Ca_{2.1}Cu_{3.0}O_y(CdO)_x$ ceramic structures have been determined using by SEM equipped with an Oxford X-ray micro-probe and IXRF System Model 550i analyzer.

3. RESULTS AND DISCUSSION

3.1. Change of microstructural and basic morphological properties of CdO added Bi-2223 ceramic structures

In the current study, we have focused sensitively on the variation of fundamental microstructural, crystalline quality, and surface morphological features of $Bi_{2.1}Sr_{2.0}Ca_{2.1}Cu_{3.0}O_y$ ceramic materials with the CdO addition in the crystal lattice by means of the standard scanning electron microscope measurements. The SEM images have enabled us to determine the varied partial melting sites, texturing, cracks, voids, micropores, and microcrystal coalescence orientations. Similarly, the change in the grain alignment distribution, boundary coupling problems, surface appearance, flaky layered structure, and grain size distribution have also been discussed in detail. The experiments have been performed by a SEM branched JEOL 6390-LV under a 20 kV external voltage and pictures have been imaged at 10000X magnification under secondary electron image. We have depicted the SEM images for only the first three samples called pure, CdO/1 and CdO/2 samples have been depicted in Fig. 1 a-c due to the decrease in the fundamental microstructural, crystalline quality, and surface morphological features of Bi-2223 ceramic compounds. It has been obvious that the presence of cadmium oxide impurity has seriously affected the surface morphology appearance of Bi-2223 ceramic system.

The change of the morphological features has stated that the cadmium oxide particles have been adopted in the crystal structure of Bi-2223 compounds successfully. At the same time, the obtained figures have shown that the crystal quality and surface morphology have been found to damage all the features discussed above.

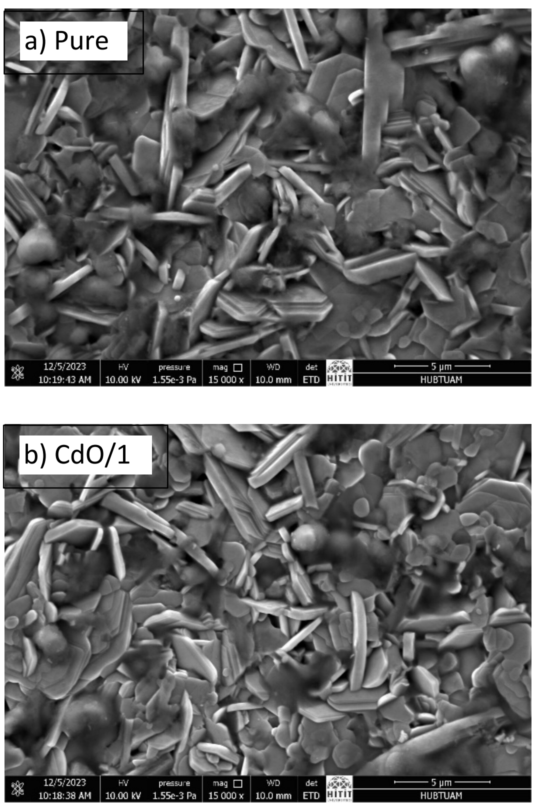

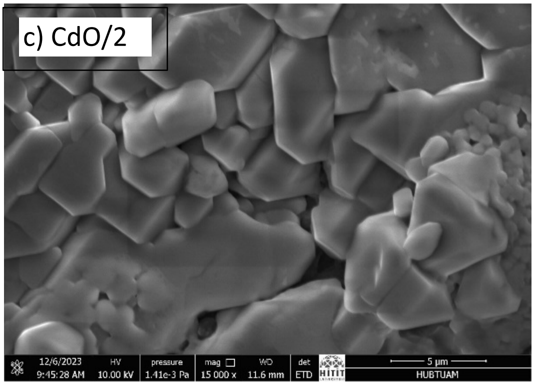

Fig.1 SEM images taken at 10000x magnification for a-) the unadded Bi-2223 structure, b-) CdO/1 sample, and c-) CdO/2 compounds prepared.

Furthermore, the figures have indicated that both the pure and CdO added Bi-2223 ceramic compounds have presented the typical granular crystal structure growth within flaky layers and random alignment distribution of grains. Interestingly, the SEM images have displayed that the presence of the cadmium oxide impurity inserted in the bulk Bi-2223 ceramic system has damage the formation of the flaky layers of platelet-like shape for grains as a result of the induction of various microcrystal coalescence orientations, new partial melting sites, and especially the degradation of particle size distributions based on the decrease in the crystallite size of samples (Fig. 1a-c). On this basis, among the $Bi_{2.1}Sr_{2.0}Ca_{2.1}Cu_{3.0}O_y(CdO)_x$ ceramic structures, the un-added Bi-2223 ceramic structure has presented the most homogenous uniform surface appearance and the best grain boundary couplings. Likewise, the same sample has exhibited the most crystal structure quality and largest particle distributions throughout the crystal structure. Besides, the bulk pure sample with the well-linked platelet shapes and crystal orientations has been noted to have the smoothest and densest surface morphology depending on its own least porous structure among the compounds studied. The pure sample has also stabilized much more the typical Bi-2223 ceramic system as seen in Fig. 1a. Conversely, with the enhancement in the cadmium oxide additions in the Bi-2223 crystal structure, the melting point of ceramic system has been observed to decrease and the partial melting sites have been observed to increase seriously. This fact has led to the increase in the irregular grain mis-orientations and especially the revival of coupling problems between adjacent layers. In fact, the presence of the cadmium oxide impurity in the system has caused to the rapid enhancement of the micropores, cracks, voids, and microcrystal coalescence orientations (Fig. 1c). In this respect, the surface appearance has been recorded to decrease more and more depending on the increase of the CdO impurity addition.

3.2. Examination of elemental composition distributions in $Bi_{2.1}Sr_{2.0}Ca_{2.1}Cu_{3.0}O_y(CdO)_x$ ceramic structures

In the current work, we have determined the differentiation in the local elemental (Cd, Cu, Sr, Ca, Bi, and O) composition distributions with the aid of typical EDX (electron dispersive X-ray) experiments in the crystal systems of $Bi_{2.1}Sr_{2.0}Ca_{2.1}Cu_{3.0}O_y(CdO)_x$ ceramic structures so that we have got knowledge about whether the desired CdO impurity addition has been performed throughout the crystal lattice or not. One can see the numeric parameters for the elemental composition distributions in Table 1. Based on the EDX results focused on the change in the elemental composition distributions, it has been recorded that all the $Bi_{2.1}Sr_{2.0}Ca_{2.1}Cu_{3.0}O_y(CdO)_x$ ceramic materials have consisted of every required composition (Ozturk, et al., 2012).

Table 1. Differentiation of Cd, Cu, Sr, Ca, Bi, and O elemental composition distributions for pure and different CdO added $Bi_{2.1}Sr_{2.0}Ca_{2.1}Cu_{3.0}O_y(CdO)_x$ ceramic materials.

Component	**Line**	**Distribution Content (wt.%)**					
		Pure	**CdO/1**	**CdO/2**	**CdO/3**	**CdO/4**	**CdO/5**
Bi	L_α	41.831	41.805	41.570	41.630	41.462	41.606
Sr	L_α	16.707	16.734	16.968	16.643	16.688	16.521
Ca	K_α	8.024	8.032	8.025	8.046	8.119	7.995
Cu	K_α	18.175	18.138	18.109	18.024	17.896	17.749
O	K_α	15.263	15.233	15.207	15.105	15.070	15.008
Cd	K_α	0	0.058	0.121	0.552	0.765	1.121

At the same time, it has been observed that the variations of calcium, strontium and bismuth elemental distributions have been obtained to be randomly whereas the elemental distribution belonging to the cadmium elements has been noted to increase systematically as desired. As for the differentiations in the copper and oxygen elemental distributions, there has appeared a dramatic decrease depending on the increase in the cadmium oxide impurity addition. We have also sketched the change in the elemental compositions in terms of the CdO impurity addition (Fig. 2).

The graphics have shown that the bismuth elemental distribution has been observed to harshly vary with respect to the impurity additions of CdO materials. Numerically, the cadmium composition has been computed to be about 0 for the pure sample, 0.058% for the CdO/1 compound, 0.121% for the bulk CdO/2 structure, 0.552% for the CdO/3 material, 0.765% for the bulk CdO/4 system, and 1.121% for the CdO/5 material, respectively.

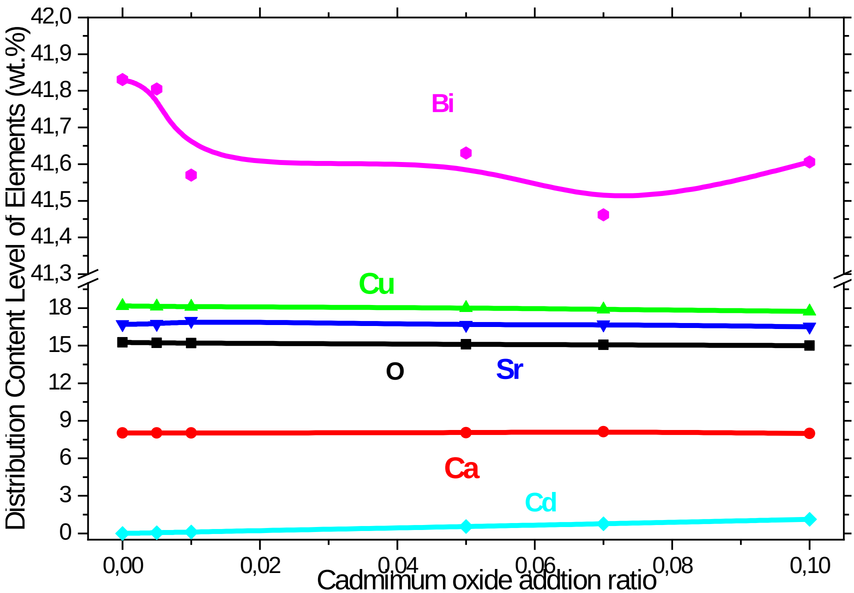

Fig.2 Local elemental distributions for ceramic materials.

As for the change in the copper composition distribution in the bulk Bi-2223 crystal system, the cadmium composition has been determined to decrease from the value of 18.175% (for the pure material) to 17.749% (for the CdO/5 ceramic sample). The other samples produced have possessed the moderate ratios in the $Bi_{2.1}Sr_{2.0}Ca_{2.1}Cu_{3.0}O_y(CdO)_x$ ceramic materials. Besides, the oxygen content level has been found to diminish from the value of 15.263% (for the pure material) to 15.008% (for the CdO/5 sample). The other ceramics have possessed the moderate ratios between these ratios. All in all, the enhancement in the cadmium oxide addition in the Bi-2223 ceramic structures has led to the systematic degradation in both the oxygen and elemental distribution throughout the $Bi_{2.1}Sr_{2.0}Ca_{2.1}Cu_{3.0}O_y$ ceramic systems. Maybe, the decrement trend has stemmed from the suppression of the fundamental microstructural, crystalline quality, and surface morphological features of $Bi_{2.1}Sr_{2.0}Ca_{2.1}Cu_{3.0}O_y$ ceramic materials with the CdO impurity addition. Similar experimental finding can be seen in the scientific publications (Ozturk, et al., 2012).

3.3. Effect of CdO impurity on reaction kinetics of nucleation mechanism for ceramic materials

In this part of paper, we have discussed on the influence of cadmium oxide impurity addition on the reaction kinetics of the nucleation (crystallization) mechanism. It is well known that the change in the fundamental microstructural, crystalline quality, and surface morphological features with the cadmium oxide impurity has stemmed from the alteration of activation energy (known as Ea) for the crystallization depending on the stoichiometry of chemical contents in the composition (Kannan & Predeep 2013). Even, the nucleation mechanism is received to play an important role in understanding the main properties of a ceramic structure. The experimental findings related to the SEM and related features have demonstrated that the existence of cadmium oxide impurity has resulted in considerable enhancement in the value of the Ea parameter because of the variation in the stoichiometry of chemical contents in the composition (based on the changed electronegativity, valance electron states, electron configurations, cation-vacancy, ionic radius dimensions), couplings between adjacent layers, and interplanar bonds of Cd ions and host ions along with the main matrix (Nilsson, et al., 2008, Koralay, et al., 2016). Similarly, the presence of cadmium oxide impurity has caused a remarkable shift of the crystallization temperature to lower temperature regions. Namely, the crystallization mechanism of different impurity phases has started in the bulk $Bi_{2.1}Sr_{2.0}Ca_{2.1}Cu_{3.0}O_y(CdO)_x$ ceramic matrix instead of the main characteristic superconducting phase. As for the behavior of pure sample, the material preparation conditions mentioned above have led to the enhancement in the nucleation temperatures towards higher temperature regions. In the rearrangement procedure to nucleate the different phases, the chemical contents that bind with neighboring ions in the main composition are placed in the lattice state of the primary crystals (Kannan & Predeep 2013). As for the nucleation stability of pure and Cd-added bulk $Bi_{2.1}Sr_{2.0}Ca_{2.1}Cu_{3.0}O_y$ ceramic systems, the preparation conditions for the pure sample have triggered thermodynamically the reduction of the stability and the augmentation in the formation of surface nucleation. Correspondingly, the pure sample has been detected to be thermodynamically unstable as compared to the other samples produced (Ianculescu, et al., 2006). All in all, the Ea values and nucleation stability of materials are known to directly depend on the chemical contents in the composition, couplings between adjacent layers, and interaction between the CdO impurity ions and host ions along the main matrix.

Additionally, with the increase in the activation energy value for the crystallization, the penetration of cadmium impurity in the bulk $Bi_{2.1}Sr_{2.0}Ca_{2.1}Cu_{3.0}O_y$ system has been obtained to be harder as possible. Similarly, the shift of crystallization temperatures to higher temperature regions has made the enter of cadmium impurities to the crystal lattices difficult. Accordingly, both nucleation and crystal growth mechanisms have been performed much slower than they should be. Shortly, the impurity ions have been noted to enter into the lattice points of bulk pure ceramic material possessing the combination of the highest surface nucleation, and the smallest Ea values and crystallization temperatures. That is to say, the presence of CdO impurity addition in the bulk $Bi_{2.1}Sr_{2.0}Ca_{2.1}Cu_{3.0}O_y$ system has led to a decrease in the nucleation rate for the first crystallization action based on the instantaneous nucleation and 3D parabolic expansion mechanism (Kannan & Predeep 2013). The significant reduction of the nucleation rate has retarded the nuclei growth as a consequence of fluctuations of chemical contents in the composition, couplings between adjacent layers, and interaction between the CdO impurity ions and host ions along the main matrix. Consequently, the existence of cadmium oxide impurity has resulted in damage to chain reaction process related to nucleation transition into 1D, 2D, and 3D growth (Karamanov & Pelino 2001).

4. CONCLUSION

In the current work, the change in the reaction kinetics of the nucleation, crystal growth mechanisms, microstructural, crystalline quality, and surface morphological properties of $Bi_{2.1}Sr_{2.0}Ca_{2.1}Cu_{3.0}O_y$ crystal structures with the different cadmium oxide addition amount changing molar ratios of $0.00 \leq x \leq 0.10$ with the aid of the scanning electron microscopy measurements. The experimental results have indicated that the bulk $Bi_{2.1}Sr_{2.0}Ca_{2.1}Cu_{3.0}O_y(CdO)_x$ ceramic matrices have been produced as required. However, the elemental distributions for the oxygen and copper atoms have been observed to decrease monotonously with the enhancement in the cadmium oxide addition amount in the Bi-2223 ceramic compounds. As expected, the local elemental distribution related to the Cd element has been noticed to increase step by step based on the augmentation in the cadmium oxide impurity. Based on the EDX findings, it has been confirmed that there may be a strong relationship between the surface morphological quality and CdO impurity amount in the Bi-2223 crystal structure. Moreover, it has been form from the SEM images that the microstructural, crystalline quality, and surface morphological features have been shown to regress due to the diminish in the formation of the flaky layers of platelet-like shape for grains based on the enhancement in various microcrystal coalescence orientations, new formation of partial melting sites, micropores, cracks, voids, and especially the degradation of particle size distributions. As for the discussion about the reaction kinetics of the nucleation for the CdO added Bi-2223 crystal system, there has been a considerable increase in the activation energy value due to the shift of the crystallization temperature to lower-temperature regions. Hence, the crystallization mechanism of different impurity phases has been caused to the formation of different impurity phases in the $Bi_{2.1}Sr_{2.0}Ca_{2.1}Cu_{3.0}O_y$ matrix.

Conversely, the pure sample has been found to show the least thermodynamic stability due to both the augmentation in the formation of surface nucleation and the decrease in the crystallization temperatures and activation energy.

REFERENCES

Abdioglu, M., Ozturk, K., Guner, S. B., Celik, S., & Kucukomeroglu, T. (2019). Investigation of magnetic force properties between different PMGs and multi-seeded YBCO superconductors with different seed distances. Physica C: Superconductivity and its Applications, 565, 1353519.

Akdemir, E., Pakdil, M., Bilge, H., Kahraman, M. F., Bekiroglu, E., Yildirim, G., ... & Oz, M. (2016). Degeneration of mechanical characteristics and performances with Zr nanoparticles inserted in Bi-2223 superconducting matrix and increment in dislocation movement and cracks propagation. Journal of Materials Science: Materials in Electronics, 27, 2276-2287.

Autret-Lambert, C., Pignon, B., Gervais, M., Monot-Laffez, I., Ruyter, A., Ammor, L., ... & Decourt, R. (2006). Microstructural and transport properties in substituted $Bi_2Sr_2CaCu_2O_{8+}$ δ-modulated compounds. Journal of Solid State Chemistry, 179(6), 1698-1706.

Bednorz, J. G., & Müller, K. A. (1986). Possible high T c superconductivity in the Ba– La– Cu– O system.

Zeitschrift für Physik B Condensed Matter, 64(2), 189-193.

Bilge, H., & Morgül, Ö. K. (2023). Analytical and Experimental Investigation of the Rotary Inertia Effects of Unequal End Masses on Transverse Vibration of Beams. Applied Sciences, 13(4), 2518.

Bilge, H., Doruk, E., Fındık, F., & Pakdil, M. (2019). Effect of fatigue crack propagation on natural frequencies of system in AISI 4140 Steel. Steel and Composite Structures, An International Journal, 32(3), 305-312.

Bordet, P., Chaillout, C., Chenavas, J., Hodeau, J. L., Marezio, M., Karpinski, J., & Kaldis, E. (1988). Structure determination of the new high-temperature superconductor $Y_2Ba_4Cu_7O_{14+x}$. Nature, 334(6183), 596-598.

Çakır, B., Öztürk, K., Güner, S. B., Çelik, Ş., & Aydıner, A. (2019). Magnetic properties of the welded joined TSMG Y123+ x wt% Y211 (x= 20 and 30) bulk superconductors. Physica C: Superconductivity and its Applications, 557, 19-25.

Dadras, S., Dehghani, S., Davoudiniya, M., & Falahati, S. (2017). Improving superconducting properties of YBCO high temperature superconductor by Graphene Oxide doping. Materials Chemistry and Physics, 193, 496-500.

Erdem, O., Abdioglu, M., Guner, S. B., Celik, S., & Kucukomeroglu, T. (2017). Improvement in levitation force performance of bulk MgB2 superconductors through coronene powder adding. Journal of Alloys and Compounds, 727, 1213-1220.

Ford, P. J., & Saunders, G. A. (2004). The rise of the superconductors. CRC press.

Guner, S. B., Celik, S., & Tomakin, M. (2017). The investigation of magnetic levitation performances of single grain YBCO at different temperatures. Journal of Alloys and Compounds, 705, 247-252.

Güner, S. B., Savaşkan, B., Öztürk, K., Çelik, Ş., Aksoy, C., Karaboğa, F., ... & Yanmaz, E. (2019). Investigation on superconducting and magnetic levitation force behaviour of excess Mg doped-bulk MgB_2 superconductors. Cryogenics, 101, 131-136.

Guner, S. B., Zalaoglu, Y., Turgay, T., Ozyurt, O., Ulgen, A. T., Dogruer, M., & Yildirim, G. (2019). A detailed research for determination of Bi/Ga partial substitution effect in Bi-2212 superconducting matrix on crucial characteristic features. Journal of Alloys and Compounds, 772, 388-398.

H.K. Onnes (1911). Further experiments with liquid helium. D. On the change of electrical resistance of pure metals at very low temperatures, etc. V. The disappearance of the resistance of mercury, K. Ned. Akad. van Wet. Proc. (in: Koninklijke Nederlandsche Akademie van Wetenschappen Proceedings) 14, 113–115.

Hilgenkamp, H., & Mannhart, J. (2002). Grain boundaries in high-T c superconductors. Reviews of Modern Physics, 74(2), 485.

Ianculescu, A., Gartner, M., Despax, B., Bley, V., Lebey, T., Gavrilă, R., & Modreanu, M. (2006). Optical characterization and microstructure of BaTiO3 thin films obtained by RF-magnetron sputtering. Applied surface science, 253(1), 344-348.

Jin, S., Tiefel, T. H., Sherwood, R. C., Davis, M. E., Van Dover, R. B., Kammlott, G. W., ... & Keith, H. D. (1988). High critical currents in Y-Ba-Cu-O superconductors. Applied physics letters, 52(24), 2074-2076.

Kannan, T., & Predeep, P. (2013). Investigation into the superconducting threshold of $Bi_{1.6}Pb_{0.4}Sr_2Ca_{n-1}Cu_nO_{2n+4+\delta}$, n= 2, 2.5, 4 perovskites synthesized by glassy precursor route with Thermal and Raman spectroscopic techniques. Journal of thermal analysis and calorimetry, 114, 635-641.

Kannan, T., & Predeep, P. (2013). Investigation into the superconducting threshold of BiPbSrCaCuO, n= 2, 2.5, 4 perovskites synthesized by glassy precursor route with Thermal and Raman spectroscopic techniques. Journal of Thermal Analysis & Calorimetry, 114(2).

Karamanov, A., & Pelino, M. (2001). Influence of the nucleation time-lag on the activation energy in non-isothermal crystallization. Journal of non-crystalline solids, 290(2-3), 173-179.

Koralay, H., Hicyilmaz, O., Cavdar, Ş., Ozturk, O., & Tasci, A. (2016). Experimental and theoretical approaches on thermal and structural properties of Zn doped BSCCO glass ceramics. Materials Science-Poland, 34(1).

Li, S., Zhao, L., Wang, C., Huang, H., & Zhuang, M. (2023). Synergistic improvement of carbon sequestration and crop yield by organic material addition in saline soil: A global meta-analysis. Science of The Total Environment, 164530.

Lian, Z., Pingxiang, Z., Ping, J., Keguang, W., Jingrong, W., & Xiaozu, W. (1990). The properties of YBCO superconductors prepared by a new approach: the'powder melting process'. Superconductor Science and Technology, 3(10), 490.

Marsh, P., Fleming, R. M., Mandich, M. L., DeSantolo, A. M., Kwo, J., Hong, M., & Martinez-Miranda, L. J. (1988). Crystal structure of the 80 K superconductor $YBa_2Cu_4O_8$. Nature, 334(6178), 141-143.

Nilsson, A., Gruner, W., Acker, J., & Wetzig, K. (2008). Critical aspects on preparation of Bi-2223 glassy precursor by melt-process. Journal of non-crystalline solids, 354(10-11), 839-847.

Ozturk, K., Dancer, C. E. J., Savaskan, B., Aksoy, C. A. N. A. N., Guner, B., Badica, P., ... & Celik, S. (2017). The investigation on the regional nanoparticle Ag doping into MgTi0. 06B2 bulk for improvement the magnetic levitation force and the bulk critical current. Journal of Alloys and Compounds, 724, 427-434.

Ozturk, O., Asikuzun, E., Erdem, M., Yildirim, G., Yildiz, O., & Terzioglu, C. (2012). The effect of Pr addition on superconducting and mechanical properties of Bi-2212 superconductors. Journal of Materials Science: Materials in Electronics, 23, 511-519.

Parinov, I. A. (2013). Microstructure and properties of high-temperature superconductors. Springer Science & Business Media.

R. Kleiner, W. Buckel (2016). Superconductivity an introduction, Wiley-VCH, New York, 3th Ed.

Roa, J. J., Jiménez-Piqué, E., Capdevila, X. G., & Segarra, M. (2010). Nanoindentation with spherical tips of single crystals of YBCO textured by the Bridgman technique: Determination of indentation stress–strain curves. Journal of the European Ceramic Society, 30(6), 1477-1482.

Salama, K., Selvamanickam, V., Gao, L., & Sun, K. (1989). High current density in bulk $YBa_2Cu_3O_x$ superconductor. Applied Physics Letters, 54(23), 2352-2354.

Sarıtekin, N. K., Bilge, H., Kahraman, M. F., Zalaoğlu, Y., Pakdil, M., Doğruer, M., ... & Oz, M. (2016, March). Improvement of mechanical characteristics and performances with Ni diffusion mechanism throughout Bi-2223 superconducting matrix. In AIP Conference Proceedings (Vol. 1722, No. 1). AIP Publishing.

Sarıtekin, N. K., Kahraman, M. F., Bilge, H., Zalaoğlu, Y., Pakdil, M., Doğruer, M., ... & Oz, M. (2016, March). Effect of Ni diffusion annealing temperature on crucial characterization of Bi-2223 superconducting system. In AIP Conference Proceedings (Vol. 1722, No. 1). AIP Publishing.

Saritekin, N. K., Pakdil, M., Yildirim, G., Oz, M., & Turgay, T. (2016). Decrement in metastability with Zr nanoparticles inserted in Bi-2223 superconducting system and working principle of hybridization mechanism. Journal of Materials Science: Materials in Electronics, 27, 956-965.

Savaskan, B., Guner, S. B., Yamamoto, A., & Ozturk, K. (2020). Trapped magnetic field and levitation force properties of multi-seeded YBCO superconductors with different seed distance. Journal of Alloys and Compounds, 829, 154400.

Savaşkan, B., Koparan, E. T., Güner, S. B., Çelik, Ş., Öztürk, K., & Yanmaz, E. (2015). Effect of $C_4H_6O_5$ Adding on the Critical Current Density and Lateral Levitation Force of Bulk MgB_2. Journal of low temperature physics, 181(1-2), 38-48.

Saxena, A.K. (2012). High-Temperature Superconductors, 2nd Ed., Springer Heidelberg New York Dordrecht London.

Sheahen, T.P. (2022). Introduction to High-temperature Superconductivity, 1st ed., Kluwer Academic Publishers, New York, Boston.

Takayama-Muromachi, E. (1998). High-pressure synthesis of homologous series of high critical temperature (T_c) superconductors. Chemistry of materials, 10(10), 2686-2698.

Taylan Koparan, E., Savaskan, B. U. R. C. U., Guner, S. B., & Celik, S. (2016). Effects of Bi-2212 addition on the levitation force properties of bulk MgB_2 superconductors. Applied Physics A, 122, 1-11.

Ulgen, A. T. (2021). Influence of cadmium addition on electrical and superconducting features of bulk $Bi_{2.1}Sr_{2.0}Ca_{1.1}Cu_{2.0}O_y$ superconducting materials. Research & Reviews in Science and Mathematics-I.

Wang, Q. (2023). Effect of preparation of organic ferroelectric P (VDF-TrFE) nanostructure on the improvement of tennis performance. Advances in nano research, 14(4), 329-334.

Wu, M. K., Ashburn, J. R., Torng, C., Hor, P. H., Meng, R. L., Gao, L., ... & Chu, A. (1987). Superconductivity at 93 K in a new mixed-phase Y-Ba-Cu-O compound system at ambient pressure. Physical review letters, 58(9), 908.

Yamauchi, H., & Karppinen, M. (2000). Application of high-pressure techniques: stabilization and oxidation-state control of novel superconductive and related multi-layered copper oxides. Superconductor Science and Technology, 13(4), R33.

RISK ANALYSIS AND ASSESSMENT OF A HOSPITAL USING THE L DECISION MATRIX METHOD

Mehmet HASKUL[1] and Ercan ÖZEN[2]

1. INTRODUCTION

People may be exposed to a variety of dangers at the institutions and organisations for which they work. To prevent such negative impacts, it is vital to identify and evaluate potential hazards ahead of time, as well as to identify and take actions to eliminate or minimise the risks. Enterprises should systematically do risk analysis and risk assessment in order to generate an analysis report for this purpose. They should also identify potential negative outcomes and take appropriate action to mitigate them. In this context, occupational health and safety in the workplace is of great importance. If one were to give an overall definition, occupational health would be defined as the science that attempts to prevent or minimise risks associated with working conditions, tools, and equipment, as well as to allow employees to live in harmony with their work environment. It also refers to the full physical, mental, moral, and social well-

[1] Assoc. Prof. Dr., Şırnak University, Faculty of Engineering, Department of Mechanical Engineering, mehmethaskul@sirnak.edu.tr, ORCID: 0000-0001-8671-4597.

[2] Biologist, Silopi State Hospital

being of employees at the highest level (Sarac, 1998). Occupational safety refers to the methodical efforts made to protect workers from potential risks that may arise while performing their jobs, as well as the harm that these risks may do to their health, as well as to provide a more comfortable and secure work environment (Dizdar, 2002). According to the Risk Assessment Regulation and Law No. 6331, "These are the studies required to identify the hazards that exist in the workplace or that may come from outside, to analyse and rank the factors that cause these hazards to turn into risks and the risks arising from the hazards, and to decide on control measures." It is defined as follows. Risk assessment refers to all of the steps done within the framework of rules, regulations, and statutes to identify the dangers that cause occupational accidents and diseases, as well as the risks that these hazards may represent. Özkılıç, (2005) and Öztaş (2007) proposed numerous definitions and methodologies for risk analysis, evaluation, and management.

With the Health Quality Standards and Health Accreditation Standards, the Ministry of Health has taken a number of steps to protect patient and employee safety. Furthermore, with the Occupational Health and Safety Law No. 6331, which entered into force in 2012, our country's protective and preventive legal regulations regarding occupational accidents and occupational diseases in working life have been addressed as a whole, and a new era in providing a safe working environment has begun. Employers are required by law to implement work-related health and safety measures, as well as to conduct or have a risk assessment conducted, to safeguard employees in the workplace from work-related or environmental risks, without regard to public or private sector. Risk analysis and evaluation make potential hazards and risks obvious and help positively to reducing the health and safety risks of employees, patients, and their families. Overall, risk analysis is critical in reducing or eliminating any negative experiences that healthcare personnel, patients, and their families may have.

Examples of studies conducted at institutions offering health services include risk analysis, risk management, risk assessment, and comparison of risk analysis methodologies (Gül et al. 2013; Aksay & Orhan, 2013; İncesu, 2019; Kantarcıoğlu et al., 2020, Buturak & Yapıcı 2022). Öztürk et al. (2012) conducted research to determine whether occupational safety is ensured for healthcare personnel working in public hospitals. Meydanlıoğlu (2013) conducted a study to remind healthcare workers of workplace hazards and to contribute to the planning of healthcare services for healthcare professionals. Basmacı and Özdemir (2019) did a study to assess the interaction between risk management and employee safety in complex, labor-intensive healthcare companies that provide services through the coordinated work of employees from multiple professional groups. Muhammed and Akbel (2020) examined the hazards and risks that healthcare personnel face. Akgün (2015) investigated the dangers that may lead to workplace accidents among healthcare workers, as well as measures to protect against these risk factors. Kırılmaz et al. (2016) investigated psychological risk variables in healthcare workers.

The L matrix risk analysis approach was used in this work to conduct risk analysis and evaluation of a hospital. The risk analysis produced a ranking based on risk severity, and preventive strategies for these risks were offered.

2. L MATRIX METHOD

An L-type matrix (5x5 matrix diagram) is made up of five columns that represent five different categories and five rows that indicate five different levels for each of those categories. The matrix's left column represents "probability," while the top row represents "severity." L-type matrix diagrams are used to analyse the relationship between many variables and to rate and assess the likelihood and consequence of an event occurring (Özkılıç, 2005).

Table 1: Probability value of an L-type matrix (Özkılıç, 2005).

Probability (P)	
1 (Very small)	Hardly ever
2 (Small)	Once a Year (only in abnormal cases, very few)
3 (Middle)	Once a Month (less)
4 (High)	Once a Week (often)
5 (Very high)	Every day (very often)

Table 2: Shows the severity intensity value of a L type matrix (Özkılıç, 2005)

***Severity* (S)**	
1 (Very Light)	No loss of work hours, requires first aid
2 (Light)	No workday loss, outpatient treatment
3 (Middle)	Minor injury, inpatient treatment

4 (Serious)	Serious injury, long-term treatment, occupational disease
5 (Very Serious)	Death, Permanent disability

Table 3: L-type Matrix Risk Score (Özkılıç, 2005)

Risk Score = *Probability (P)* X *Severity* (S)						
R	***SEVERITY***					
PROBABILITY		**1 (Very Light)**	**2 (Light)**	**3 (Middle)**	**4 (Serious)**	**5 (Very Serious)**
	1(Very small)	**1 Insignificant**	**2 Low**	**3 Low**	**4 Low**	**5 Low**
	2(Small)	**2 Low**	**4 Low**	**6 Low**	**8 Middle**	**10 Middle**
	3(Middle)	**3 Low**	**6 Low**	**9 Middle**	**12 Middle**	**15 High**
	4 (High)	**4 Low**	**8 Middle**	**12 Middle**	**16 High**	**20 High**
	5 (Very high)	**5 Low**	**10 Middle**	**15 High**	**20 High**	**25 Not Tolerable**

Table 4: L-type Matrix Risk Results (Özkılıç, 2005)

Results	Actions
Unbearable Risk (25)	Work should not begin until the identified hazards have been reduced to an acceptable level, and any ongoing work should be terminated immediately. If, despite attempts, the risks cannot be lowered to an acceptable level, the work should be terminated.
Significant Risks (15,16,20)	Activity should not begin, and existing activity should be halted, until the identified risks are mitigated. If a risk occurs while the work is being done, safeguards should be taken immediately, and it should be considered whether or not the activity should be continued.
Intermediate Risks (8,9,10,12)	Attempts should be taken to mitigate the identified hazards. These research could take some time.
Bearable Risks (2,3,4,5,6)	An additional control process may not be required to eliminate the identified risks. It should be checked whether ongoing checks are continuing.

Inconsequential Risks (1)	In order to eliminate the identified risks, it may not be necessary to plan the control process and keep records of the work to be done.

3. RESEARCH AND FINDINGS

In this study, the emergency service unit of the hospital were examined and a risk analysis evaluation was made according to the L-type matrix.

Table 5: Identified Risks and Risk Degrees in the Emergency Service Unit

Hazard	Risk	Affected Persons	P	S	RS	Result	Precaution
Fire alarm system	Death Injury Poisonin g	Employees Visitors patients	**5**	**4**	**20**	**High Risk**	The fire alarm system in the building must be activated as soon as possible.
Fire cabinets	Death, injury	Employees Visitors, Patients	**5**	**4**	**20**	**High Risk**	All fire cabinets in the building must be activated so that water flows.
Fire extinguis hing spring	Death, injury, poisonin g	Employees Visitors, Patients	**5**	**4**	**20**	**High Risk**	Fire extinguishing sprints must be activated by making a water connection.
Working standing for long periods of time	Musculos keletal disorders , Varicose veins	Employees	**4**	**4**	**16**	**High Risk**	Appropriate rest areas should be provided for employees. Regular rest breaks should be determined and the number of personnel should be increased.
Physical or verbal violence	Death, injury, stress, depressio n	Employees,	**4**	**4**	**16**	**High Risk**	Employees should be given training on stress management and coping with violence.
Slippery, wet or damaged floor/stai	Falling, Tripping, Injury	Employees, Visitors, Patients	**3**	**4**	**12**	**Middle Risk**	Relevant personnel should be informed that they should use slippery floor warning

rs							signs, slippery floor tapes on the stairs should be renewed, and when necessary, the employees should report any negativities to the authorized supervisor verbally and in writing.
Sitting exercises	Musculoskeletal system disorders	Employees	**3**	**4**	**12**	**Middle Risk**	When working while sitting, breaks should be taken at regular intervals, feet and eyes should be rested, and ergonomically ideal desks and chairs should be preferred.
Front of electrical panel	Death, injury, electrocution	Employees Visitors, Patients	**3**	**4**	**12**	**Middle Risk**	Insulating material should be placed in front of all electrical panels in the building and danger warning signs should be placed on the panels.
Electrical panel leakage current relay	Death, injury Don't get electrocuted	Employees Visitors, Patients	**3**	**4**	**12**	**Middle Risk**	There should be a leakage current relay in all panels and they should be checked regularly.
Working with vehicles which have monitor	Vision loss	Employees,	**3**	**4**	**12**	**Middle Risk**	In order to prevent vision loss for emergency service personnel working in front of computers, the time spent in front of the screen should be kept short, eye exercises should be performed during breaks, and a restful second screen should be used to prevent eyes from getting tired.
Narcotic analgesic drugs	Suicide, theft, misuse	Employees Visitors, Patients	**3**	**4**	**12**	**Middle Risk**	Narcotic drugs should be kept in locked cabinets, and the key should be kept in a safe place where only the authorities can reach

							them.
Using cutting tools	Injury, infectious disease	Employees Patients	**3**	**4**	**12**	**Middle Risk**	Workers should be provided with durable gloves and protective equipment used to break medicine ampoules. Training should be given regarding the procedure to be followed in case of sharp object injuries and immunization should be repeated every 5-6 years.
Contact with medical waste	Injury, infectious diseases	Employees Visitors, Patients	**3**	**4**	**12**	**Middle Risk**	Medical waste should not be mixed with household waste, the necessary training should be given to the personnel, the personnel should be immunized, and immunization should be repeated every 5-6 years. Medical waste should be transferred to the medical waste depot at regular intervals. Quality unit employees must control waste.
Glove	Infectiou s diseases	Employees, patients	**3**	**4**	**12**	**Middle Risk**	Staff should use gloves when intervening with patients and change gloves even for different interventions on the same patient.
Oxygen tubes	Explosio n, injury, death	Employees, Visitors, Patients	**3**	**4**	**12**	**Middle Risk**	Adequate precautions should be taken to prevent oxygen cylinders from tipping over, and employees should be informed not to contaminate oxygen cylinder valves with flammable substances such as oil, diesel, gasoline, and

							not to smoke near oxygen cylinders or to approach them with fire.
Emergency observation rooms and corridor cleaning	Infectious disease, visual pollution	Employees, Visitors, Patients	**3**	**4**	**12**	**Middle Risk**	Patients and visitors should be warned not to leave food and drinks in random places in patient observation rooms, and cleaning times in the emergency room should ensure adequate hygiene.
PPE use	Injury, infectious diseases	Employees	**3**	**4**	**12**	**Middle Risk**	All employees should be trained on the use of PPE. Unit managers should control the use of PPE by all employees.
Noise caused by patients and their relatives	Distraction, headache, stress	Employees	**3**	**3**	**9**	**Middle Risk**	Noise measurement should be repeated at regular intervals with a more sensitive device, if it exceeds the lowest exposure action value (80 dB≥), noise insulation should be made and the work area should be rearranged, and ear protection equipment should be made available for use by employees.
Eemergency exit routes	Injury, Crushing, Death	Employees, Visitors, Patients	**2**	**4**	**8**	**Middle Risk**	In order to prevent rapid escapes and crowding, employees should be informed and warning signs should be placed on emergency exit routes to ensure that no materials are placed to prevent escape.
Patient lifting and carrying	Musculoskeletal system disorders	Employees, Patients	**2**	**4**	**8**	**Middle Risk**	In manual lifting and carrying operations, heavy materials should be transported with

							appropriate transport vehicles and ergonomic rules should be followed.
Drill for fire	Death, injury	Employees Visitors, Patients	**2**	**4**	**8**	**Middle Risk**	Fire drills should be conducted regularly within the periods specified in the regulation.
Electric panel sheet metal protectio n	Death, injury, electrocu tion	Employees Visitors, Patients	**2**	**4**	**8**	**Middle Risk**	Sheet metal panels should be checked at intervals deemed appropriate by the relevant technical service personnel and any deficiencies should be eliminated.
Exposed electrical sockets, switches and cables	Death, injury, electrocu tion	Employees Visitors, Patients	**2**	**4**	**8**	**Middle Risk**	All sockets and buttons in the emergency department should be checked by the relevant technical service personnel, and sockets and buttons deemed risky should be repaired.
Machiner y and devices	Incorrect result/tre atment	Employees, patients	**2**	**4**	**8**	**Middle Risk**	Specific personnel should be assigned to monitor the control calibrations of the machines and the necessary controls should not be interrupted.
Ventilati on	Depressi on, sweating, chills	Employees, Visitors, Patients	**2**	**3**	**6**	**Low Risk**	Air conditioning maintenance should be done at regular intervals for adequate ventilation.
Lighting	Headach e, eye discomfo rt, hitting objects	Employees, Visitors, Patients	**2**	**3**	**6**	**Low Risk**	Lighting should be at least 300 lux, sufficient spare parts of the LED panel fixtures that have failed or have completed their life should be kept in the warehouse and the fault should be repaired

4. CONCLUSION

Conducting risk analyzes in workplaces is important beyond compliance with the law in terms of occupational health and safety. With risk analysis, most possible risks in the workplace can be predicted, the effects of these risks can be calculated, and who or how many people may be affected by the risks can be determined. Occupational accidents that occur or are likely to occur in the workplace are largely prevented, and health problems such as illness, injury, disability and death are prevented.

In this study, the risk assessment of the emergency department of a hospital providing health services was made and the precautions to be taken for possible dangers and risks were included in the study. Since the possible risks in the study are realized with the current conditions and the equipment and methods used, the risk assessment should be repeated in case of changing equipment and working methods.

In this study, risk analysis and evaluation were carried out according to the L-type land matrix in the emergency department of a hospital. In the assessment, the hazards that may occur, the risks that these hazards will pose, and the people affected by these risks are determined. In the evaluation, the measures to be taken according to the risk score result are specified separately for each risk. According to the evaluation results, 5 high risk, 19 middle risk and 2 low risk hazard situations were identified. Since the possible risks in the study are realized with the current conditions and the equipment and methods used, the risk assessment should be repeated in case of changing equipment and working methods.

Employees should be encouraged to participate in training about the dangers they may encounter in the work environment and protection methods.

REFERENCES

Akgün, S. (2015). Sağlık sektöründe iş kazaları. Sağlık Akademisyenleri Dergisi, 2(2), 67-75.

Aksay, K., & Orhan, F. (2013). Hastanelerde İnovasyon Sürecinin Risk Yönetimi Bağlamında Değerlendirilmesi: Bir Model Önerisi. Dicle Üniversitesi İktisadi ve İdari Bilimler Fakültesi Dergisi, 2(3), 10-23.

Basmaci, G., & Özdemir, A. H. A. (2019). Sağlık hizmetlerinde risk yönetiminin çalışan güvenliğine etkisi ve bir uygulama. Journal of Academic Value Studies, 3(17), 103-118.

Buturak, G. K., & Yapıcı, N. (2022), Kamu Sağlık Kurumlarında Farklı Risk Analiz Yöntemlerinin İncelenmesi: Örnek Bir Uygulama. Çukurova Üniversitesi Mühendislik Fakültesi Dergisi, 37(3), 753-764.

Dizdar E. İş güvenliği. ABP Yayınevi & Matbaacılık, Ankara-2002. ss: 98.)

Gül, G., Bol, P., & Erbaycu, A. E. (2013), Hasta ve Çalışan Güvenliğinde Risk Yönetimi: Bir Eğitim Araştırma Hastanesi'nde Yapılan Risk Analizi ve İyileştirme. Sağlıkta Performans Ve Kalite Dergisi, 5(1), 1-16.

İncesu, E. (2019). Sağlık Hizmetlerinde Kurumsal Risk Yönetim Modeli Önerisi. Sağlıkta Kalite ve Akreditasyon Dergisi, 2(1), 47-54.

Kantarcıoğlu, H., Kantarcıoğlu, A., & Hamza, Dinç (2020). Sağlık kurumlarında iş sağlığı ve güvenliği: Kamu hastanelerinde risk değerlendirme yöntemlerine yönelik bir inceleme. Sağlık Akademisyenleri Dergisi, 7(1), 61-67.

Kırılmaz, H., Yorgun, S., & Atasoy, A. (2016). Sağlık çalışanlarında psikososyal risk faktörlerini belirlemeye yönelik bir araştırma. Uluslararası Kültürel Ve Sosyal Araştırmalar Dergisi, 2 (Special Issue 1), 66-82.

Meydanlıoğlu, A. (2013). Sağlık çalışanlarının sağlığı ve güvenliği. Balıkesir Sağlık Bilimleri Dergisi, 2(3), 192-199.

Muhammed, A. & Akbel, E. (2020). Sağlık Çalışanlarında Fiziksel Risk Etmenlerinin Değerlendirilmesi. Ohs Academy, 3(3), 230-237.

Özkılıç, Ö., 2005, İş sağlığı ve güvenliği, yönetim sistemleri ve risk değerlendirme metodolojileri, Türkiye İşveren Sendikaları Konfederasyonu, 246.

Öztaş, S., 2007, Risklerin analizi ve değerlendirilmesine farklı bir bakış, Maden İşletmelerinde İş Sağlığı ve Güvenliği Sempozyumu, Adana.

Öztürk, H., Babacan, E., & Anahar, E. Ö. (2012). Hastanede çalışan sağlık personelinin iş güvenliği. Gümüşhane Üniversitesi Sağlık Bilimleri Dergisi, 1(4), 252-268.

Saraç, C. (1998) Sosyal Sigortalar Kurumları ve İşveren Açısından İş Kazası Kavramı. Ankara: YODÇEM Yayın No:10

EXAMINATION OF SCATTING PARAMETER ON SOME ELEMENTS WITH ATOMIC NUMBERS RANGING FROM 48<Z<82

Ahmet TURŞUCU[1]

1. INTRODUCTION

The discovery of X-rays, frequently used as a non-destructive testing technique in atomic and molecular physics, was made by German physicist Wilhelm Conrad Roentgen in 1895. With this critical discovery, he was awarded the Nobel Prize in Physics in 1896. X-ray fluorescence spectroscopy, which was used as a new field of study after its discovery, has become an important research technique with different application methods in science.

In recent years, many studies on X-rays and their usage areas have become very popular and have been added to the literature by researchers. Providing non-destructive testing and allowing experiments to be carried out quickly in a laboratory environment are just a few factors that pave the way for studies on this subject. Calculations made based on the different behaviours of photons with the X-ray spectroscopy technique, which stands out as a non-destructive testing technique, are essential. The absorption, scattering, or complete recoil of X-ray photons on matter forms the basis of calculations. For this

[1] Assoc. Prof. Dr., (Şırnak University, Engineering Faculty, Electric-Electronic Engineering Dept.), ahmettursucu@sirnak.edu.tr, ORCID: 0000-0002-4963-697X.

purpose, the analysis to be made at the beginning of the experiment must be determined, and the experimental geometry must be prepared accordingly.

The interaction of radiation with a surface and the calculation of its behaviour after interaction stand out as frequently encountered problems in radiation protection studies. Here, techniques for transferring radiation between surfaces are often needed to make detailed calculations of the scattered dose. However, under certain conditions, a simplified approach based on albedo can be used quite effectively in performing these calculations. Researchers specialized in different fields have conducted critical studies on radiation's effects and protection properties using the same technique and other materials. At the same time, studies on the impact of magnetic fields on plants gave rise to investigations of the effects of radiation on biological structures.

Different studies come to the fore in the field of determination of the albedo parameter and the effects of the magnetic field on biological organisms, which come to the fore in studies made by taking advantage of the scattering feature of X-rays. Yılmaz and Akkuş have measured the albedo parameters of TLD 100, TLD 100h, TLD 200, and TLD 400 samples experimentally to determine the radiation scattering properties (Yılmaz and Akkuş 2024). Also, the effective atomic number was determined using the coherent and Compton scattering peaks in the scattering geometry. Additionally, several radiation parameters were calculated for the investigated TLD materials. Yılmaz *et al.* have conducted a current study to describe the distinctive features of thermoplastic materials with different colour centres from a gamma-ray scattering perspective. Their study determined the effective atomic number and number, energy, and dose albedo of several thermoplastic mask materials for a photon energy of 59.54 keV. Gamma-ray spectroscopy examined Rayleigh and Compton scattering peaks to determine Z_{eff} as well as number, energy, and dose albedo(Yılmaz, Kurucu, and Gürol 2023). Açıkgöz *et al.* have analyzed the effects of CeO_2 and Er_2O_3 additives on the mechanical, structural, and optical properties of B_2O_3-Na_2O-Al_2O_3 glasses. Studies of CeO_2 and Er_2O_3 doped glasses are commonly performed on borosilicate glasses, obsidian glasses, and bismuth borate glasses(Acikgoz et al. 2022).

As part of life, humans are irradiated by natural sources such as space and cosmic rays from the sun, radioactive isotopes in the earth's crust, soil and construction materials, water, and food. In addition, it receives doses due to artificial sources used in many fields, such as energy production, medicine, industry, research, agriculture, and animal husbandry. For example, as the electron structures of living cell atoms exposed to ionizing radiation change, serious illnesses, especially cancer, occur. Radiation, which causes irreparable damage to living organisms, also forms the basis of experiments to develop critical technological and medical applications. For example, radiation research techniques are used in nuclear power plants, medical diagnostic applications, and space research. Minimizing the harmful effects of radiation and investigating the impact of the magnetic field on living things constitute the basis of recent studies. Hamisu *et al.* have been measured the protective properties of polymers and composites/nanocomposites against benign radiation have been investigated. For this purpose, polymers such as polymethyl methacrylate (PMMA), polyethene and epoxy, and additives such as bismuth, boron and tungsten were also considered(Hamisu et al. 2024). Babeer et al. have examined the radiation shielding parameters on glass materials doped with different amounts of La_2O_3, NiO and BaO. In their research, they found that while an increase in the protective properties was observed with increasing rates of some additives, there was a decrease with increasing density of some additives (Babeer et al. 2024). Thakur et al. have obtained nickel-doped bismuth borate glass systems using the traditional melt-quenching method. After obtaining the materials, kinetic and trapping parameters of the glass were studied, as well as its radiation shielding efficiency through simulations using an easy-to-use Phy-X/PSD software program (Thakur et al. 2024). Unlike these essential studies, studies on the effects of the magnetic field also attract attention. Ulgen et al. have conducted experimental studies on developing plant forms to which different magnetic field intensities were applied. As a result of the experimental results, they found that the magnetic field had positive effects on plant growth (Ulgen et al. 2021; Ulgen, Birinci Yıldırım, and Uçar Turker 2017; Ülgen, Yıldırım, and Türker 2020). These and similar studies are important research reports revealing that magnetic fields at certain levels have positive effects on some living forms when the harmful effects of magnetic fields are frequently mentioned.

In this study, albedo values of some elements, which are among the radiation scattering parameters, were determined. Many parameters are used to determine the radiation protection values of materials used for armouring. Of these, the most popular recently are albedo factor parameters. It is mentioned in the plural as albedo factor parameters because it consists of 3 components. These components are represented separately as albedo number, energy, and dose. In determining the albedo factor parameters that are the subject of our study, the americium 241 radioactive isotope was used as the stimulating source, and an HPGe detector was used to detect photons scattered from the target material.

2. EXPERIMENTAL

2.1. Experimental Management

In this section, we tried to explain the scattering features of some elements with atomic numbers varying between 48<Z<82. For this purpose, we prepared an experimental setup and sample chamber that is shown in Figures 1 and 2, respectively. This setup included an HPGe semiconductor detector that collected photons scattered from the radioactive source (^{241}Am) and target material. We calculated the albedo parameters because of processing and calculating the values obtained by processing and calculating the spectra obtained by the detector.

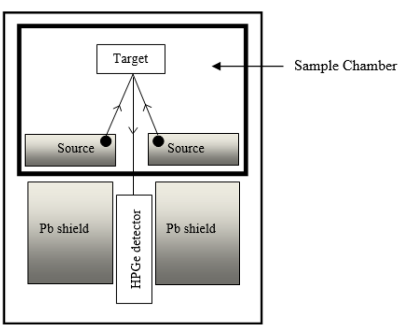

Figure 1. Experimental setup (radius of collimator is 0.53 cm).

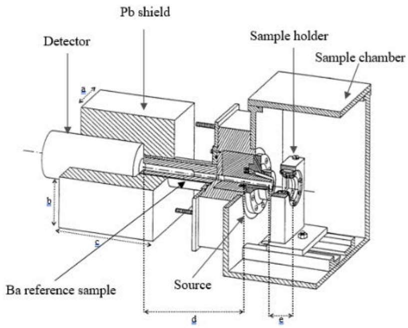

Figure 2. Sample chamber
(a=6.5 cm, b=6.3 cm, c=13.5cm, d=11 cm, e=5 cm).

While the sample chamber protects researchers from radiation effects, it minimizes the impact of unwanted scattering on the characteristic spectrum. For this purpose, the sample chamber, whose inner walls are coated with lead, has a conical structure and the feature of minimizing unwanted multiple backscattering.

2.2. Albedo Factor Calculations

This section will discuss the evaluation of the data regarding the scattering of gamma rays emitted from the source over the target sample and the calculation of albedo parameters. As mentioned before, studies were continued with an experimental setup consisting of a radioactive source and a semiconductor detector. The data obtained with this mechanism was analyzed with the computer-aided Genie-2000 program. Spectrum data taken from the Genie-2000 program were processed with the Origin 7.5 program, and area values of Compton and coherent spectra were determined.

This section will discuss the evaluation of the data regarding the scattering of gamma rays emitted from the source over the target sample and the calculation of albedo parameters. The albedo number is the first albedo parameter to be calculated with the obtained area values. The equation to be used for this purpose is presented below,

$$A_N = \left[\frac{N_{bs}/\varepsilon(E_{bs})}{(N_i/\varepsilon(E_i))(1/d\Omega)(1/2)}\right] \tag{1}$$

The terms N_{bs} and N_i used in this equation express the number of primary photons and scattered photons coming from the source. Among the terms used in the same equation, terms $\varepsilon(E_{bs})$ and $\varepsilon(E_i)$ represent the detector efficiency for backscattered and incident photons, respectively. Finally, one of the terms used in equation $(d\Omega)$ is the solid angle, defined as the angle between the center of the target material causing scattering and the collimator aperture leading to the detector.

After obtaining the albedo number with equation (1), we can calculate the albedo energy by using the value obtained from this expression with the equation given below,

$$A_E = \left[\frac{E_{bs}}{E_i}\right] A_N \tag{2}$$

In equation 2, some terms we have not explained before are used. These are the terms E_i and E_{bs}, which represent the incident and scattered photons, respectively.

The following equation is used to calculate the albedo dose, which is the last of the albedo parameters,

$$A_D = \left[\frac{\sigma_{a(E_{bs})}}{\sigma_{a(E_i)}}\right] A_E \tag{3}$$

Equation 3, unlike the others, includes the air absorption correction coefficients ($\sigma_{a(E_i)}$ *and* $\sigma_{a(E_{bs})}$) for incident and scattered photons. These values can be calculated with the help of XCOM(Gerward et al. 2001), a computer-based program. Different elements found in the air and used in calculating the air absorption coefficient are given in the table with their abundance percentages.

Table 1. Table of gaseous composition of dry air

Constituent	Chemical symbol	Mole percent
Nitrogen	N_2	78.084
Oxygen	O_2	20.947
Argon	Ar	0.934
Carbon dioxide	CO_2	0.0350
Neon	Ne	0.001818
Helium	He	0.000524
Methane	CH_4	0.00017
Krypton	Kr	0.000114
Hydrogen	H_2	0.000053
Nitrous oxide	N_2O	0.000031
Xenon	Xe	0.0000087
Ozone	O_3	0.00000001

3. RESULT AND DISCUSSION

This section discusses the calculations of the data we obtained as a result of our experimental study using the relevant equations. In general terms, it would be correct to say that we obtained values close to the data obtained in radiation shielding studies. Unlike other studies, this study used pure materials, not an alloy or compound. Therefore, as expected, an almost linear increase in shielding properties was observed with increasing atomic number (Fig.3-5). We have achieved this theoretically expected increase experimentally.

These and similar studies aimed at designing materials for radiation protection need to be spread on a broader basis to obtain more comprehensive data. In other words, the data obtained from pure materials aims to guide more extensive studies by creating alloys and compounds. The subject of our future work will be more comprehensive armoring materials created by adding different elements in different proportions.

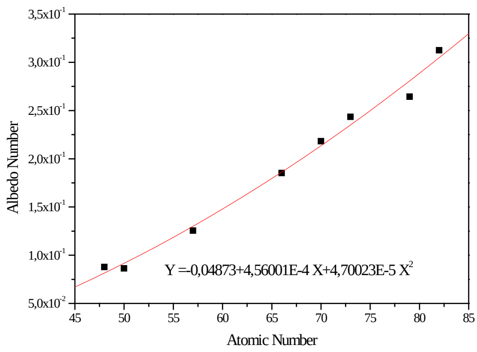

Figure-3. The albedo number distribution of target samples as a function of the atomic number.

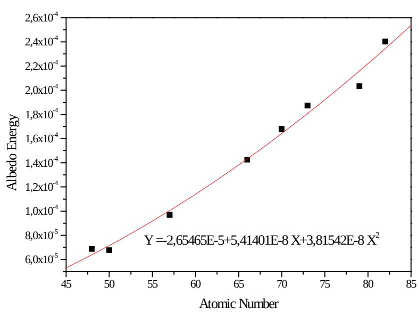

Figure-4. The albedo energy distribution of target samples as a function of the atomic number.

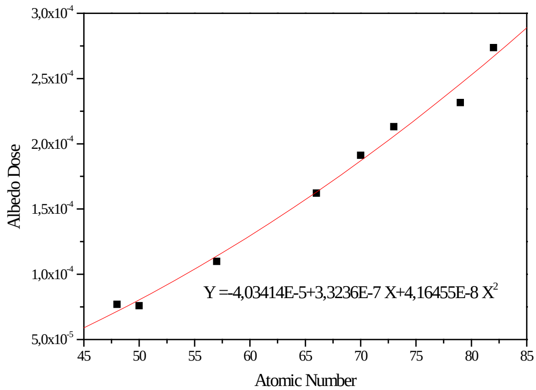

Figure-5. The albedo dose distribution of target samples as a function of the atomic number.

REFERENCES

Acikgoz, Abuzer et al. 2022. "Structural, Mechanical, Radiation Shielding Properties and Albedo Parameters of Alumina Borate Glasses: Role of CeO2 and Er2O3." *Materials Science and Engineering: B* 276.

Babeer, Afaf M. et al. 2024. "Composition Impacts of La2O3 on the Structure and Radiation Shielding Parameters of NiO–BaO–B2O3 Glasses." *Optical Materials* 147.

Gerward, L, N Guilbert, K Bj(rn Jensen, and H Levring. 2001. 60 Radiation Physics and Chemistry *X-Ray Absorption in Matter. Reengineering XCOM*. http://www.intellix.

Hamisu, Ahmad et al. 2024. "The Use of Nanomaterial Polymeric Materials as Ionizing Radiation Shields." *Radiation Physics and Chemistry* 216.

Thakur, Seema et al. 2024. "Thermo- and Photoluminescent Properties and Gamma Radiation Shielding Efficiency of NiO Doped B2O3–Bi2O3 Glass System." *Radiation Physics and Chemistry* 216: 111402.

Ulgen, C., Yıldırım, A. B., & Turker, A. U. (2017). Effect of magnetic field treatments on seed germination of melissa officinalis L. *International Journal of Secondary Metabolite*, *4*(3, Special Issue 1), 43-49.

Ulgen, C., Yildirim, A. B., Sahin, G., & Turker, A. U. (2021). Do magnetic field applications affect in vitro regeneration, growth, phenolic profiles, antioxidant potential and defense enzyme activities (SOD, CAT and PAL) in lemon balm (Melissa officinalis L.)?. *Industrial Crops and Products*, *169*, 113624.

Ulgen, C., Yıldırım, A.B. and Türker, A. U. 2020. "Enhancement of Plant Regeneration in Lemon Balm (Melissa Officinalis L.) with Different Magnetic Field Applications." *International Journal of Secondary Metabolite* 7(2): 99–108.

Ulgen, C., Yıldırım, A., & Türker, A. (2023) Melissa officinalis: Antibacterial and Antioxidant Potential, Phenolic Profile and Enzyme Activities. Kahramanmaraş Sütçü İmam Üniversitesi Tarım ve Doğa Dergisi, 26(5), 1075-1085.

Yılmaz, Demet, and Tuba Akkuş. 2024. "An Experimental Work on Radiation Scattering Features of Some Thermoluminescent Dosimetry Materials." *Radiation Physics and Chemistry* 216.

Yılmaz, Demet, Yakup Kurucu, and Ali Gürol. 2023. "Effective Atomic Numbers and Number, Energy and Dose Albedos of Different Colored Thermoplastic Materials." *Radiation Effects and Defects in Solids* 178(3–4): 325–34.

STRUCTURAL, ELECTRONIC, ELASTIC AND PHONON PROPERTIES OF CUBIC Ca_3N_2 COMPOUND STUDIED BY DENSITY FUNCTIONAL THEORY

Cihan KÜRKÇÜ[1]

1. INTRODUCTION

Metal nitride materials have attracted significant research due to their intriguing properties, such as exceptional hardness, excellent thermal conductivity, and broad bandgap. Alkaline-earth metal nitrides are being used more and more in various industries (Metselaar, 1994; Niewa & DiSalvo, 1998). They are used as a catalyst to create cubic BN, a highly hard material, and as host materials for white light emitting diodes (Bocquillon, Loriers-Susse, & Loriers, 1993; Uheda, Hirosaki, & Yamamoto, 2006; Yin et al., 2003). Pressure is a manipulable thermodynamic parameter that has the ability to not only trigger phase changes in established substances but also generate novel phases with distinct characteristics. Consequently, doing research on Ca_3N_2 under pressure would be advantageous for enhancing the material's properties.

[1] Assoc. Prof. Dr., Kırşehir Ahi Evran University, Vocational School of Technical Sciences, Department of Electronics and Automation, ckurkcu@ahievran.edu.tr, 0000-0003-3597-1950

Ca_3N_2 has a cubic lattice structure with the Ia-3 space group under normal conditions. Nevertheless, there remain unresolved disagreements regarding the high-pressure configurations of Ca_3N_2. Römer forecasted a sequential transformation of the current Ia-3 structure into the Pbcn structure, followed by the C2/m structure, and ultimately the P-3m1 structures (Römer, Schnick, & Kroll, 2009). This phase sequence adhered to the experimental study methodology that involved the integration of synchrotron X-ray diffraction and Raman spectroscopy to elucidate the phase transition. However, the expected Pbcn phase was not seen in the experimental observation (Hao et al., 2010). Following that, Zhu made a prediction about a clear and noticeable phase shift, when the current phase transformed into the Pmn21 structure (Zhu et al., 2016). The high pressure behavior of Ca_3N_2 remains uncertain. Obtaining precise structural information is essential for defining its qualities. Ca_3N_2 is commonly acknowledged to have a direct bandgap. The exact value of the gap is currently indeterminate, varying between 1.16 eV and 1.55 eV (Reckeweg, Lind, Simon, & DiSalvo, 2003; Römer et al., 2009). Nevertheless, the relatively low value of Ca_3N_2 makes it appropriate for use in solar cells. The gap value is consistently controlled by pressure to promote increased interaction. For instance, the bandgap of Mg_3N_2 has been seen to expand under pressure (Li, Fan, Dong, Jin, & He, 2014; Wu et al., 2022). Regrettably, there is a lack of studies regarding the evolutionary changes in the high pressure gap of Ca_3N_2. Additional investigation is necessary to have a deeper comprehension of the impact of pressure on the bandgap of calcium nitride.

In this study, an ab-initio study on the Pm-3m phase, which has not been studied so extensively in the literature for the Ca_3N_2 compound, was carried out by density functional theory. The structural, electronic, elastic and phonon properties of the Pm-3m phase of the Ca_3N_2 compound have been studied in detail. We believe that the results obtained will contribute to the literature and guide experimental workers.

2. CALCULATION METHOD

In this study, the structural, electronic, elastic and phonon properties of the Ca_3N_2 compound were investigated within the framework of Density Functional Theory (DFT) using the Siesta Programme (Ordejón, Artacho, & Soler, 1996). Generalized gradient approximation and Perdew-Burke-Ernzerhof (PBE) (Perdew, Burke, & Ernzerhof, 1998) parameter were used as exchange-correlation energy in the calculations. After the necessary structure optimization, the k-point values in the first Brillouin zone for Ca_3N_2 compound were determined as 12 × 12 × 12. In the calculations, 350 Ry was considered sufficient as the cut-off energy. Moreover, the convergence tolerance was fixed at 10-6 eV/atom and calculated by taking a smearing parameter value of 0.02 Ry. The KPlot program was used to obtain information about the space group, atom positions and lattice parameter values of the Pm-3m phase of the Ca_3N_2 compound (Hannemann, Hundt, Schön, & Jansen, 1998; Hundt, SchoÈn, Hannemann, & Jansen, 1999).

3. RESULTS AND DISCUSSIONS

3.1. Structural Properties

Ca_3N_2 compound used in this study, crystallizes in a cubic structure with space group Pm-3m. Initially, the experimental lattice constant value was found to start the calculations. These parameters were then varied until a minimum energy was reached. Therefore, detailed structural optimizations of the unit cell geometries were performed, minimizing the total energy. The lattice parameter value for the Pm-3m structure of Ca_3N_2 was calculated as a_0=4.701 Å and this value was used where relevant in the study. In the Pm-3m structure of Ca_3N_2, Ca atoms are located at 3c (0, 1/2, 1/2) Wyckoff positions while N atoms are located at 1a (0, 0, 0) and 1b (1/2, 1/2, 1/2) Wyckoff positions. In Table I, structural properties such as lattice constant value and volume value calculated for Ca_3N_2 are given. An image of the Pm-3m crystal structure of Ca_3N_2 is given in Figure 1.

Table 1. The calculated lattice parameters and volume value of Ca_3N_2 compound.

	References	$\boldsymbol{a_0}$ **(Å)**	**V(Å^3)**
Ca_3N_2	This Study	4.701	103.889

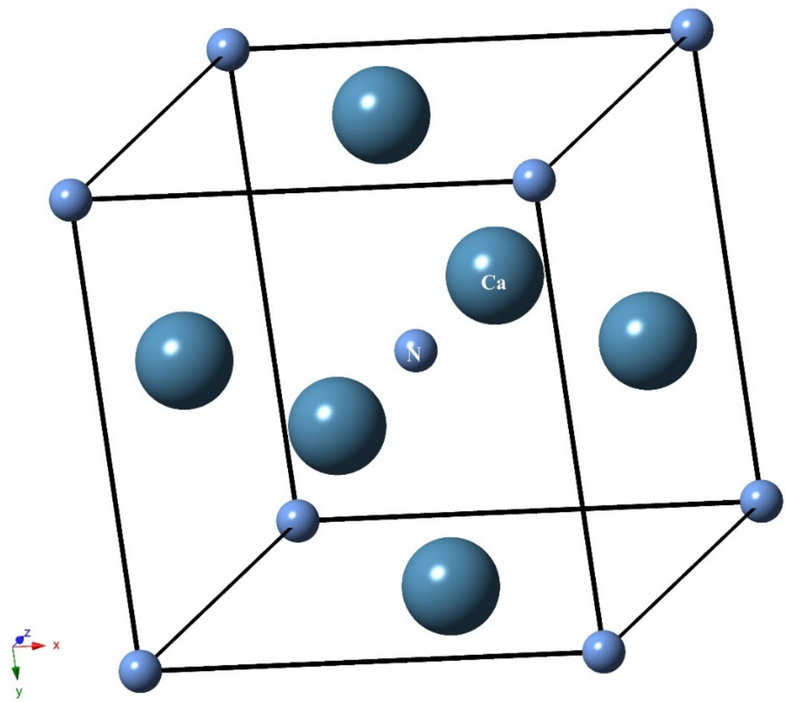

Figure 1: Crystal Structure of Pm-3m Phase of Ca_3N_2 compound.

3.2. Electronic Properties

Electronic band structure and density of state calculations were performed for the cubic Pm-3m type crystal structure of Ca_3N_2 and are given in Figures 2. The Fermi Energy (EF) level was set to 0 eV in all electronic structure calculations. The Fermi Energy level is indicated by the red dashed line. The bands below the Fermi energy level are called valence bands. Above the Fermi energy level are the conduction bands. If there is a gap between the point where the valence band is closest to the Fermi energy level, i.e. the point where the valence band is maximum, and the point where the conduction band is closest to the Fermi energy level, i.e. the point where the conduction band is minimum, it is said that the material is a semiconductor and insulator. If this band gap value is less than about 3.5 eV, the material is a semiconductor, otherwise it is an insulator. If the material is a semiconductor, then we can talk about two different properties. If the maximum of the valence band and the minimum of the conduction band are on the same symmetry point, then the material is called a direct bandpass semiconductor. If the maximum of the valence band and the minimum of the conduction band are not located at the same symmetry point, then the material is called an indirect bandpass semiconductor.

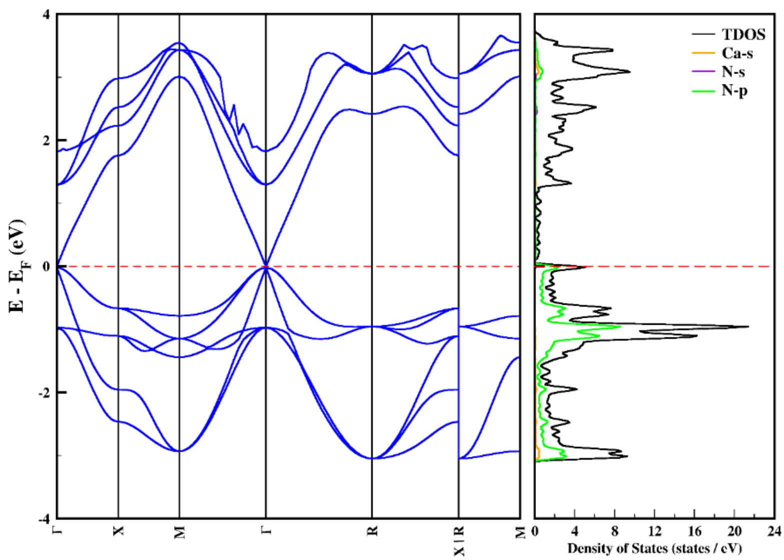

Figure 2. Electronic Band Structure of the Pm-3m Phase of Ca_3N_2 compound.

Another situation is that the material has metallic properties. If some of the valence bands and conduction bands overlap and cut each other at the Fermi energy level, then we can say that the material has metallic character. As seen in Figure 2, the bands are crossed at the Fermi Energy level. There is no band gap. In this case, Ca_3N_2 compound has metallic character in the Pm-3m phase. In order to have more detailed information about the electronic nature of the material, the total and partial density of states were calculated in the next step and given in Figure 2. As can be seen from Figure 2, the Fermi Energy level is set to 0 eV and is indicated by a red dash line. As in the electronic band structure graph, the Fermi energy level is interrupted by bands. Thus, it is once again understood that the material has a metallic base. If we also examine the contribution from the orbitals, it is clear that the largest contribution above and below the Fermi Energy level comes from the N-p state.

3.3. Elastic Properties

The second-order independent elastic constant values (C_{ij}), which provide information about the mechanical stability and stiffness of the material, were calculated for the cubic Pm-3m type structure of Ca_3N_2 compound. The ability of a material to resist applied pressure is determined by its elastic constants, which are very important physical parameters in determining structural stability. Elastic properties also provide information about physical properties such as atomic bonding, hardness, ductility, brittleness and mechanical stability. For cubic structures there are three different independent values of elastic constants (C_{11}, C_{12} and C_{44}). In addition, Born stability criteria for cubic structures (Born, 1940), which help us to decide whether the material is mechanically stable or not, are as follows:

$$C_{11} > 0, C_{44} > 0, C_{11} > |C_{12}|, (C_{11} + 2C_{12}) > 0 \quad (1)$$

When the elastic constant values we obtained are substituted into the above equation, the cubic Pm-3m type structure of Ca_3N_2 compound is mechanically stable since all conditions are met. The elastic constant values obtained as a result of the calculations are given in Table 2 and other elastic quantities that give us information about the hardness of the materials are given in Table 3.

Table 2. The calculated Elastic Constant values for the Cubic Pm-3m Type Structure of Ca_3N_2 compound.

Phase	**C_{11} (GPa)**	**C_{12} (GPa)**	**C_{44} (GPa)**
Pm-3m	161.396	11.669	36.815

Table 3. The calculated Bulk Modulus (B), Shear Modulus (G), B/G Ratio, Young's Modulus (E) and Poisson's Ratio (ν) values for the Cubic Pm-3m Type Structure of Ca_3N_2 compound.

Phase	**B (GPa)**	**G (GPa)**	**B/G**	**E (GPa)**	**ν**
Pm-3m	61.578	49.122	1.254	116.411	0.185

The data were computed utilizing values for second order elastic constants. The Bulk Modulus (B), which represents the resistance to volume change under pressure, was computed using the second order elastic constant values. Subsequently, the Shear Modulus (G) was computed by utilizing elastic constant values, representing the resistance to deformation under the influence of pressure. G is a crucial factor in determining the hardness measurement. Hardness, in turn, quantifies a material's ability to withstand the force applied by another substance on its surface.

The cubic Pm-3m type structure of the Ca_3N_2 compound was analyzed to determine the values of the bulk modulus (B) and shear modulus (G). These calculations provide insights into the material's brittleness and ductility. A material is considered ductile if its B/G ratio exceeds 1.75, whereas it is considered brittle if the ratio is below. Pugh (Pugh, 1954) defined this ratio and set the limit value at 1.75. Upon examining the data shown in Table 3, it is evident that the B/G ratio for the cubic Pm-3m type structure of the Ca_3N_2 compound is less than 1.75. Consequently, the substance exhibits brittleness throughout this stage. Equation 2 was used to obtain the Poisson's ratio (v) for the cubic Pm-3m type structure of the Ca_3N_2 compound.

$$\nu = [(3B - E)/6B] \tag{2}$$

The higher the Poisson's ratio, the higher the plasticity of the materials. The Poisson's ratio is around 0.1 for covalent materials and 0.25 for ionic materials. The Poisson value calculated for the cubic Pm-3m type structure of Ca_3N_2 compound is 0.185. This value is closer to 0.25. Therefore, in the cubic Pm-3m type structure of Ca_3N_2 compound, the atoms are connected to each other by ionic bonds.

The final measure, Young's Modulus (E), represents the material's level of hardness. The Young's Modulus is determined from the Bulk Modulus and Poisson's ratio, and it represents the ratio of stress to strain when a material is subjected to a tensile or compressive force.

3.4. Phonon Properties

The phonon dispersion calculation, which provides information about the dynamic stability of the materials, was he-scoped along the high symmetry directions using a 2x2x2 supercell and is given in Figure 3.

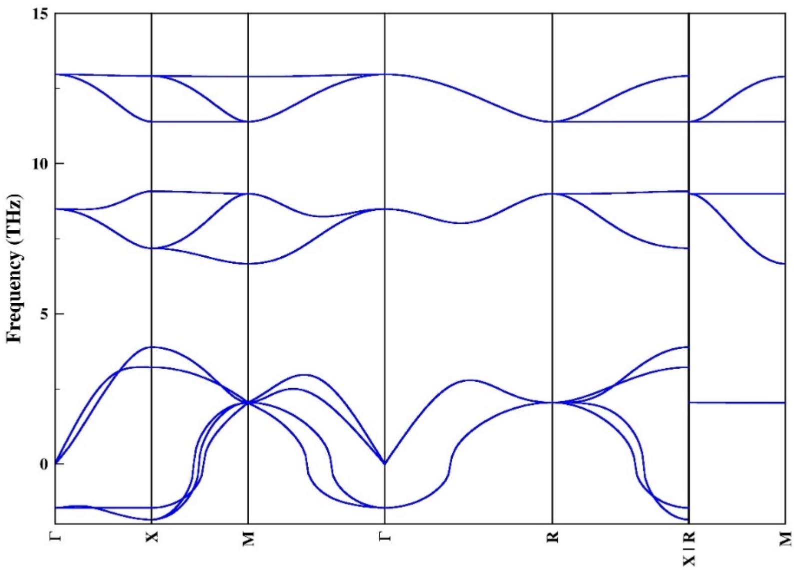

Figure 3: Phonon dispersion curve for the cubic Pm-3m type structure of Ca_3N_2 compound.

Ca_3N_2 compound has 5 atoms per unit cell in the Pm-3m phase. The total number of phonon branches in the material is calculated by multiplying the number of atoms in the unit cell by the number of degrees of freedom of each atom. Since each atom can oscillate in 3 axes (x,y,z), the total number of phonon branches is 15. Of these branches, there are as many Acoustic Phonon branches as the number of degrees of freedom (3). The remaining 12 are Optical Phonon branches. The energy of optical phonons is higher than the energy of acoustic phonons.

As can be seen from Figure 3, not all phonon branches are positive. There are negative phonon branches. Since not all phonon branches are positive, Ca_3N_2 compound is dynamically unstable in the Pm-3m phase.

4. CONCLUSION

In this study, the structural, electronic and elastic properties of the cubic Pm-3m type structure of Ca_3N_2 were investigated using density functional theory. The lattice constant value for the Pm-3m type structure of Ca_3N_2 was calculated as a_0=4.701 Å and found to be in good agreement with other results. In addition, the electronic band structure and density of state curves were calculated for the Pm-3m type structure of Ca_3N_2 and it was observed that this structure has a metallic character. On the other hand, elastic constant calculations were made for the Pm-3m type structure of Ca_3N_2. From the data obtained, it was concluded that Ca_3N_2 with Pm-3m phase is mechanically stable. From the elastic constant values, values for Bulk, Young's and Shear modulus and Poisson's ratio were also calculated. According to the Bulk modulus and Shear modulus calculations, which give information about the hardness of the material, the material is brittle and according to the Poisson's ratio, it is seen that the atoms forming Ca_3N_2 are connected to each other by ionic bonds. Phonon calculations were also performed to obtain information about the dynamic stability of the Ca_3N_2 compound.

It was concluded that Ca_3N_2 is dynamically unstable because it has a negative branch in the Pm-3m phase.

REFERENCES

Bocquillon, G., Loriers-Susse, C., & Loriers, J. (1993). Synthesis of cubic boron nitride using Mg and pure or M′-doped Li 3 N, Ca 3 N 2 and Mg 3 N 2 with M′= Al, B, Si, Ti. *Journal of materials science, 28*, 3547-3556.

Born, M. (1940). *On the stability of crystal lattices. I.* Paper presented at the Mathematical Proceedings of the Cambridge Philosophical Society.

Hannemann, A., Hundt, R., Schön, J., & Jansen, M. (1998). A new algorithm for space-group determination. *Journal of applied crystallography, 31*(6), 922-928.

Hao, J., Li, Y., Wang, J., Ma, C., Huang, L., Liu, R., . . . Li, X. (2010). Experimental determinations of the high-pressure crystal structures of Ca3N2. *The journal of physical chemistry C, 114*(39), 16750-16755.

Hundt, R., SchoÈn, J. C., Hannemann, A., & Jansen, M. (1999). Determination of symmetries and idealized cell parameters for simulated structures. *Journal of applied crystallography, 32*(3), 413-416.

Li, J., Fan, C., Dong, X., Jin, Y., & He, J. (2014). Theoretical investigation of the high-pressure structure, phase transition, and mechanical and electronic properties of

Mg3N2. *The journal of physical chemistry C, 118*(19), 10238-10247.

Metselaar, R. (1994). Progress in the chemistry of ternary and quaternary nitrides. *Pure and applied chemistry, 66*(9), 1815-1822.

Niewa, R., & DiSalvo, F. (1998). Recent developments in nitride chemistry. *Chemistry of materials, 10*(10), 2733-2752.

Ordejón, P., Artacho, E., & Soler, J. M. (1996). Self-consistent order-N density-functional calculations for very large systems. *Physical review B, 53*(16), R10441.

Perdew, J. P., Burke, K., & Ernzerhof, M. (1998). Perdew, burke, and ernzerhof reply. *Physical Review Letters, 80*(4), 891.

Pugh, S. (1954). XCII. Relations between the elastic moduli and the plastic properties of polycrystalline pure metals. *The London, Edinburgh, and Dublin Philosophical Magazine and Journal of Science, 45*(367), 823-843.

Reckeweg, O., Lind, C., Simon, A., & DiSalvo, F. J. (2003). Rietveld refinement of the crystal structure of α-Be3N2 and the experimental determination of optical band gaps for Mg3N2, Ca3N2 and CaMg2N2. *Zeitschrift für Naturforschung B, 58*(1), 159-162.

Rö̈mer, S. R., Schnick, W., & Kroll, P. (2009). Density functional study of calcium nitride: refined geometries and prediction of high-pressure phases. *The journal of physical chemistry C, 113*(7), 2943-2949.

Uheda, K., Hirosaki, N., & Yamamoto, H. (2006). Host lattice materials in the system Ca3N2–AlN–Si3N4 for white light emitting diode. *physica status solidi (a), 203*(11), 2712-2717.

Wu, G., Wang, L., Bao, K., Li, X., Wang, S., & Xu, C. (2022). Bandgap evolution of Mg3N2 under pressure: Experimental and theoretical studies. *Chinese Physics B, 31*(6), 066205.

Yin, L. W., Li, M. S., Liu, Y. X., Xu, B., Sui, J. L., & Qi, Y. X. (2003). Novel route to cubic boron nitride dendritic nanostructures under electron beam irradiation. *Advanced Materials, 15*(9), 720-723.

Zhu, S., Peng, F., Liu, H., Majumdar, A., Gao, T., & Yao, Y. (2016). Stable calcium nitrides at ambient and high pressures. *Inorganic Chemistry, 55*(15), 7550-7555.

IMAGE PROCESSING METHODS

Mehmet GÜL[1]

1. INTRODUCTION

Image processing applications, which are used in various areas today, are extremely vital in the studies used. Many different methods are used to carry out image processing applications. Image processing applications are particularly useful in the defense industry, medical science, industrial applications, agricultural applications, traffic, and many other fields. It is a fact that it plays an important role in defense industry applications such as enemy target monitoring, specific mission specifications, and the destruction of crucial targets. Image processing applications help medical doctors diagnose diseases with increasing success rates. Tracking and monitoring the production process in industrial areas, product packaging, sorting out faulty products, etc. Image processing is especially applied in agricultural applications when spraying open land; only weeds are identified, and less pesticide is applied; crop harvesting is done in greenhouses or open agricultural areas, etc. It appears in applications such as traffic, particularly license plate identification, face recognition, etc. This section will give

[1] Assist. Prof. Dr., Şırnak University, Faculty of Engineering, Computer Engineering, Şırnak-Türkiye, 73100, email: mgul@sirnak.edu.tr; mehmetgul@ymail.com ; ORCID: 0000-0002-4819-4743

information about some effective methods used in medical image processing studies.

2. IMAGE PROCESSING IN MEDICINE

It is an undeniable fact that medical images are extremely important in disease diagnosis. Medical images include X-ray, computer tomography (CT), magnetic resonance imaging (MRI), positron emission tomography (PET), and microscopic imaging (MI). Determining the disease diagnosis on the image is an example of medical image processing application studies. Particularly useful information is gathered during the diagnosis of the malignant area. The most important advantage of the implemented applications can be shown as saving time and minimizing the margin of error (Apsari et al., 2021). Determining the 3D brain tumor area on multiple and serial images is a process that takes weeks to be performed by a radiologist; this can be done in minutes by using image processing methods. On the other hand, considering the experience of the radiologist examining the image, extremely sensitive work is carried out with image processing methods in such a vital study, where the risk of error is exceedingly high.

2.1. Convolutional Neural Network

There has been a significant increase in convolutional neural network (CNN) based studies recently. It serves as the foundation for many investigations, particularly in the field of deep learning (DL). Among the main applications developed based on CNN, applications such as image enhancement, face and gesture recognition, self-service supermarkets, and smart health device development can be listed. CNN is basically inspired by the Artificial Neural Network (ANN) method. ANN is a central nervous system-inspired system. ANN is made up of computing nodes called neurons that are linked together (Figure 1). The final output is obtained by optimizing the connected nodes. In the multidimensional ANN method, the network system, also defined as the hidden layer, takes place immediately after the input layer. Each hidden-layer network makes decisions based on the previous layer. Structurally, it consists of a layer chain consisting of multiple layers stacked on top of each other.

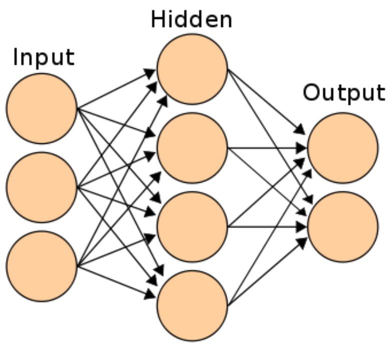

Figure 1: The ANN architecture (https://www.analyticsvidhya.com/blog/2014/10/ann-work-simplified/, n.d.)

CNN learning is accomplished through self-optimizing neurons. This approach itself is also incorporated into the ANN algorithm. The most significant difference between the CNN and the ANN is that the CNN is largely utilized in the field of pattern recognition on images. It is particularly possible to encode the unique properties of each image and to make the network more suitable for image-oriented tasks by further reducing the parameters required for these operations. This is because image processing using ANN-based models struggles with the computational complexity required to calculate image data.

As a result, when the CNN architecture is examined in detail, it can be said that it is basically similar to the LeNet-5 multilayer neural network method (Lecun et al., 1998). Until 2006, the difficulties encountered in training CNN models could not be entirely resolved (Karen Simonyan & Andrew Zisserman, 2014; Niu & Suen, 2012; Olga Russakovsky et al., 2014a). The study (Olga Russakovsky et al., 2014b) was the most striking study carried out. In the study, AlexNet architecture, which forms the path of modern CNN architecture to some extent, was introduced. Although AlexNet architecture is basically similar to LeNet architecture, the main distinction is that it has a more complex structure. This situation represents a tipping point in terms of the ability of CNN architectures to increase their performance. The VGGNet (Karen Simonyan & Andrew Zisserman, 2014), GoogleNet (Christian Szegedy et al., 2014), and ResNet (Kaiming He et al., 2015a) methods are a few examples of performance improvement. The most important feature of these exemplary methods is that they have deep network structures. ResNet architecture, for example, has a 20-times deeper structure than AlexNet architecture but only an 8-times deeper structure than VGGNet architecture.

2.2. MobileNet

MobileNet is an open-source CNN-based method first developed by Google to rub on mobile devices. The ley layer utilized to minimize the number of features is a profoundly separable convolution architecture. Its CNN-based network structure has a depth-separable convolutional network model that significantly reduces the number of parameters compared to other networks with the same depth in its CNN-based network structure. This method has a structure that includes profoundly separable folds, in-depth folds, and point folds with two core layers (Figure 2).

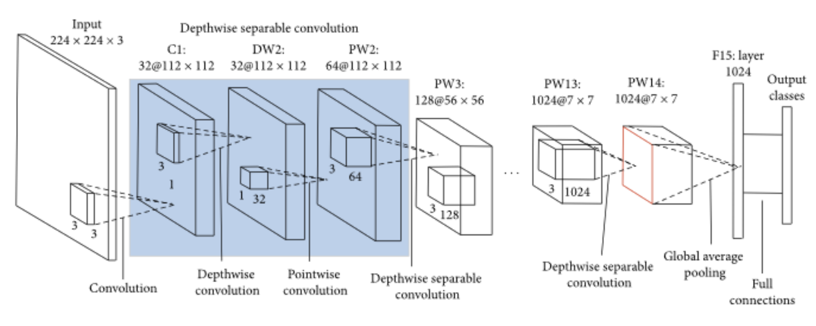

Figure 2: The MobileNet architecture
(https://wikidocs.net/165429, n.d.)

Deep convolution is the stage used to filter the input without creating new features. As a result, new features known as point convolutions are formed. The final stage defines the combination of two layers as depth-separable convolution. For each convolution utilized in the model, batch normalization (BN) and a rectified linear unit (ReLU) are used. The MobileNet method includes approximately four million parameters, which is extremely small compared to other models.

2.3. MobileNetV2

The MobileNetV2 method is a variation of the MobileNet method and was also developed by Google. It is a CNN-based method used to improve the performance of mobile devices, like the MobileNet method. The architecture of the MobileNetV2 method consists of 32 convolution layers and 19 bottleneck layers. The MobileNetV2 architecture is shown in Figure 3. The MobileNetV2 method uses the Depthwise Separable Convolutions (DSC) technique for portability. When depth convolution and point convolution techniques are combined, the total number of parameters and computational costs decrease. The MobileNetV2 method overcomes the problem of losing information in non-linear layers in convolution blocks by using linear bottlenecks as well as the DSC technique. In this way, while the compiled information is protected, a new structure called inverted residuals is also presented (Mark Sandler et al., 2018).

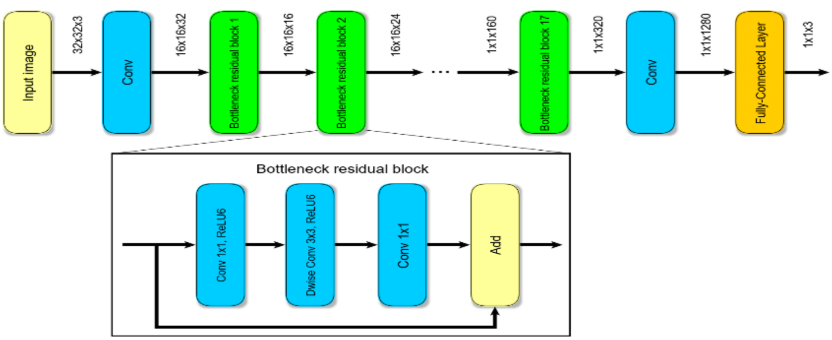

Figure 3: The architecture of MobileNetV2 (Seidaliyeva et al., 2020)

2.4. U-Net

Among neural network architectures, the U-Net architecture is the leading segmentation method that has recently demonstrated high performance. The U-Net model uses two main strategies to perform extremely fast and precise segmentation. The most basic approach of the U-Net method focuses on making more precise segmentation by working with fewer training images. The first of the two fundamental arms serves as the encoder, while the other serves as the decoder (Figure 4). As can be understood, the shape of U-Net takes its name from the shape of the model created. It consists of two consecutive 3x3 convolution structures consisting of a ReLU activation layer and a maximum pooling layer, where each block is repeated several times to ensure that information is learned during the development of the network.

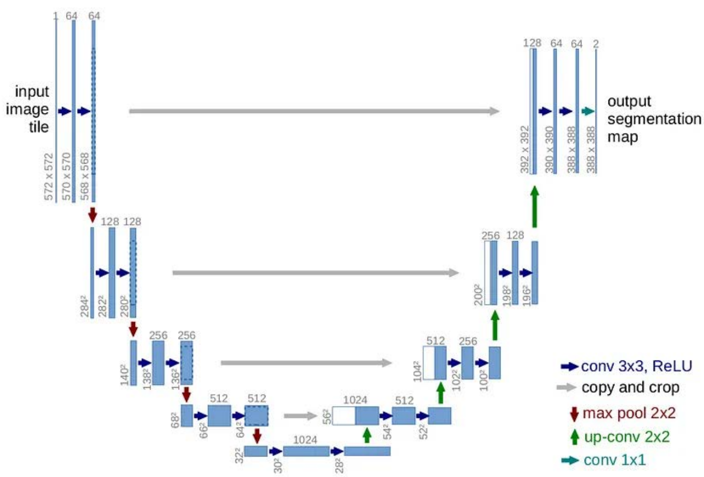

Figure 4: The U-Net architecture (https://towardsdatascience.com/unet-line-by-line-explanation-9b191c76baf5, n.d.)

In the created U-structure model, the feature map of the layer corresponding to the narrowing process is trimmed, and thus merging is performed on the upsampled feature map. In the final stage, a 1x1 convolution layer is applied to reduce the number of feature maps necessary and generate the segmented image. During the processing, phase-edge pixels with the least amount of contextual information should be discarded. The biggest innovation of this model, in which the feature map is up-sampled using 2x2 up-convolution at each stage, is the most significant novelty of this model, which was originally described in the literature in 2015 (Siddique et al., 2021).

2.5. U-NET++

The U-Net++ method is a high-performance method that is extremely effective, especially in medical images, based on the semantic segmentation architecture developed based on U-Net. The U-Net++ method has a versatile image segmentation architecture specifically designed to improve image segmentation (Jonathan Long et al., 2014). It uses the same encoder-decoder architecture as the U-Net architecture. Dense block and convolution layers between the encoder and decoder are included in the revised assignment paths in the U-Net++ method architecture. Thanks to internal layers, image segmentation accuracy is increased. When compared to the U-Net approach, highly high-performance results are obtained in medical images incorporating electron microscopes (EM), cells, nuclei, brain tumors, and liver and lung nodules (Zhou et al., 2018). The most important feature of the U-Net++ method that distinguishes it from the U-Net method is that it has a structure that allows the use of redesigned bypass paths and deep control that connects two subnets, as shown in Figure 5.

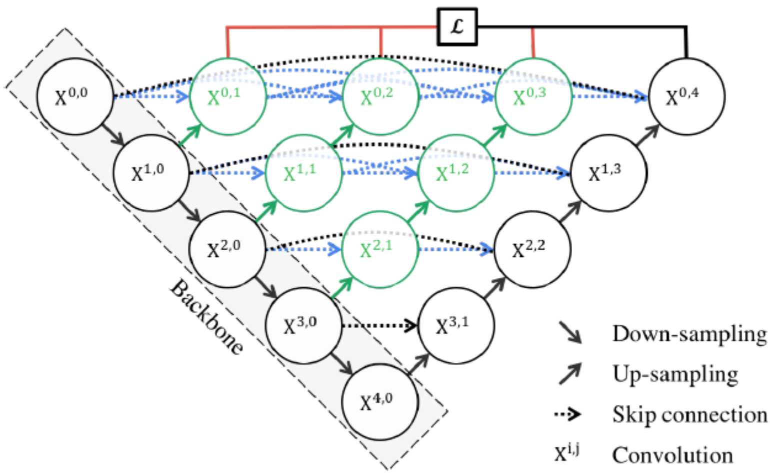

Figure 5: The U-Net++ architecture (https://sh-tsang.medium.com/review-unet-a-nested-u-net-architecture-biomedical-image-segmentation-57be56859b20, n.d.)

2.6. U-NET3+

The U-Net3+ method is another method with an encoder-decoder architecture derived from the U-Net method, like the U-Net++ method (Huimin Huang et al., 2020). To reduce the semantic gap of the U-Net++ method, its efficiency was boosted by omitting the layered network structure's connections. As the coding layer increases, the spatial information of the feature map reduces. This occurs by using the remaining spatial information from the feature map at a lower level. To solve these problems, the U-Net3+ method was developed, and the loss of spatial information obtained through interconnection and interconnection paths was minimized. In this way, when all previous feature maps are used via interconnectivity, computing costs are lowered compared to U-Net++, and learning is more effective. As with the U-Net++ method, high-performance semantic segmentation results must be produced through extensive inspection of network products in the U-Net3+ method (Figure 6).

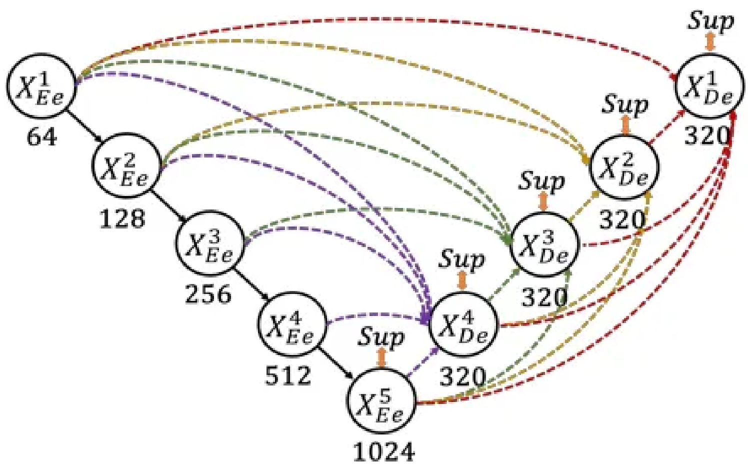

Figure 6: The U-Net3+ architecture (Huimin Huang et al., 2020)

2.7. Inception-ResNet-V2

Inception-ResNet-V2 is a hybrid model consisting of residual connections and a recent version of the Inception architecture (Christian Szegedy et al., 2015; Kaiming He et al., 2015b). This method is architecturally built on the Residual Inception Block. The dimensionality of the filter bank is scaled before insertion to accommodate the input depth, and the 1x1 convolution filter expansion layer is used after this scaling. This architectural structure creates BN only valid on traditional layers. In terms of architecture, Inception-ResNet-V2 has a depth of 164 layers and an image input of 299x299 pixels. These blocks consist of Input, Stem, 10xInception-ResNet-A, Reduction-A, 20xInception-ResNet-B, 10xInception-ResNet-C, Average Pooling, Dropout, and Softmax blocks, respectively. The residual Inception Block architecturally contains multidimensional convolutional filters containing residual connections. Using residual connections eliminates corruption issues, particularly in deep networks, and also reduces training time. The architecture of Inception-ResNet-V2 is shown Figure 7.

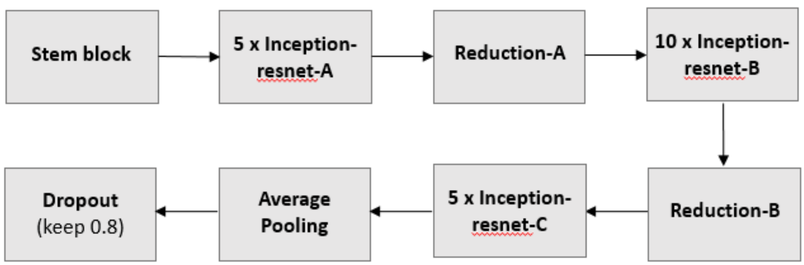

Figure 7: The Inception-ResNet-V2 architecture (Christian Szegedy et al., 2015)

2.8. Local Binary Patterns

The Local Binary Patterns (LBP) method is basically based on questioning the relationship between the central pixel in any 3x3 pixel segment selected on the image and the neighboring pixels around it (Figure 8) (Kaplan et al., 2020).

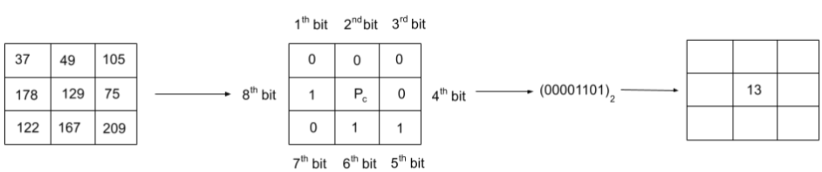

Figure 8: Architecture of basic Local Binary Patterns method

In the query phase, the relationship between the pixel in question and the center pixel is questioned based on the following formula;

$$LBP_{P,R} = \sum_{i=0}^{P-1} s(g_i - g_c)2^i, \qquad s(x) = \begin{cases} 1 & x \geq 0 \\ 0 & x < 0 \end{cases} \quad (1)$$

When the query performed, an 8-digit base 2 number is obtained. The decimal equivalent of the resulting number is assigned as the new value of the center pixel. This operation is applied to all pixels of the image and a new image is obtained. The desired feature query can be performed with the new image obtained using the LBP method. Figure 9 shows the evaluation result of the brain tumor image with the classical LBP method.

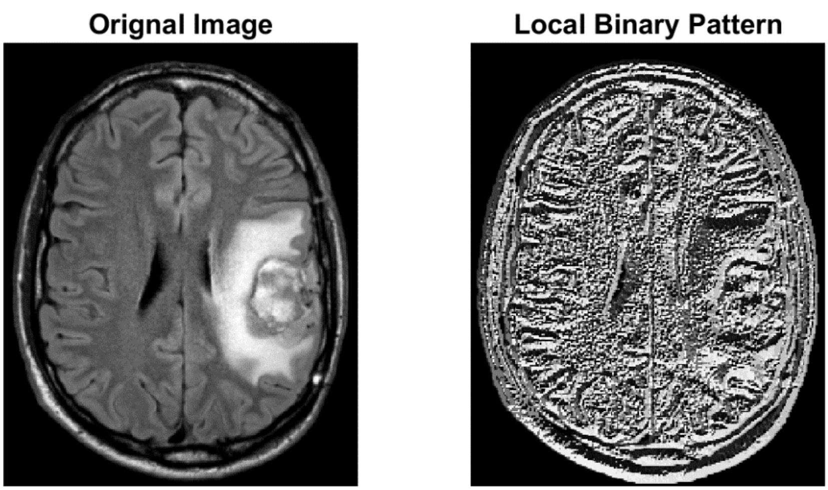

Figure 9: Image obtained by classic LBP method

Since the LBP method is a powerful method that gives extremely effective results, many derivative methods are being developed based on the classical LBP method.

2.9. Step-Local Binary Patterns

In the Step-LBP method (n-LBP) approach, which was developed as an alternative to the classical LBP method, the surrounding pixels in the 3x3 pixel segment are compared with neighboring pixels, not with the center pixel (Kaplan et al., 2020). The n-LBP method employs the following formula:

$$S(P_i > P_j) = \begin{cases} 1 & if \quad P_i > P_j \\ 0 & \quad\quad P_i \le P_j \end{cases} \tag{2}$$

Because the LBP method is a powerful method that produces exceptionally successful outcomes, various derivative methods based on the classical LBP method are being developed.

In the n-LBP method, the number of steps varies between 1-4 (Figure 10).

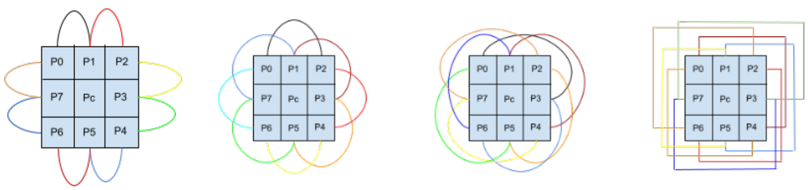

Figure 10: The architecture of n-LBP method

The comparison process of 8 neighboring pixels around the center pixel when the step number is 1;

$P_c = \mathrm{S}(P_0 > P_1), \mathrm{S}(P_1 > P_2), \mathrm{S}(P_2 > P_3), \mathrm{S}(P_3 > P_4), \mathrm{S}(P_4 > P_5), \mathrm{S}(P_5 > P_6), \mathrm{S}(P_6 > P_7), \mathrm{S}(P_7 > P_0)$

If the number of steps is 2;

$P_c = \mathrm{S}(P_0 > P_2), \mathrm{S}(P_1 > P_3), \mathrm{S}(P_2 > P_4), \mathrm{S}(P_3 > P_5), \mathrm{S}(P_4 > P_6), \mathrm{S}(P_5 > P_7), \mathrm{S}(P_6 > P_0), \mathrm{S}(P_7 > P_1)$

If the number of steps is 3;

P_c = S(P_0 > P_3), S(P_1 > P_4), S(P_2 > P_5), S(P_3 > P_6), S(P_4 > P_7), S(P_5 > P_0), S(P_6 > P_1), S(P_7 > P_2)

If the number of steps is 4;

P_c = S(P_0 > P_4), S(P_1 > P_5), S(P_2 > P_6), S(P_3 > P_7), S(P_4 > P_0), S(P_5 > P_1), S(P_6 > P_2), S(P_7 > P_3)

Figure 11 shows four different results of the brain tumor image obtained between step numbers 1-4.

Figure 11: Images obtained by Step-LBP (A: Cancer Image, B: n=1, C: n=2, D: n=3, E: n=4)

2.10. Angle-Local Binary Patterns

Angle-LBP (αLBP) method is a method derived from the classical LBP method (Kaplan et al., 2020). The following formula is valid for the αLBP method;

$$\alpha LBP = \sum_{i=0}^{P} u(P_i - P_c)2^t \quad (3)$$

In the αLBP method, the basic principle is that the relationship of eight pixels located on the angle values determined as 0, 45, 90, 135 degrees with the center pixel is questioned (Figure 12).

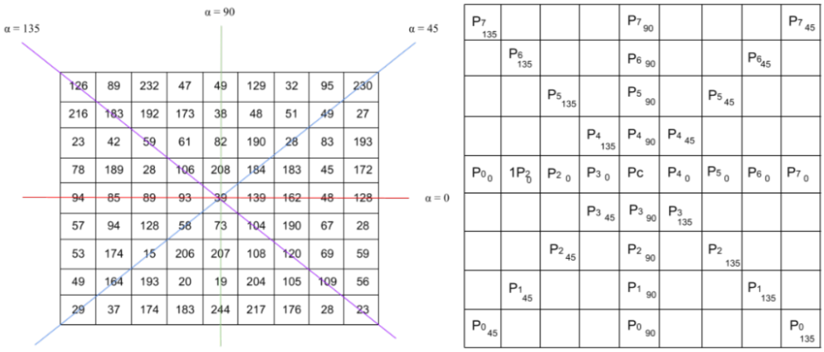

Figure 12: The architecture of αLBP method

Depending on the change in angle value, the obtained patterns change. In case α = 0;

$P_c = S(P_{0_0} > P_c), S(P_{1_0} > P_c), S(P_{2_0} > P_c), S(P_{3_0} > P_c), S(P_{4_0} > P_c), S(P_{5_0} > P_c), S(P_{6_0} > P_c), S(P_{7_0} > P_c)$

In case α = 45;

$P_c = S(P_{0_{45}} > P_c), S(P_{1_{45}} > P_c), S(P_{2_{45}} > P_c), S(P_{3_{45}} > P_c), S(P_{4_{45}} > P_c), S(P_{5_{45}} > P_c), S(P_{6_{45}} > P_c), S(P_{7_{45}} > P_c)$

In case α = 90;

$P_c = S(P_{0_{90}} > P_c), S(P_{1_{90}} > P_c), S(P_{2_{90}} > P_c), S(P_{3_{90}} > P_c), S(P_{4_{90}} > P_c), S(P_{5_{90}} > P_c), S(P_{6_{90}} > P_c), S(P_{7_{90}} > P_c)$

In case α = 135;

$P_c = S(P_{0_{135}} > P_c), S(P_{1_{135}} > P_c), S(P_{2_{135}} > P_c), S(P_{3_{135}} > P_c), S(P_{4_{135}} > P_c), S(P_{5_{135}} > P_c), S(P_{6_{135}} > P_c), S(P_{7_{135}} > P_c)$

Brain tumor image obtained depending on the angle values of the αLBP method is shown in Figure 13.

Figure 13: Images obtained by Angle-LBP (A: Cancer Image, B: angle=0, C: angle=45, D: angle=90, E: angle=135)

3. CONCLUSION

Image processing methods are becoming more diverse and this diversity is particularly visible in deep learning and artificial intelligence applications. In this section, information was given about some of the most commonly used successful methods, particularly in deep learning and artificial intelligence applications. Specifically, the defense industry, disease detection using medical image analysis, agricultural applications, and etc. are such applications that are just a few examples of ongoing research in this topic. Depending on where they are used, each of them produces incredibly beneficial results. Within the scope of this study, information was provided regarding various successful methods used, particularly in the diagnosis of medical diseases. This study is expected to give a road map for researchers interested in using image enhancement technologies in deep learning applications.

REFERENCE

Apsari, R., Aditya, Y. N., Purwanti, E., & Arof, H. (2021). *Development of lung cancer classification system for computed tomography images using artificial neural network*. 050013. https://doi.org/10.1063/5.0042195

Christian Szegedy, Vincent Vanhoucke, Sergey Ioffe, Jonathon Shlens, & Zbigniew Wojna. (2015). Rethinking the inception architecture for computer vision. *Computer Vision and Pattern Recognition*.

Christian Szegedy, Wei Liu, Yangqing Jia, Pierre Sermanet, Scott Reed, Dragomir Anguelov, Dumitru Erhan, Vincent Vanhoucke, & Andrew Rabinovich. (2014). Going Deeper with Convolutions. *Computer Vision and Pattern Recognition*.

https://sh-tsang.medium.com/review-unet-a-nested-u-net-architecture-biomedical-image-segmentation-57be56859b20. (n.d.). *Review: UNet++ — A Nested U-Net Architecture (Biomedical Image Segmentation)*.

https://towardsdatascience.com/unet-line-by-line-explanation-9b191c76baf5. (n.d.). *UNet — Line by Line Explanation*.

https://wikidocs.net/165429. (n.d.). *K_04 Understanding of MobileNet - EN*.

https://www.analyticsvidhya.com/blog/2014/10/ann-work-simplified/. (n.d.). *ANN method*.

Huimin Huang, Lanfen Lin, Ruofeng Tong, Hongjie Hu, Qiaowei Zhang, Yutaro Iwamoto, Xianhua Han, Yen-Wei Chen, & Jian Wu. (2020). UNet 3+: A Full-Scale Connected

UNet for Medical Image Segmentation. *Image and Video Processing*.

Jonathan Long, Evan Shelhamer, & Trevor Darrell. (2014). Fully Convolutional Networks for Semantic Segmentation. *Computer Vision and Pattern Recognition*.

Kaiming He, Xiangyu Zhang, Shaoqing Ren, & Jian Sun. (2015a). Deep Residual Learning for Image Recognition. *Computer Vision and Pattern Recognition*.

Kaiming He, Xiangyu Zhang, Shaoqing Ren, & Jian Sun. (2015b). Deep residual learning for image recognition. *Computer Vision and Pattern Recognition*.

Kaplan, K., Kaya, Y., Kuncan, M., & Ertunç, H. M. (2020). Brain tumor classification using modified local binary patterns (LBP) feature extraction methods. *Medical Hypotheses*, *139*, 109696. https://doi.org/10.1016/j.mehy.2020.109696

Karen Simonyan, & Andrew Zisserman. (2014). Very Deep Convolutional Networks for Large-Scale Image Recognition. *Computer Vision and Pattern Recognition*.

Lecun, Y., Bottou, L., Bengio, Y., & Haffner, P. (1998). Gradient-based learning applied to document recognition. *Proceedings of the IEEE*, *86*(11), 2278–2324. https://doi.org/10.1109/5.726791

Mark Sandler, Andrew Howard, Menglong Zhu, Andrey Zhmoginov, & Liang-Chieh Chen. (2018). MobileNetV2: Inverted Residuals and Linear Bottlenecks. *Computer Vision and Pattern Recognition*.

Niu, X.-X., & Suen, C. Y. (2012). A novel hybrid CNN–SVM classifier for recognizing handwritten digits. *Pattern Recognition*, *45*(4), 1318–1325. https://doi.org/10.1016/j.patcog.2011.09.021

Olga Russakovsky, Jia Deng, Hao Su, Jonathan Krause, Sanjeev Satheesh, Sean Ma, Zhiheng Huang, Andrej Karpathy, Aditya Khosla, Michael Bernstein, Alexander C. Berg, & Li Fei-Fei. (2014a). ImageNet Large Scale Visual Recognition Challenge. *Computer Vision and Pattern Recognition*.

Olga Russakovsky, Jia Deng, Hao Su, Jonathan Krause, Sanjeev Satheesh, Sean Ma, Zhiheng Huang, Andrej Karpathy, Aditya Khosla, Michael Bernstein, Alexander C. Berg, & Li Fei-Fei. (2014b). ImageNet Large Scale Visual Recognition Challenge. *Computer Vision and Pattern Recognition*.

Seidaliyeva, U., Akhmetov, D., Ilipbayeva, L., & Matson, E. T. (2020). Real-Time and Accurate Drone Detection in a Video with a Static Background. *Sensors*, *20*(14), 3856. https://doi.org/10.3390/s20143856

Siddique, N., Paheding, S., Elkin, C. P., & Devabhaktuni, V. (2021). U-Net and Its Variants for Medical Image Segmentation: A Review of Theory and Applications. *IEEE Access*, *9*, 82031–82057. https://doi.org/10.1109/ACCESS.2021.3086020

Zhou, Z., Siddiquee, M. M. R., Tajbakhsh, N., & Liang, J. (2018). *UNet++: A Nested U-Net Architecture for Medical Image Segmentation*.

TERM WEIGHTING AND TECHNIQUES IN TEXT CLASSIFICATION

Rasım ÇEKİK[1]

1. INTRODUCTION

The rapid advancement of technology has had an impact on all aspects of human life. Human-computer interaction has reached new heights, particularly with the advancement of web technologies, with information gathering and dissemination centers such as social media, online shopping sites, news, sports, and magazine news platforms. Human-computer interaction has resulted in the creation of a massive amount of data. This massive amount of data is highly contaminated. Dirty data is data that is meaningless, inconsistent, inaccurate, incomplete, or useless. Big data must be mined for meaningful and useful information. People, for example, want to index only the web pages that interest them, and they want to see only the products that interest them on online shopping sites. They do not wish to squander their time. To make the data meaningful, a number of data mining processes are used. The vast majority of the data is textual. Because of the rapid increase in text documents, it is more important than ever to ensure that these documents can be accessed effectively. Textual documents can be quickly and easily

[1] Assist. Prof. Dr., Şırnak Üniversite, Şırnak University, Faculty of Engineering, Computer Engineering, rasimcekik@sirnak.edu.tr, ORCID: 0000-0002-7820-413X.

accessed by organizing, indexing, and categorizing them. As a result, text classification studies pique the interest of researchers.

Text classification is the process of categorizing or classifying text data. This process is carried out by analyzing the content of text data and making a decision based on that content using machine learning algorithms. Text classification is a critical application in natural language processing (NLP). It aids in the organization, analysis, and comprehension of text data. The text classification process is made up of several operations and processes. Preprocessing, feature extraction, feature weighting, feature selection, and classification are the processes involved (Çekik, 2020). Weighting based on terms The weight of the term is calculated for each term of the documents using a term weighting algorithm during the term weighting process, which is an important stage in text classification. The main goal is to differentiate between terms that provide distinct and unique information in the classification and terms that are found in all documents and do not carry any special information. For this purpose, various approaches have been developed. Serious research is still being conducted in this field. This demonstrates its significance in this field as well as its impact on text classification. Text classification performance is significantly influenced by term weighting. As a result, offering effective feature weighting techniques entails offering effective text categorization. There are two types of term weighting techniques: supervised and unsupervised (Sebastiani, 2002). Unsupervised methods do not use class information during the calculation and assignment of term weights, whereas supervised methods do.

Because text classification is a popular artificial intelligence application, this study discusses term weighting and techniques that have a significant impact and importance in text classification.

2. TERM WEIGHTING PROCESS

The term weighting process is a strategy for determining and emphasizing the importance of terms in a text document. The frequency of terms appearing in the content of a text document and the importance of the document within the overall collection are typically used in this process. The frequency of a term within a document can serve as an indicator of its importance. Weighting this frequency based on its overall frequency within the collection, on the other hand, may allow more meaningful and informative terms to stand out. This method is used to highlight similarities and differences between documents, to improve systems that extract useful information from data, and to achieve better results in text classification applications. There are several stages to the process (Doğan, 2019).

Preprocessing: It consists of a number of operations on raw text collections, such as data cleaning, finding semantic values of words, data normalization and ensuring data integrity. At this stage, basic operations such as tokenization, removal of stop words, lower case conversion and root finding are commonly performed.

Term extraction: After completing pre-processing operations on unstructured text documents, terms can be extracted from these documents. The process of identifying features that represent text documents is known as feature extraction. Classifiers use these features to categorize text documents. The main goal is to identify features in text documents that represent the content and are important for classification. These elements can be words, phrases, sentences, or more complex structures. Feature extraction from text documents uses different approaches. For example, word extraction, phrase extraction, sentence extraction, and pattern extraction are some of them. The choice of feature extraction methods may vary depending on the requirements of the application. For example, word extraction methods may be sufficient for simple text classification applications. However, more advanced methods can be used for more complex applications.

Feature representation: It is the conversion of features into a digitization format that machine learning methods can understand and work on. Depending on the contents of text documents, document-term vectors are created in the vector space model and the relationship between each term and the document is transformed into a representation. The strength of this relationship depends on the success of the weighting method.

Term weighting: The weighting method chosen for the feature-document vectors created at this stage is used to create value sets. The value set depicts the term's relationship to the document and class. Classifiers use this information to categorize documents.

Figure 1 shows the operational stages of the term weighting process.

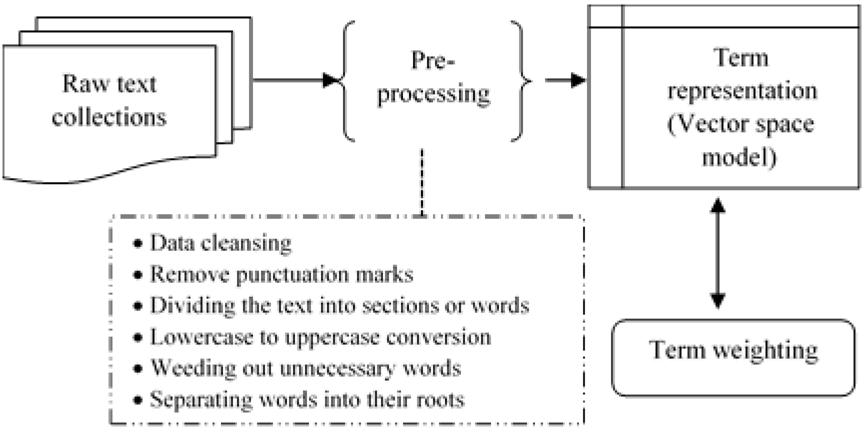

Figure 1. Term weighting process

Term weighting processes employ a variety of techniques for identifying and emphasizing the importance of terms in text documents. The following section contains information on these techniques.

3. TERM WEIGHTING TECHNIQUES

Term weighting processes are useful tools for improving the extraction of meaning and information from text documents. The term weighting method used may differ depending on the intended use and the dataset under consideration. Depending on the use of class information in the data set, either supervised or unsupervised methods are used. Furthermore, if the dataset under consideration is binary or multi-class, the preferred method may change. That is why the literature contains weighting techniques with various working mechanisms. This section will provide information on these techniques. Table 1 is provided below because the weighting equations of the techniques have mostly common expressions.

Table 1. Relationship between term and class contingency table

D (Number of documents)	Presence of the term t	Absence of term t
C (given class C)	t_x	$\overline{t_x}$
$\bar{C}$ (not given class C)	t_y	$\overline{t_y}$
M *indicates* total number of classes in the document collection.		

3.1. TF-IDF

Words that appear frequently in text data can raise the computational cost. In English, for example, the word "the" is widely used and has a high frequency, which means it appears in all documents. Because such words have low distinctiveness in text classification processes, they may need to be removed. As a result, the IDF (inverse document frequency) of a rarely occurring word will be high, while the IDF of a frequently occurring word will be low (Sparck Jones, 2004). Therefore, the TF-IDF method assigns low scores to common terms in the text collection and high scores to rare terms by calculating inverse document frequency values. In mathematical terms, TF-IDF:

$$W_{TF.IDF}(t) = TF(t, d_k) * \log\left(\frac{D}{d(t)}\right) \quad \textbf{(1)}$$

The number of occurrences of term t in document d_k is indicated by $TF(t, d_k)$, while the number of occurrences of term

t in the document is indicated by $d(t)$. D denotes the total number of documents as shown in Table 1.

3.2. TF-PB

TF-PB is an effective method for unbalanced data sets and two-class classification that uses intra-class and inter-class probability distributions (Liu Y., Loh H., & Sun A., 2009). This method computes the weighting as shown in Equation (2):

$$W_{TF.PB}(t) = TF(t, d_k) * max_{i=1}^{M}(\log\left(1 + \frac{t_x}{\overline{t_x}} * \frac{t_x}{t_y}\right)) \tag{2}$$

M denotes the total number of classes in the text collection in the equation.

3.3. TF-RF

TF-RF is a supervised method that performs weighting and is designed specifically for two-class classification (M. Lan, C. L. Tan, J. Su, & Y. Lu, 2009). This method focuses on the frequency of occurrence of terms in positive and negative classes. The TF-RF weighting formula is shown in Equation (3) below.

$$W_{TF.RF}(t) = TF(t, d_k) * max_{i=1}^{M}(\log\left(2 + \frac{t_x}{t_y}\right)) \tag{3}$$

3.4. TF-TRR

TF-TRR is a term weighting method that uses positive and negative class distributions to weight terms appropriately for two-class classification. In the TF-TRR weighting method, the TF value is used to determine how frequently a term appears in the document (Y. Ko, 2015). The TRR value is used to determine how relevant a term is to a document's subject matter. Also, its mathematical representation is as Equation (4).

$$W_{TF.TRR}(t) = \log\left(TF(t, d_k)\right) * max_{i=1}^{M}\left(\log\left(2 + \frac{\frac{t_x}{t_x + \overline{t_x}}}{\frac{t_y}{t_y + \overline{t_y}}}\right)\right) \quad \textbf{(4)}$$

3.5. TF-IDF-ICF

TF-IDF-ICF is a supervised method that employs data on the total number of documents in which terms appear as well as the total number of classes in which they appear. The weight values of the terms are obtained using this weighting method by multiplying the weight values calculated by TF-IDF for each term by the inverse class frequency (ICF) values of that term (Ren & M. G. Sohrab, 2013). Equation (5) expresses its mathematical calculation.

$$W_{TF.IDF.ICF}(t) = TF(t, d_k) * \left(1 + \log\left(\frac{D}{d(t)}\right)\right) * \left(1 + \log\left(\frac{M}{C}\right)\right) \quad \textbf{(5)}$$

Where, C indicates the number of classes in which the term occurs.

3.6. TF-IDF-ICSDF

The weight values of the terms are obtained using this weighting method by multiplying the TF-IDF weight value of each term by the inverse class space density frequency (ICSDF) value of that term (Ren & M. G. Sohrab, 2013). The main difference between this method's formula and the previous method's formula is that the weighting includes the number of documents in each class and the ratio of the total number of documents in that class, rather than the total number of classes in which each term occurs. Equation (6) contains the relevant weighting formula.

$$W_{TF.IDF.ICSDF}(t) = TF(t, d_k) * (1 + \log(\frac{D}{d(t)})) * (1 + \log(\frac{M}{\sum_{k=1}^{M} \frac{d(t)_k}{D_k}})) \quad \textbf{(6)}$$

In this formula, D_k represents the total number of documents in the k class, and $d(t)_k$ represents the total number of documents in which the term t occurs in class k.

3.7. TF-IGM

The TF-IGM is a recently proposed supervised weighting method that provides weighting for multi-class classification. The terms are calculated using the Inverse Gravitational Moment (IGM) (K. Chen & Zhang, 2016). This method calculates IGM by counting the number of documents in which each term appears at least once for each class. These numbers are then sorted in ascending order from largest to smallest. Equation (7) shows the mathematical formula for calculating a term's IGM value.

$$IGM(t) = \frac{f_1}{\sum_{r=1}^{M} f_r * r} \quad \textbf{(7)}$$

The frequency f_1 $(r = 1,2, \ldots, M)$ indicates the term's class-based document frequency. In other words, r represents the number of text documents in the rth class that contain the term

t, arranged from largest to smallest. Equation (8) is used to calculate a term's TF-IGM weight.

$$W_{TF.IGM}(t) = TF(t, d_k) * (1 + \lambda * \mathrm{IGM(t)}) \quad \textbf{(8)}$$

Where, λ is an adjustable constant value that is typically defined in studies in the range of 5.0–9.0.

4. DISCUSSION AND CONCLUSION

Text classification is popular today, and it is a focus of researchers' attention. The success and rapid development of artificial intelligence applications such as ChatGPT and Google Bard, in particular, have heightened interest in this field. Therefore, conducting successful and effective text classification studies remains a need and necessity. This study presented data on term weighting, which has a significant impact on the efficient and effective classification process in the field of text classification. The term weighting process's operation and techniques were investigated. Effective working weighting techniques from the literature are presented. This will make studies in this field easier.

As a result, term weighting schemes are generally composed of three basic components: term frequency factor, collection frequency factor, and normalization factor. However, the proposed new methods for term weighting in the literature primarily focus on the term frequency factor and collection frequency factor components.

REFERENCES

Aggarwal, C. C., & Aggarwal, C. C. (2016). Model-based collaborative filtering. Recommender systems:. *the textbook* (s. 71-138.). içinde

Aygün, C., & Yildiz, O. (2016). (2016). Genetik Algoritma Kullanılarak İçerik Tabanlı Kitap Tavsiye Sistemi Geliştirilmesi Development Of Content Based Book Recommendation System Using Genetic Algorithm. *Fen Bilimleri Enstitüsü, Yüksek Lisans Tezi, Ankara,*, 43s.

Çekik, R. (2020). Kısa metin sınıflandırma için öznitelik seçimi. Doktora Tezi. Eskisehir, Türkiye.

Doğan, T. (2019). Metin sınıflandırma için terim ağırlıklandırma, Doktora Tezi. Eskişehir, Türkiye.

Herlocker, J. L., Konstan, J. A., Borchers, A., & al., e. (1999). An algorithmic framework for performing collaborative filtering. *Proceedings of the 22nd Annual International ACM SIGIR Conference on Research and Development in Information Retrieval.*

K. Chen, Z. Z., & Zhang, H. (2016). Turning from TF-IDF to TF-IGM for term weighting in text classification. *Expert Systems with Applications*, vol. 66, pp. 245-260.

Kwan, C. K., & Jasser, M. (2020). A Comparison Study Between Content-Based and Popularity-Based Filtering via Implementing a Book Recommendation System. *IJARET* (s. 11(12), 1121-1135.). içinde

Liu Y., Loh H., L., & Sun A. (2009). Imbalanced text classification: A term weighting approach,. *Expert Systems with Applications*, 690-701.

M. Lan, C. L. Tan, J. Su, & Y. Lu. (2009). Supervised and traditional term weighting methods for automatic text categorization. *IEEE transactions on pattern analysis and machine*, vol. 31, no. 4, pp. 721-735, 2009.

Manouselis, N., Drachsler, H., Vuorikari, R., Hummel, H., & Koper, R. (2011). Recommender systems in technology enhanced learning. . *Recommender systems handbook,* (s. 387-415.). içinde

Özgöbek, Ö., & Erdur, R. C. (2015). Öneri sistemleri ve bir uygulama alanı olarak haber öneri sistemleri. *Akademik Bilişim Konferansları*, (s. 31).

Pazzani, M. J., & Billsus, D. (2007). Content-based recommendation systems. *In The adaptive web: methods and strategies of web personalization* (s. pp. 325-341). Berlin, Heidelberg: : Springer Berlin Heidelberg.

Ren, F., & M. G. Sohrab. (2013). Class-indexing-based term weighting for automatic text classification. *Information Sciences*, vol. 236, pp. 109-125.

Sebastiani, F. (2002). Machine learning in automated text categorization. . *ACM computing surveys (CSUR),* , 34, 1-47.

Seyrek, H. (2020). Genetik algoritma ile ağırlıklandırılmış hibrit bir film öneri sistemi/A hybrid film recommendation system weighted with genetic algorithm. *Doctoral dissertation*.

Shen, J. W., & Yang, Y. (2013). Collaborative filtering recommendation algorithm based on two stages of similarity learning and its optimization. *IFAC Proceedings Volumes,* , (s. 46(13), 335-340.).

Sieg, A. M., & Burke, R. D. (2007). Learning ontology-based user profiles: A semantic approach to personalized web search. *IEEE Intell. Informatics Bull.*, 8(1), 7-18.

Sparck Jones, K. (2004). A Statistical Interpretation of Term Specificity and Its Application in Retrieval. . *Journal of Documentation,*, 28, 11-21.

SU, X., & Khoshgoftaar, T. M. (2009). A survey of collaborative filtering techniques. *Advances in artificial intelligence*.

Terzi, İ. (2017). (2017). Kullanıcı/ürün çiftleri için en iyi öneri algoritmalarının tespit edilmesi . *Master's thesis, Anadolu Üniversitesi*.

Y. Ko. (2015). A new term-weighting scheme for text classification using the odds of positive and negative class probabilities,. *Journal of the Association for Information Science and Technology*, vol. 66, no. 12, pp. 2553-2565.

EVALUATION OF CORONAVIRUS IN TERMS OF OCCUPATIONAL HEALTH AND SAFETY

Edip TAŞKESEN[1], Selman İLBEYOĞLU[2*] and Rüzgar ÜREN[3]

1. INTRODUCTION

Holistic Approach to Occupational Health and Safety and Safety Culture Occupational Health and Safety is a field related to the health and safety of people working in any institution and sector. Especially in this time period where industry and technology are advancing rapidly, new business sectors are opening up every day. This situation brings with it new measures and new controls. The aim in OHS is always to protect and secure the mental and physical health of the employees. In order to explain the current situation in the work place, it is necessary to minimize the existing risks and protect the employees. Making the workplace a healthy and safe space is among the main tasks.

[1] Assist. Prof. Dr, Şırnak University, Faculty of Engineering, Energy Systems Engineering, ediptaskesen@sirnak.edu.tr, ORCID: 0000-0002-3052-9883.

[2*] Engineer, Şırnak University, Graduate Education Institute, Energy Science and Technologies, 220030003@st.sirnak.edu.tr, ORCID: 0009-0006-5374-7548

[3] Engineer, Şırnak University, Graduate Education Institute, Energy Science and Technologies, ruzgaruren@proton.me, ORCID: 0000-0002-0313-9337

2. OHS FIELDS OF STUDY

When focusing on the discipline of protecting the health and safety of employees who start working in a workplace, there are primarily two areas of emphasis. The situation of ensuring the health of employees in the workplace, which is examined and safeguarded by professionals specialized in the field, along with the discipline of identifying the presence of physical, biological, or chemical hazards, should be carefully considered. Therefore, the collaborative efforts and coordination of occupational medicine and workplace safety become crucial in accordance with the aspects mentioned below. Managing and coordinating the collaborative efforts of these two areas, especially adhering to occupational health and safety (OHS) standards within their respective domains, holds great significance. The joint efforts of these two aspects effectively focus on the health and safety of employees.

These two crucial aspects:

- Occupational Medicine
- Work safety The existence of OHS by a workplace depends on workplace medicine and workplace safety in that workplace. With the coordination of both working groups, real security can be achieved (Ahmed et al., 2023a; Mohammadi et al., 2023a).

2.1. Areas Of Interest Of The Working Groups

The areas of interest of the working groups for Occupational Health and Safety (OHS) can vary depending on the organization and industry, but some common areas of interest include; Hazard identification and risk assessment (Bentley et al., 2023), Safety training and education, Workplace ergonomics, Occupational health, Continuous improvement.

2.1.1. Occupational Medicine

Occupational disease is one of the biggest problems encountered. In determining this (Cai, 2023; Dine et al., 2023; Khiba et al., 2023; Mohammadi et al., 2023b), the priority task falls to the workplace physicians. They should have duties and responsibilities such as providing healthy working environments, conducting examinations of the employees, and investigating the interest of the employees in the work. To take measures against the risks that may occur in the workplace. Example: giving the tetanus vaccine to their employees against the risks that may arise in the workplace. Example: Someone who has had a previous lung disease should not work in dusty environments. Investigating whether the illness of any employee that may occur in the workplace is related to the work he/she does. To take the necessary measures in this direction. Conducting and monitoring health checks of employees at regular intervals. Informing employees about ways to prevent diseases. A guide for OHS (Figure 1) is below.

Figure 1. A Guide for OHS(Occupational Health and Safety (OHS): A Guide | SafetyCulture, 2023).

3. OHS - THE ENGINEERING/TECHNICAL SIDE

It is important to try to analyze and identify any situation that may pose a health and safety risk(Bentley et al., 2023; Khiba et al., 2023; Prasetyo, 2023) in working environments (Dine et al., 2023; Mohammadi et al., 2023b).

- Making measurements that may pose a risk in the workplace
- Presence and detection of chemical or biological substances used in work_places
- Detecting and minimizing the noises that may come from the machines.
- Measurement and detection of ionizable rays.
- Collaboration with relevant units in the determination of ergonomic and biological risks. Intervention against identified risks.
- Working on 'Occupational Hygiene' with all employees for a healthy and safe workplace.

4. RISKS

People may encounter life-threatening risks throughout their daily lives and are always at risk. This process is possible not only in workplaces, but also in homes, roads, outdoors and in many other areas. There are dangers and risks at every stage of life. it is impossible to reduce them to zero. However, as it is known, these risks at every stage of life are:

- can be distinguished,
- can be learned,
- can be protected,
- measurable,
- can be analyzed,
- can be evaluated,
- It can be managed and controlled.

The main risk assessment methods(Figure 2) ;these methods can be used to identify and evaluate potential risks(Ahmed et al., 2023b; Liu et al., 2023) in different contexts, and to help develop strategies for managing and minimizing those risks. There are various methods for assessing risks, including:

Figure 2. Risk Management (Khalda Petroleum Company, 2023).

- Pre-Hazard Analysis,
- Primary Risk Analysis,
- Security Function Analysis,
- Risk Map,
- Occupational Safety Inspection,
- Occupational Safety Analysis,
- Process/System Checklists,
- Transactions Review Technique,
- Relative Ranking - Dow and Mond Indices Analysis,
- Risk analysis,
- What Happens If It Happens? Analysis,
- Hazard and Operability Analysis,
- Error Types, Effects and Criticality Analysis,
- Fault Tree Analysis,
- Event Tree Analysis,
- Cause - Effect Analysis,

- Human Error Analysis,
- Human Error Identification ,
- Human Reliability Assessment ,
- Human Error Rate Estimation Technique,
- Hierarchical Task Analysis,
- Management View and Risk Tree Analysis,
- Energy Analysis • Safety Barrier Diagrams,
- Kinney Model • Zurich Hazard Analysis,
- Machinery Risk Assessment,
- Hazard Early Warning Model,
- Mean Deviation Technique,
- Deviation from Weighted Averages Technique.

5. PROTECTION FROM DANGER AND RISKS

Protection from danger and risks (Ahmed et al., 2023b; Liu et al., 2023; Mohammadi et al., 2023b) in Occupational Health and Safety (OHS) is essential to prevent harm to workers, their families, and society. Employers have a legal and ethical responsibility to provide a safe and healthy workplace for their employees. To ensure safety in the workplace, employers need to identify potential hazards and risks, assess their likelihood and severity, and take measures to eliminate or control them.

5.1. Primary Protection

- While there is no risk or dangerous situation, HR and OD are to warn, inform and train employees against possible dangers and risks before they occur (Ahmed et al., 2023b).

- health education,
- Raising the age of exposure,
- Employment health examinations examples such as.

5.2. Secondary Protection

If there is a risk, minimizing the dangers that this risk may create, reducing the impact and controlling, it is the secondary protection (Assegaf et al., n.d.; Haroun & Ghomari, n.d.; Zaman et al., 2023).

Examples of secondary protection methods include:

- Periodic health examinations,
- Early diagnosis,
- Evaluation,
- To increase the possibility of intervention,
- To prevent the problem from growing,
- Developing harm reduction strategies,
- Problem solving,
- Developing coping skills.

5.3. Tertiary Protection

If the existing risks cannot be controlled, tertiary protection options come into play (Assegaf et al., n.d.; Symanzik & John, 2023). These :

- Treatment,
- Improvement,
- Renovation.

It is the name given to the interventions made after the events have happened. These are tertiary protection (Figure 3).

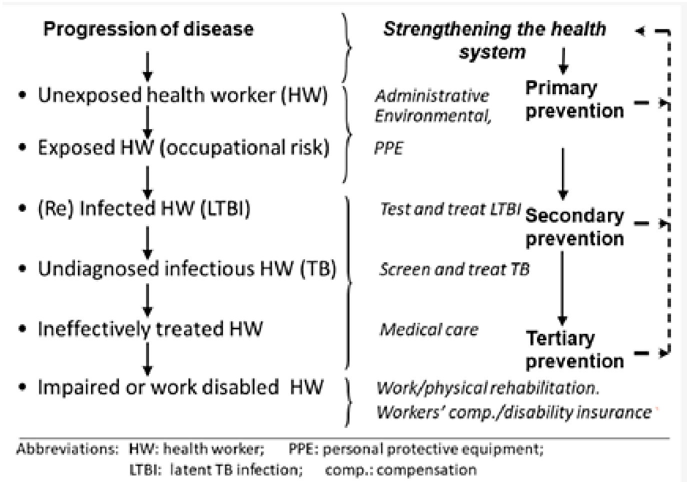

Figure 3. The Place of Tertiarity Prevention in Occupational schema (Ehrlich et al., 2020).

6. HEALTH AND SAFETY

Health and safety (Figure 4) are integral building blocks of personal and social development (Ahmed et al., 2023b; Assegaf et al., n.d.; Haroun & Ghomari, n.d.; Liu et al., 2023; Zaman et al., 2023). It is a wide-ranging field in which multiple disciplines work together. For this reason, it acts in accordance with certain principles.

Figure 4. OHS policities(CSS NCII (COC1) | Occupational Health and Safety Policy – ICTTechTips, *2023)* .

The principles adopted are as follows:

- The right to health and safety belongs to all employees.
- Certain policies in the field of OHS should be established and developed.
- A coordinated work should be carried out especially with the state, employers and workers on the social side.
- All programs and policies in this area should relate to disease prevention and safety protection.
- Necessary information should be given. Education, politics and programs should be relevant to the subject.
- The most basic approach of OHS's occupational health practices should be on health promotion.
- OHS services should cover all employees.

- Individuals who have been exposed to occupational accidents should be provided with the right to compensation, recovery and treatment.
- Relevant policies must be implemented and implemented.
- Necessary training should be given on the subject and awareness should be created.
- Workers, employers and related institutions must fulfill their responsibilities.

7. DIMENSIONAL BASIC SECURITY

This study expresses the fundamental principles applied to ensure health and safety in a workplace. It delineates the strategic disciplines established to prevent various hazards and illnesses in workplaces. Attention should be paid to safety dimensions such as physical, biological, chemical, ergonomic, psychological, and emergency preparedness and interventions. Considering these fundamental aspects is crucial for creating a safe working environment.

8. EVALUATION OF CORONAVIRUS IN TERMS OF OHS

The coronavirus, which was detected in the last quarter of 2019 and named as Covid-19, spread rapidly after the first instances of it were seen in our country. Thereupon, both companies, institutions and organizations resorted to ways to take measures quickly. OHS quickly gained importance in taking and imple_menting these measures. In this case, the issue of what the rights of employees exposed to this virus will be in the workplace, which is one of the biggest responsibilities of OHS, gains importance. Precautions to be Taken by the Employer in the Scope of Coronavirus Epidemics are directly related to occupational health and safety legislation(*Türkiye - Act No. 6331 on Occupational Health and Safety.*, n.d.). In accordance with the provision of Occupational Health and Safety Law No. 6331, article 4 (*Türkiye - Act No. 6331 on Occupational Health and Safety.*, n.d.), "Employers are responsible for ensuring the health and safety of em_ployees at work."

In this context (*Türkiye - Act No. 6331 on Occupational Health and Safety.*, n.d.):

- Prevention of occupational risks,
- Taking all kinds of measures, including providing education and information,
- Organizing the organization,

To promote workplace safety and prevent accidents, employers should:

Provide workers with appropriate tools and equipment;

Continuously adapt health and safety measures to changing conditions and seek to improve the current situation;

Monitor and inspect the workplace to ensure compliance with occupational health and safety measures and eliminate any nonconformities;

Conduct or commission a risk assessment to identify and manage potential hazards and risks;

Consider employees' health and safety suitability when assigning duties and tasks;

Restrict access to areas with inherent danger or risk only to authorized personnel who have received sufficient information and instructions.

Employers have a responsibility to maintain a safe and healthy work environment, which involves:

Supplying workers with the necessary tools and equipment to perform their jobs safely;

Adapting health and safety measures as needed and striving to improve existing conditions;

Monitoring and inspecting the workplace to ensure compliance with health and safety regulations and promptly addressing any noncompliance issues;

Conducting or arranging for risk assessments to identify and mitigate potential hazards and risks;

Considering employees' health and safety fitness when assigning job duties;

Restricting access to hazardous or dangerous areas to authorized personnel who have received proper training and instructions.

All units in a work area(Bentley et al., 2023) should be monitored indirectly in the environment they are working and outside of work. Risk assessment should be made for this and similar hazards. This requires a risk management team.

9. RISK ASSESSMENT

It is obvious that there is a lot of progress in the field of OHS in our country. Most of these studies have been adopted by the relevant institution, the State, and there are constitutional regulations. In this direction, in order to evaluate the risks In article 3/¨o of the law in the Constitution, “Works to be carried out in order to determine the dangers that exist in the workplace or that may come from outside, the factors that cause these hazards to turn into risks, and the analysis and grading of the risks arising from the hazards, and the determination of control measures” The Occupational Health and Safety Risk Assessment (Figure 5)(*Risk Assessment OHS Training - Skill Security HQ*, n.d.) Regulation outlines the principles and procedures for risk assessment, including the evaluation of dangers posed by the coronavirus. Under the 8/3/g provision of this regulation, which addresses "the dangers that may arise from the hygiene conditions of the working environment and the personal hygiene habits of the employees," the employer should take the following steps to manage risks associated with the coronavirus:

Figure 5. Risk Assessment Ohs Training(Risk Assessment OHS Training - Skill Security HQ*, 2023)*.

- Identify who may be harmed, how, and to what degree
- Determine the frequency of risk occurrence
- Consider the characteristics of the business and the risks identified
- Assess the nature of hazards or risks in the workplace.
- Should pay attention to the constraints of the workplace. Based on these factors, attention should be paid to national or international standards. Analyzes should be started on the basis of one or more of these standards. The identified risks should start with the problem with the highest level of risk,
- To take the most appropriate and optimum measures for the identified risks,
- To implement optimum measures and to make regular checks,
- The risk assessment process should be documented and retained,
- The employer must comply with the above principles.

As long as the employer does not comply with the necessary principles(Bentley et al., 2023), he may face administrative fines due to the violation of his obligations in the 4th and 10th articles of the constitution, which is one of the relevant articles. Regarding Occupational Health and Safety regarding the danger of coron_avirus Another important point: It was announced as ”Occupational Medicine” under the title of

”OHS Fields of Study”(*16 Jobs You Can Do With an Occupational Health and Safety Degree | Indeed.Com*, n.d.; Ahmed et al., 2023c).

In Article 9 of the relevant Regulation; “In addition to prevention and immunization studies for the control of com_municable diseases, providing the necessary hygiene training, ensuring that the necessary examinations and examinations are carried out” statement is included.

In line with these statements, when a coronavirus is detected in a workplace, workplace doctors are obliged to take the necessary precautions and provide training on the subject.

The coronavirus covered by an occupational accident; Covid19 In accordance with article 3/g of the Occupational Accident Law: ”An event that occurs in the workplace or due to the conduct of the business, causing death or rendering bodily integrity mentally or physically disabled” Covid19, which has still become a topic of discussion in our country, contin_ues to be examined by relevant academics and trainers.

10. CONCLUSION

A comprehensive examination has been conducted from the perspective of occupational health and safety. In this context, engineering and technical fields are particularly explored in-depth in terms of occupational health and safety. The existing risks in the workplace, their analyses, protection methods, and strategies are detailed.

The fundamental safety needs of employees in any workplace have been identified, and the rights and ways of protection for employees to meet these needs have been thoroughly examined. Within the framework of occupational health and safety (OHS), the implementation of measures to ensure the safety of employees, along with the strategic application of these measures, is crucial.

Furthermore, emphasizing the importance of determining a risk plan, control plan, and action plan against the ongoing Covid-19 pandemic in light of this information. The compliance of the measures taken during the pandemic with OHS standards and considering the rights of employees in this process have been taken into account.

Lastly, from the perspective of Occupational Accidents, a detailed explanation is provided regarding what Covid-19 is and the specific measures taken in workplaces against this pandemic. Within the framework of OHS principles, the effects of Covid-19 and protective methods are addressed with a focus on ensuring the safety and health of employees.

REFERENCES

16 Jobs You Can Do With an Occupational Health and Safety Degree | Indeed.com. (n.d.). Retrieved April 4, 2023, from https://www.indeed.com/career-advice/finding-a-job/with-occupational-health-safety-degree

Ahmed, T., Hoque, A. S. M., Karmaker, C. L., & Ahmed, S. (2023a). Integrated approach for occupational health and safety (OHS) risk Assessment: An Empirical (Case) study in Small enterprises. *Safety Science*, *164*, 106143.

Ahmed, T., Hoque, A. S. M., Karmaker, C. L., & Ahmed, S. (2023b). Integrated approach for occupational health and safety (OHS) risk Assessment: An Empirical (Case) study in Small enterprises. *Safety Science*, *164*, 106143.

Ahmed, T., Hoque, A. S. M., Karmaker, C. L., & Ahmed, S. (2023c). Integrated approach for occupational health and safety (OHS) risk Assessment: An Empirical (Case) study in Small enterprises. *Safety Science*, *164*, 106143.

Assegaf, S. T., Pramadita, S., & Jati, D. R. (n.d.). ANALYSIS OF CONSTRUCTION SAFETY RISK MANAGEMENT BASED ON PU MEMORY NUMBER 10 THE YEAR 2021 "Case Study: Provision of Sanitation Facilities in Institutions Religious Education." *Jurnal Teknik Sipil*, *23*(1), 125–134.

Bentley, T. A., Caponecchia, C., Onnis, L., Brunetto, Y., Farr-Wharton, B., Cattani, M., Neto, A., & Vassiley, A. (2023). A systems model for the design of occupational health and safety management systems inclusive of work-from-home arrangements. *Applied Ergonomics*, *109*, 103966.

Cai, M. (2023). Occupational health and safety. In *Encyclopedia of Human Resource Management* (pp. 279–280). Edward Elgar Publishing.

CSS NCII (COC1) | Occupational Health and Safety Policy – ICTTechTips. (2023, April 4).

Https://Icttechtips.Wordpress.Com/2018/07/09/Css-Coc1-Occupational-Health-and-Safety-Policy/ .

Dine, G., Reed, S., Oosthuizen, J., & Masaka, E. (2023). Identifying occupational health and safety risks among environmental health officers in Australia and New Zealand through an online survey. *Medicine*, *102*(12), e33270–e33270.

Ehrlich, R., Spiegel, J. M., Adu, P., & Yassi, A. (2020). Current guidelines for protecting health workers from occupational tuberculosis are necessary, but not sufficient: Towards a comprehensive occupational health approach. *International Journal of Environmental Research and Public Health*, *17*(11), 3957.

Haroun, H., & Ghomari, A. R. (n.d.). A spatial data integration and visualization approach for occupational health and safety risks management: Application to Algerian electricity and gas company. *The Electronic Journal of Information Systems in Developing Countries*, e12265.

Khalda Petroleum company. (2023, April 4). Https://Www.Slideshare.Net/MahmoudHamdy64/Khalda-Petroleum-Company .

Khiba, K., Seda, O., & Fourie, A. (2023). Occupational Health and Safety concerns within the live events industry at selected venues in Gaborone, Botswana: a pragmatic and utilitarian approach. *South African Theatre Journal*, 1–22.

Liu, R., Liu, H.-C., Shi, H., & Gu, X. (2023). Occupational health and safety risk assessment: A systematic literature review of models, methods, and applications. *Safety Science*, *160*, 106050.

Mohammadi, H., Rabiei, H., & Farhang Dehghan, S. (2023a). Emerging technologies in occupational health and safety. *Frontiers in Public Health*, *11*, 136.

Mohammadi, H., Rabiei, H., & Farhang Dehghan, S. (2023b). Emerging technologies in occupational health and safety. *Frontiers in Public Health*, *11*, 136.

Occupational Health and Safety (OHS): A Guide | SafetyCulture. (2023, April 4). Https://Www-Sandpit.Safetyculture.Com/Topics/Occupational-Health-and-Safety.

Prasetyo, D. (2023). ANALYSIS OF OCCUPATIONAL HEALTH AND SAFETY RISK IN THE 76MM SHOOTING PROCESS USING HAZARD IDENTIFICATION, RISK ASSESSMENT AND RISK CONTROL (HIRARC) METHODS. *Journal of Industrial Engineering & Management Research*, *4*(2), 74–87.

Risk assessment OHS training - Skill Security HQ. (2023, April 4). Https://Www.Securityguardexam.Com/Risk-Assessment-Ohs-Training/ .

Symanzik, C., & John, S. M. (2023). Occupational Skin Cancer by Solar Ultraviolet Radiation. In *Handbook of Occupational Dermatoses* (pp. 47–55). Springer.

Türkiye - Act No. 6331 on Occupational Health and Safety. (n.d.). Retrieved April 4, 2023, from https://www.ilo.org/dyn/natlex/natlex4.detail?p_lang=en&p_isn=92011

Zaman, M. B., Pitana, T., Prastowo, H., Priyanta, D., Siswantoro, N., Maulana, F. S., & Busse, W. (2023). Occupational health and safety risk assessment of shipyard using HIRARC method. *AIP Conference Proceedings*, *2482*(1), 130005.

THE EFFECT OF SEMI-ACTIVE AND PASSIVE CONTROL ON SYSTEM PERFORMANCE IN STRUCTURAL VIBRATION CONTROL

Hüseyin AGGÜMÜŞ[1]

1. INTRODUCTION

Structural vibration control is important in protecting the structure and its residents. There are many control applications made in this field to save the structure from the effect of an excitation force that affects the structure and causes vibrations (Aggumus and Cetin 2018; Aggumus and Guclu 2020; Guclu and Yazici 2007; Leung and Zhang 2009; Ohtori et al. 2004; Turan and Aggumus n.d.; Wang and Dyke 2013). Although passive control elements are easy to apply to systems, their performance is limited due to the constancy of their parameters. Semi-active control applications are superior to the same type of passive control applications in terms of performance, as the parameters of the damping or spring elements or both can change while interacting with the system (Aggumus and Cetin 2018). In the literature, Tuned Mass Dampers (TMD) are often preferred because they give successful results in passive control performance (Hadi and Arfiadi 1998; Warburton 1982). Parameter determination

[1] Assist. Prof. Dr., Şırnak University, Şırnak Vocational School, Department of Mechanical and Metal Technologies, haggumus@sirnak.edu.tr, ORCID: 0000-0002-7158-677X.

methods (Den Hartog 1947; Leung and Zhang 2009; Warburton 1982) have been developed to increase the vibration suppression performance of TMD on the structure and optimization algorithms (Bekdaş and Nigdeli 2011; Zahrai, Akhlaghi, and Rabipour n.d.) have been used to obtain better performance.

Semi-active control applications include rigidity and damping elements. Among the damping elements, MR dampers are preferred for important reasons such as high power capacities and durability. The semi-active control element feature of MR dampers is obtained by changing the damping force with the transmitted stresses (Dyke et al. 1996; Terasawa et al. 2004a). For this, it is necessary to design control algorithms suitable for the system. Both the placement of the MR damper on the structure and the development of the applied control algorithms continue to work in this field (Aggumus and Guclu 2020; Paksoy and Aggümüş 2022).

This study investigates how MR damper and TMD affect system responses by using them together on the same structure. For this purpose, the system performance was examined for the situation where MR damper and TMD were together. The groundhook control algorithm determined the MR damper voltage.

2. MODELING AND PARAMETERS

The six-story building model examined in this study is given in Figure 1a. The control status examined is given in Figure 1b. Lateral vibrations, which occur during the excitation forces, where the most dangerous situation for the structure occurs, were evaluated. The models' most general equations of motion in Figure 1 are as follows.

$$M_s\ddot{x}(t) + C_s\dot{x}(t) + K_s x(t) = -Hf(t) - M_s L\ddot{x}_g \qquad (1)$$

Here M_s, C_s ve $K_s \in R^{6x6}$ are the matrices of mass, damping, and stiffness, respectively. $\ddot{x}(t)$, $\dot{x}(t)$ ve $x(t) \in R^{6x1}$ are acceleration, velocity, and displacement vectors, respectively. Displacement vector,

$$x = [x_1 \quad x_2 \quad x_3 \quad x_4 \quad x_5 \quad x_6 \quad x_d]^T \qquad (2)$$

The seismic input vector L and, H_s vector showing the location of the semi-active control element is as follows

$$L = [1 \quad 1 \quad 1 \quad 1 \quad 1 \quad 1 \quad 1] \qquad (3)$$

$$H_s = [1 \quad 0 \quad 0 \quad 0 \quad 0 \quad 0]^T \qquad (4)$$

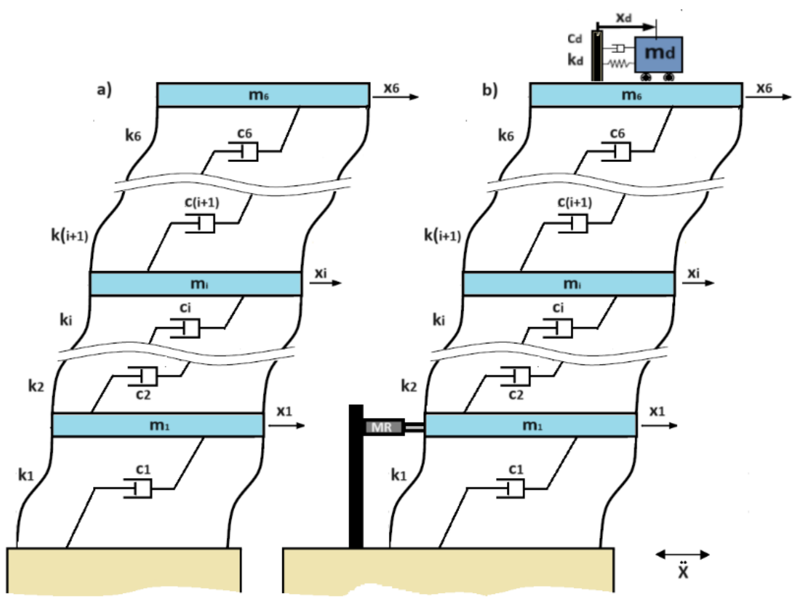

Figure 1. The building model: a) The situation in which there is no control, b) The situation in which the control is applied.

The mass of the building model, $m_{1\ldots5} = 862.85$ kg, $m_6 = 803.98$ kg, rigidity, $k_1 = 1.26 * 10^6$ N/m, $k_{2..6} = 1.23 * 10^6$ N/m, and damping, $c_{1\ldots6} = 36.7052 * 10^6$ Ns/m. TMD parameters are calculated as in Eqs 5, 6, and 7.

$$m_d = \mu M_{top} \tag{5}$$

$$k_d = m_d(f_{opt}W_n)^2 \tag{6}$$

$$c_d = 2\xi_{opt}(f_{opt}W_n)m_d \tag{7}$$

The μ parameter shows the ratio of the mass of TMD (m_d) to the mass of the structure (M_{top}). the mass of the structure, ω_n , k_d and c_d the natural frequency, stiffness, and damping values of the TMD, respectively, are shown. f_{opt}, the frequency ratio is calculated in Eq. 10 ξ_{opt} opt, and the damping ratio is calculated in Eq. (Warburton 1982).

$$f_{opt} = \sqrt{\frac{1-\mu/2}{(1+\mu)}} \tag{8}$$

$$\xi_{opt} = \sqrt{\frac{\mu(1-\mu/4)}{4(1+\mu)(1-\mu/2)}} \tag{9}$$

For a mass ratio of 0.03, $m_d = 153.5469$ kg, $k_d = 1.2148*10^4$ N/m c_d=233.9678 Ns/m.

3. MR DAMPER AND THE CONTROL ALGORITHM

This study used the MR damper as a semi-active control element. According to the LuGre friction model, the force generated by the MR damper is obtained by the following expression (Terasawa et al. 2004b).

$$f = \sigma_a z + \sigma_0 z v + \sigma_1 \dot{z} + \sigma_2 \dot{x}_1 + \sigma_b \dot{x}_1 v \tag{10}$$

$$\dot{z} = \dot{x}_1 - a_0 |\dot{x}_1| z \tag{11}$$

f is the MR damper force, z is the MR fluid internal dynamic variable, and v is the voltage, σ_2 is the viscous damping coefficient. σ_0 is the stiffness of z(t) varying with v(t) σ_1, the damping coefficient of z(t) is σ_2, the viscous damping coefficient, σ_a is the stiffness of z(t), σ_b is the viscous damping coefficient varying with v(t), and a_0, is the constant coefficient (Sakai, Ohmori, and Sano 2003).

The groundhook control algorithm has been designed to determine the voltage transmitted to the MR damper. (Kim and Kang 2012; Koo et al. 2004). The groundhook control algorithm is seen in Eq. 12.

$$V = \begin{Bmatrix} V_{max} & \rightarrow & x_1(\dot{x}_1) \leq 0 \\ V_{min} & \rightarrow & x_1(\dot{x}_1) > 0 \end{Bmatrix} \tag{12}$$

V_{min} is minimum voltage and V_{max} is maximum voltage. The maximum voltage is 10v, and the minimum voltage is 0v.

4. SIMULATIONS

In this study, displacement and acceleration time responses were researched to examine the effect of TMD and MR damper on a six-story building model. In addition, the maximum of the time responses and the root mean square (rms) values were analyzed. The system affected the acceleration input of the Erzincan and Kocaeli earthquakes. System performance was evaluated by comparing the non-control and control states (TMD+MR_1).

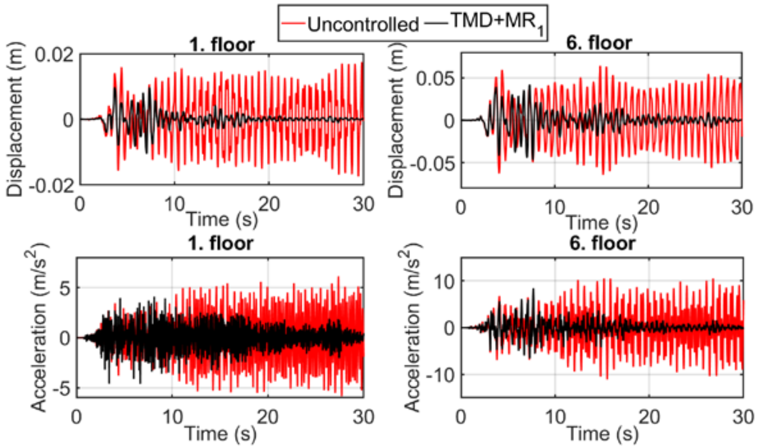

Figure 2. Time responses of the system affected by the Kocaeli earthquake

Figure 2 shows the displacement and acceleration time responses of the 1st and 6th floors of the system under the influence of the Kocaeli earthquake. In the displacement response control state, the system responses were effectively suppressed. In acceleration responses, although there is an improvement in system responses, performance is lower than in displacement responses. Figure 3 shows the maximum displacement and acceleration responses of all floors and the rms values of these responses. The control condition suppressed the system responses on all floors, as in the 1st and 6th-floor performances in Figure 2.

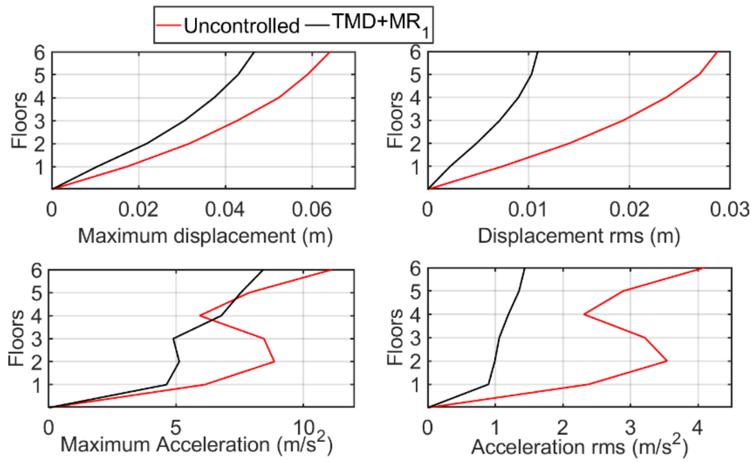

Figure 3. Maximum responses of the system affected by the Kocaeli earthquake

Figure 4 shows the displacement and acceleration time responses of the 1st and 6th floors of the system under the influence of the Erzincan earthquake. As with the Kocaeli earthquake, the control performance of the system suppressed the displacement responses more effectively than the acceleration responses. Figure 5 shows the maximum displacement and acceleration responses of all floors and the rms values of these responses. The control application suppressed the system responses in both displacement and acceleration responses.

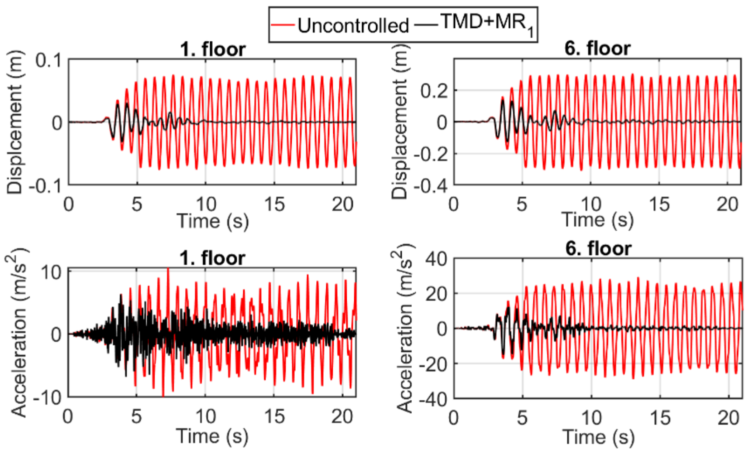

Figure 4. Time responses of the system affected by the Erzincan earthquake

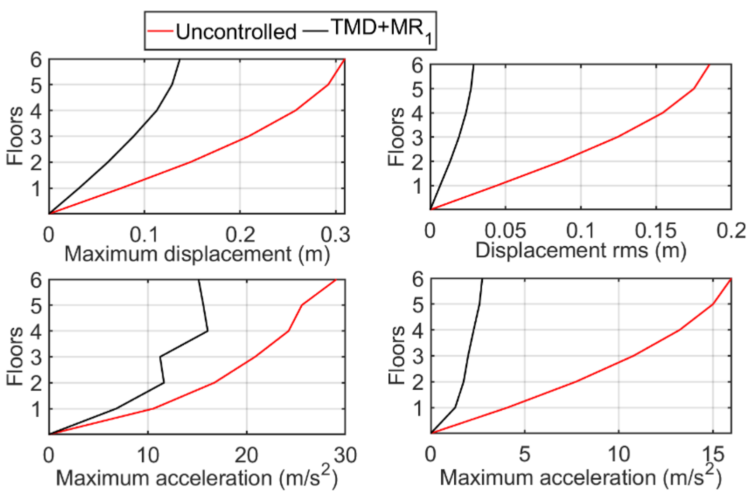

Figure 5. Maximum responses of the system affected by the Erzincan earthquake

In general, the combination of semi-active and passive control applied to the system in performance values effectively suppressed system responses. Since the primary goal is to suppress displacement responses, this is acceptable for the current control system since the performance decrease in acceleration responses does not increase when the system responses are not controlled. System performance acceleration in displacement responses and differences in system performance due to the effect of Kocaeli and Erzincan earthquakes are because these excitations do not have the same effect on the system.

5. CONCLUSIONS

This study used semi-active and passive control elements to suppress the vibrations of an earthquake-excitation six-story building. The passive control element TMD was applied to the top floor of the building, and the semi-active control element MR damper was applied to the first floor of the building. A groundhook control algorithm was used to change the MR damper voltage that produces the necessary control force for the system. The data of the Erzincan and Kocaeli earthquakes affected the structural system, and the system responses and control performance were examined. The results have shown that TMD and MR Damper worked harmoniously and suppressed system responses. Studies on the optimum determination of TMD parameters and different control algorithms for MR damper voltage may increase the control system's performance.

REFERENCES

Aggumus, Huseyin, and Saban Cetin. 2018. "Experimental Investigation of Semiactive Robust Control for Structures with Magnetorheological Dampers." *Journal of Low*

Frequency Noise, Vibration and Active Control 37(2):216–34. doi: 10.1177/0263092317711985.

Aggumus, Huseyin, and Rahmi Guclu. 2020. "Robust H∞ Control of STMDs Used in Structural Systems by Hardware in the Loop Simulation Method." *Actuators* 9(3):55. doi: 10.3390/act9030055.

Bekdaş, Gebrail, and Sinan Melih Nigdeli. 2011. "Estimating Optimum Parameters of Tuned Mass Dampers Using Harmony Search." *Engineering Structures* 33(9):2716–23. doi: 10.1016/j.engstruct.2011.05.024.

Den Hartog, J. P. 1947. *Mechanical Vibrations*. 3rd ed. New York, N.Y. : McGraw-Hill.

Dyke, S. J., B. F. Spencer, M. K. Sain, and J. D. Carlson. 1996. "Modeling and Control of Magnetorheological Dampers for Seismic Response Reduction." *Smart Materials and Structures* 5(5):565–75. doi: 10.1088/0964-1726/5/5/006.

Guclu, Rahmi, and Hakan Yazici. 2007. "Fuzzy Logic Control of a Non-Linear Structural System against Earthquake Induced Vibration." *Journal of Vibration and Control* 13(11):1535–51. doi: 10.1177/1077546307077663.

Hadi, Muhammad N. S., and Yoyong Arfiadi. 1998. "Optimum Design of Absorber for MDOF Structures." *Journal of Structural Engineering* 124(11):1272–80. doi: 10.1061/(ASCE)0733-9445(1998)124:11(1272).

Kim, Hyun-Su, and Joo-Won Kang. 2012. "Semi-Active Fuzzy Control of a Wind-Excited Tall Building Using Multi-

Objective Genetic Algorithm." *Engineering Structures* 41:242–57. doi: 10.1016/j.engstruct.2012.03.038.

Koo, Jeong-Hoi, Mehdi Ahmadian, Mehdi Setareh, and Thomas Murray. 2004. "In Search of Suitable Control Methods for Semi-Active Tuned Vibration Absorbers:" *Journal of Vibration and Control*. doi: 10.1177/1077546304032020.

Leung, A. Y. T., and Haijun Zhang. 2009. "Particle Swarm Optimization of Tuned Mass Dampers." *Engineering Structures* 31(3):715–28. doi: 10.1016/j.engstruct.2008.11.017.

Ohtori, Y., R. E. Christenson, B. F. Spencer, and S. J. Dyke. 2004. "Benchmark Control Problems for Seismically Excited Nonlinear Buildings." *Journal of Engineering Mechanics* 130(4):366–85. doi: 10.1061/(ASCE)0733-9399(2004)130:4(366).

Paksoy, Mahmut, and Hüseyin Aggümüş. 2022. "MR Sönümleyicili Yarı Aktif Ayarlı Kütle Sönümleyicisinin Uyarlamalı Kontrolü." *Avrupa Bilim ve Teknoloji Dergisi* (33):68–73. doi: 10.31590/ejosat.1020498.

Sakai, C., H. Ohmori, and A. Sano. 2003. "Modeling of MR Damper with Hysteresis for Adaptive Vibration Control." Pp. 3840–45 vol.4 in *42nd IEEE International Conference on Decision and Control (IEEE Cat. No.03CH37475)*. Vol. 4.

Terasawa, T., C. Sakai, H. Ohmori, and A. Sano. 2004b. "Adaptive Identification of MR Damper for Vibration Control." Pp. 2297-2303 Vol.3 in *2004 43rd IEEE Conference on*

Decision and Control (CDC) (IEEE Cat. No.04CH37601). Vol. 3.

Turan, Abdullah, and Huseyin Aggumus. n.d. "Implementation of Advanced PID Control Algorithm for SDOF System." 10.

Wang, Yumei, and Shirley Dyke. 2013. "Modal-Based LQG for Smart Base Isolation System Design in Seismic Response Control: MODAL-BASED LQG FOR SMART BASE ISOLATION SYSTEM IN SEISMIC CONTROL." *Structural Control and Health Monitoring* 20(5):753–68. doi: 10.1002/stc.1490.

Warburton, G. B. 1982. "Optimum Absorber Parameters for Various Combinations of Response and Excitation Parameters." *Earthquake Engineering & Structural Dynamics* 10(3):381–401.

Zahrai, S. M., M. M. Akhlaghi, and M. Rabipour. n.d. "Application of Particle Swarm Optimization for Improving Seismic Response of Structures with MR Dampers."

INSPECTION OF ORIGINAL MICROINDENTATION HARDNESS PARAMETERS OF $Bi_{2.1}Sr_{2.0}Ca_{2.1}Cu_{3.0}O_y$ CERAMIC STRUCTURES

Tahsin TURGAY [1], Cabir TERZİOĞLU[2] and Asaf Tolga ÜLGEN[3]

1. INTRODUCTION

It is widely acknowledged that hardness is intricately linked to a material's resistance to permanent shape alterations, influenced by crystal structure quality. This parameter holds significant importance in determining fundamental mechanical performances and characterizing mechanical properties. Consequently, hardness stands out as a crucial parameter for materials destined for use in power transmission, metallurgical, advanced engineering, heavy-industrial, and energy-related sectors. In essence, a material's hardness performance, in relation to mechanical strength, stiffness, ductility, toughness, and

---

[1] Prof. Dr., Sakarya University, Department of Architecture, Department of Architecture, Sakarya-Turkey e-mail:turgay@sakarya.edu.tr ORCID: 0000-0003-0304-1097

[2] Prof. Dr., Abant Izzet Baysal University, Department of Physics, Bolu–Turkey, 14280, e-mail:terzioglu_c@ibu.edu.tr, ORCID: 0000-0002-3944-0367.

[3] Assoc. Prof. Dr., Şırnak University, Department of Electric-Electonic Engineering, Şırnak–Turkey, 73000. e-mail:asaftolgaulgen@gmail.com ORCID: 0000-0002-7112-5607.

durability, can serve as a guiding factor in determining its application fields (Awad et al., 2012).

Hardness testing methods offer distinct advantages, being less deformative, destructive, simple, reliable, and cost-effective (Awad, et al., 2012, Altunpak, et al., 2016, Guner, et al.,2019, Jr. Callister & Rethwisch, 2013, Yasar & Altunpak, 2009). These tests apply substantial force to create a diogonal impression on the sample surface. In literature, widely utilized routes as regards Rockwell, Knoop, Brinell, and Vickers microhardness are employed to evaluate the mechanical endurance and characteristic nature of ceramic materials (Altunpak, et al., 2016). These methods, operating on different force scales, are easily convertible during experimental tests (Yasar & Altunpak, 2009, Bilge et al., 2019). Among them, Knoop and Vickers microhardness methods are particularly suitable for evaluating the mechanical performance and characteristic features of ceramic compounds due to their intrinsic nature. Their smaller indenter sizes, microscale measurements on specimen surfaces, and lighter force make them superior to other methods. Notably, the Vickers microhardness method is preferred, especially for analyzing load-independent hardness results in the saturation limit sites. At the same time, nowadays the researchers are extensively working on the development in the mechanical strengths and electrical properties to increase the application fields (Altunpak & Akbulut, 2017, Bilge & Morgül 2023).

This study specifically aims to evaluate the impact of cadmium particles on generral mechanical endurance and identification of $Bi_{2.1}Sr_{2.0}Ca_{2.1}Cu_{3.0}O_y(CdO)_x$ ceramic structures.

Vickers microhardness tests were conducted under varied applied external test forces sorting between 0.295N to 2.940N. The choice of bulk Bi-2223 ceramic material from the Bi-containing parents stems from its versatility in numerous application fields (Altunpak & Akbulut, 2017, Bilge & Morgül, 2023, Savaskan, et al., 2020, Takayama-Muromachi, 1998, Yamauchi & Karppinen, 2000). Main mechanical characteristic features and original indentation hardness were analyzed in the plateau limit regions using semi-empirical mechanical approaches, including modified proportional sample resistance (MPSR), Meyer's law (ML), elastic/plastic deformation (EDP), proportional sample resistance (PSR), Hays–Kendall (HK), and indentation-induced cracking (IIC) mechanical analyzing methods. However, detailed assessments primarily focus on ML, HK, and IIC approaches in the plateau sites due to their comparatively more fitting outcomes than other methods. Based on the findings, the data inferred from IIC emerge as the most practical method for discussing true hardness findings in the limit sites of pure and CdO-added bulk Bi-2223 products (Awad, et al., 2011, Elmustafa & Stone, 2003, Sangwal, 2000).

2. EXPERIMENTAL DETAILS FOR Bi-2223 CERAMICS

Ceramic $Bi_{2.1}Sr_{2.0}Ca_{2.1}Cu_{3.0}O_y$ materials were synthesized using the classical ceramic preparation technique, employing high-purity powders (exceeding 99.99%) of $SrCO_3$, CdO, Bi_2O_3, CuO, and $CaCO_3$ chemicals. In this study, six distinct $Bi_{2.1}Sr_{2.0}Ca_{2.1}Cu_{3.0}O_y(CdO)_x$ ceramic structures were fabricated with varying cadmium oxide impurity amounts, ranging from molar ratios of 0.00 to 0.10. To achieve stoichiometric ratios, 2 grams of chemical powders were meticulously weighed using an electronic balance in the ambient air.

The powders, composed of oxides and carbonates, underwent a 9-hour mixing process in a porcelain crucible within atmospheric air conditions. This mixing aimed to reduce particle sizes and ensure a homogeneous powder blend. Subsequently, the homogenous mixture was ground for 40 minutes in the agate. The resulting reduced particle size facilitated the formation of new atomic bonds within the main crystal matrix. The homogenous mixture was then calcined in a programmable furnace at 800°C for 36 hours under atmospheric air conditions, effectively eliminating impurity phases from the $Bi_{2.1}Sr_{2.0}Ca_{2.1}Cu_{3.0}O_y(CdO)_x$ solid ceramic materials at cooling/heating ratios of 5°C for a minute.

The calcined homogenous mixtures were molded into rectangular bars ($2.0x0.5x0.2\ cm^3$), enhancing interactions between stacked layers to minimize systematic issues within the crystal structures. These solid bars underwent the main heating process at a sintering temperature of 850°C for 36 hours. The resulting $Bi_{2.1}Sr_{2.0}Ca_{2.1}Cu_{3.0}O_y(CdO)_x$ solid ceramic materials, produced with varying cadmium oxide amounts (x=0.000, 0.005, 0.010, 0.050, 0.070, and 0.100), were denoted as pure or unadded, CdO-1, CdO-2, CdO-3, CdO-4, and CdO-5, respectively.

For measurement systems, standard Vickers microhardness experiments were conducted using a digital testing tool. The experiments aimed to define the impact of cadmium oxide impurities on the main mechanical identifications and real microindentation hardness of $Bi_{2.1}Sr_{2.0}Ca_{2.1}Cu_{3.0}O_y(CdO)_x$ ceramic structures in the plateau limit regions. Experimental data were collected under atmospheric air conditions at external test forces.

The study primarily focused on assessing deviation of main mechanical identification features and real hardness quantities in plateau sites. This assessment employed semi-empirical mechanical approaches, including modified proportional sample resistance (MPSR), Meyer's law (ML), elastic/plastic deformation (EDP), proportional sample resistance (PSR), Hays–Kendall (HK), and indentation-induced cracking (IIC) mechanical analyzing methods. Based on calculations from semi-empirical mechanical approaches, ML, HK, and IIC models were identified as providing the best approximation to real Vickers hardness parameters. The discussion is centered around these semi-empirical findings, presenting all modeling outcomes.

3. RESULTS AND DISCUSSION

Before delving into the discussions of semi-empirical mechanical results obtained from the models, we provided a brief explanation of the impact of various CdO impurity levels on the microhardness features of Bi-2223 crystal structures. This explanation was aided by the differentiation of Vickers microindentation hardness parameters based on applied external forces. Detailed graphs depicting pure and CdO-impurity-added Bi-2223 ceramics are presented in Figure 1.

The graphs clearly illustrate a rapid decrease in main mechanical performance findings with an increase in cadmium oxide impurity within the Bi-2223 system. The presence of cadmium oxide in the bulk Bi-2223 ceramic system leads to a degradation of crystal structure quality and intrinsic slip systems. Consequently, the reduction in Vickers hardness parameters is attributed to the consistent rise in stress considerations and associated stress raiser sites throughout the Bi-2223 crystal system. In essence, the mechanical strength and durability of the bulk Bi-2223 main matrix are adversely affected by the cadmium oxide addition mechanism.

Furthermore, the changes in Hv parameters concerning applied test forces, as depicted in Figure 1 for both pure Bi-2223 and CdO-added Bi-2223 ceramic structures, reveal a notable reduction in Vickers microhardness parameters up to an applied external force of 2N. However, beyond this critical force magnitude (referred to as saturation sites), the values of Vickers hardness parameters remain relatively constant due to increased crystal structure issues in the main matrix.

As seen in Figure 1, Bi-2223 product added with the maximum cadmium impurity amount (CdO-5) reaches the saturation limit sites even under smaller external forces. Conversely, the unadded sample, with higher mechanical strength and durability performance, reaches its saturation limit region at a slower rate. This shift in the behavior of the Bi-2223 main matrix is a result of the heightened stress considerations and associated stress raiser sites along with Bi-2223 ceramics, leading to a decline in crystal structure quality and intrinsic slip systems (Güner, et al., 2020, Ulgen, et al., 2022).

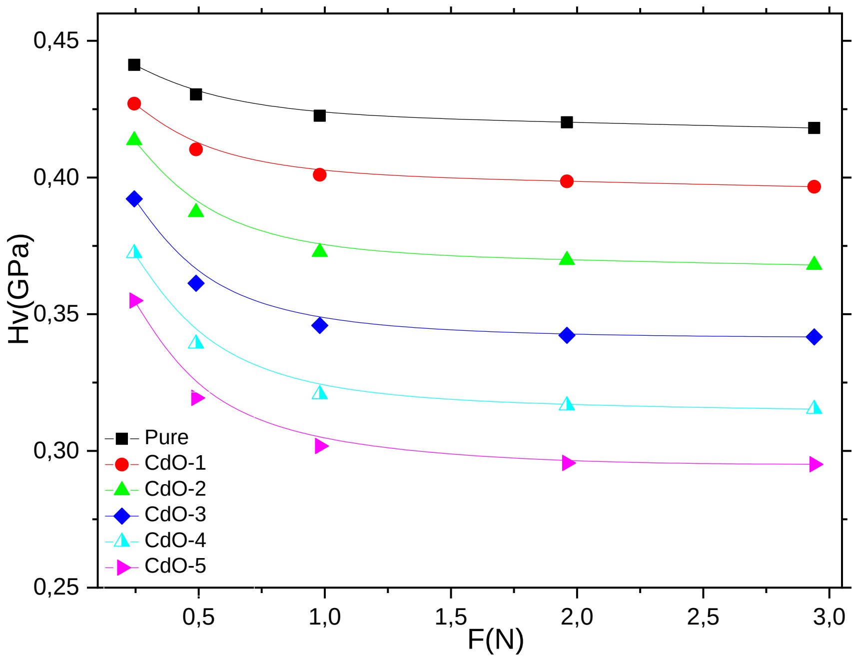

Figure. 1 Variation of microindentation hardness parameters over the external test loads between 0.245 N and 2.940 N.

Regarding the examination of the impact of cadmium oxide impurity addition on real Vickers tests, we have provided a detailed discussion of the results obtained from three semi-empirical mechanical models. However, it is important to note that we have also compiled results from other mechanical models.

3.1. Application of Meyer's Law Model for Evaluating True Hardness Quantities in Saturation Limits

In our analysis of the influence of cation/anion addition in ceramic matrices on load-independent microindentation hardness parameters in satiety risk zones and the main mechanical characteristic features, we first employed Meyer's law. A ceramic compound can exhibit two distinct mechanical behaviors: i- ISE or ii- RISE in response to applied test forces. The former is linked with the non-linearly decreased real hardness quantitates with external applied test forces, while the latter involves a non-linear increment in real Vickers hardness parameters with external applied test forces (Awad, et al., 2011, Elmustafa & Stone, 2003). The variation in mechanical behavior under applied test forces is correlated with the surface energy coefficient of the studied products (Zalaoglu, et al., 2013, Altunpak & Akbulut, 2009, Saritekin, et al., 2016).

In the Meyer's law (ML) approach, the relationship between the values of microindentation quantitites and external forces (F) is defined by an exponential power (n) related to the diagonal impression indentation lengths (d^n). The relation between the external applied test forces and diagonal indentation depths is expressed in Eq. 1 (Ling & Yan, 1988):

$$F = A_{Meyer} d^n$$

in this formula, A_{Meyer} represents values of microhardness quantities for both unadded and various CdO impurity-added ceramic products, and the exponential power n signifies the Meyer number associated with the materials studied.

Exponential power for n coefficient, also known as the Meyer number, can take one of three values: less than 2, equal to 2, or greater than 2. These values define general mechanical behaviors of ceramic products. Specifically, when $n<2$, the product exhibits the conventional ISE characteristic behavior under applied test forces. Conversely, when 2*n*=2, the ceramic product demonstrates Kick's sample behavior, confirming that Vickers microhardness parameters are entirely independent of externally applied test forces (Mohammed, et al., 2009). In the case of 2*n*>2, the product displays unconventional RISE characteristic behavior under applied test forces.

In this study, the characteristic behavior of both pure and CdO-added bulk Bi-2223 ceramic products were determined by analyzing the curves of applied test loads *Ln*(F) as a function of diagonal impression indentation depths *Ln*(d). This analysis yielded exponential power constants (*n*) and crossing points on the y-axis (denoted as A_{Meyer}). The computations are detailed in Table 1. Notably, both unadded and CdO-added bulk Bi-2223 ceramic products exhibited exponential power constants (*n*) smaller than 2, indicating typical ISE features under externally applied test forces (Dogruer, et al., 2013). Interestingly, *n* values ranged numerically between 1.954 (for the unadded sample) and 1.864 (for the CdO-5 ceramic sample). The decrease in n parameters with impurity is attributed to the reduction in ISE behavior.

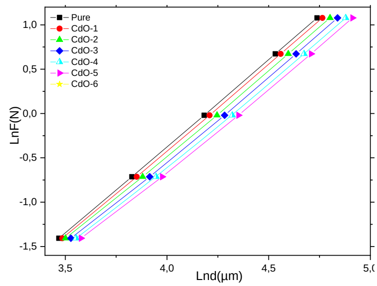

Figure. 2 Change of *Ln*(F) versus *Ln*(d) plots for pure and different CdO added bulk Bi-2223 ceramic matrices.

Table 1 Computations deduced from PSR, EPD, MPSR, HK, and IIC theoretical models for pure and CdO added bulk Bi-2223 ceramic compounds.

Samples	ML		PSR		MPSR			EPD		HK		IIC	
	A_{MEYER} $x10^{-4}$ ($N/\mu m^2$)	n	$\alpha x10^{-4}$ ($N/\mu m$)	$\beta x10^{-4}$ ($N/\mu m^2$)	$Wx10^{-2}$ (N)	A_{0MPSR} $x10^{-3}$ ($N/\mu m$)	A_{1PSR} $x10^{-4}$ ($N/\mu m^2$)	$d_e x10^{-1}$ (μm)	A_{2EPD} $x10^{-1}$ ($N^{1/2}/\mu m$)	$Wx10^{-1}$ (N)	A_{3HK} $x10^{-4}$ ($N/\mu m^2$)	$Kx10^{-2}$ ($N^{(3-5mA)/3}/\mu m^{(2-3m)}$)	m
Pure	2.728	1.959	5.188	2.208	0.677	0.276	2.226	0.171	0.1486	0.154	2.244	5.966	-0.160
CdO-1	2.761	1.945	6.492	2.080	1.767	0.032	2.124	0.219	0.1443	0.1868	2.126	2.933	-0.210
CdO-2	2.965	1.913	9.601	1.898	3.936	-0.374	1.989	0.333	0.1379	0.2703	1.966	0.597	-0.330
CdO-3	2.958	1.898	10.700	1.747	5.704	-0.802	1.870	0.382	0.1323	0.2975	1.821	0.242	-0.400
CdO-4	3.024	1.878	12.600	1.594	6.043	-0.657	1.715	0.467	0.1265	0.3729	1.677	0.064	-0.490
CdO-5	3.022	1.864	13.6	1.479	6.717	-0.706	1.606	0.520	0.1219	0.4154	1.566	0.025	-0.560

Simultaneously, the values of A_{Meyer} parameters truncated methodically with an enhancement of cadmium particles. This consistent decrease at A_{Meyer} parameters is linked to the heightened stress considerations and related stress raiser sites in the bulk Bi-2223 structure, resulting in degradation of ceramic quality and intrinsic slip systems.

3.2. Hays–Kendall Approach for Analyzing True Microindentation Quantities in Saturation Limits

The second semi-empirical mechanical model employed is the HK approach, widely chosen for assessing the main mechanical performance features and mechanical identificaitons of ceramic products. This model is particularly recognized for examining ceramic products exhibiting conventional ISE characteristics (Hays & Kendall, 1973).

In the calculations using the HK semi-empirical mechanical model, a critical force value leading to irreversible deformation in the main matrix is determined and referred to as the effective force. This force, causing plastic deformation, is denoted as W. In the equation, $F_{eff} = F - W$ the W parameter represents a critical force constant, signifying the point where the indenter begins to penetrate deeper, leaving a trace of diagonal impression indentation length on the specimen surfaces (Hays & Kendall, 1973). Additionally, the values of W parameters are utilized to ascertain whether the prepared product displays standard ISE or unconventional RISE behavior. More specifically, the sign of the W parameter determines the mechanical characteristic behavior. A positive sign indicates ISE nature, while a negative sign suggests RISE nature. Irreversible deformation commences only when the applied external test force exceeds the value of W.

The variation in the diagonal impression indentation length trace versus the externally applied test force is deduced from formula depicted:

$$F - W = A_{3HK} d^2$$

Here, constant of A_{3HK} parameter in Equation 2 signifies Vickers hardness values for the ceramic material, and the *W* parameter represents the applied external forces. Linear relationship between external forces (F) and the diagonal impression length traces (d^2) is illustrated in Fig. 3. Computed values of A_{3HK} and *W* parameters are numerically presented in Table 1.

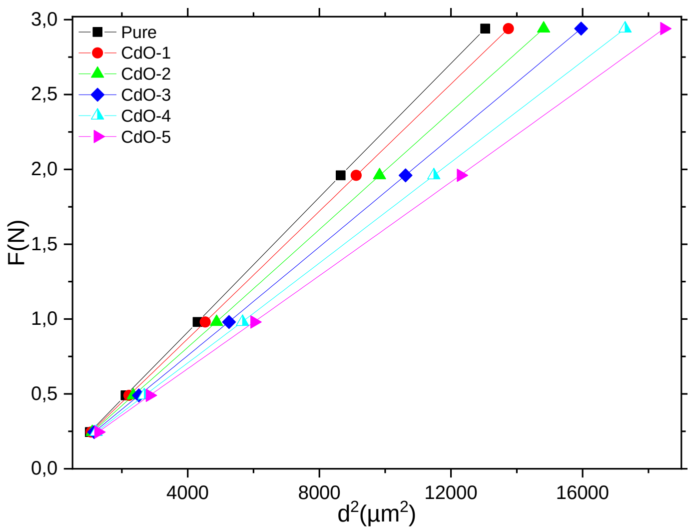

Figure. 3 Linear relations for the graphs related to the variation in the diagonal impression indentation depths with the externally applied test forces for all the unadded and CdO impurity added bulk Bi-2223 ceramic materials.

Based on the computed constants presented in Table 1, where both the unadded and CdO-impurity-added bulk Bi-2223 ceramic samples exhibit positive values for the *W* coefficients, ranging from 0.1540×10^{-1} 0.1540×10^{-1} N to 0.4154×10^{-1} 0.4154×10^{-1} N. This indicates that every compound prepared displays standard ISE behavior. Unadded sample possesses the smallest value of *W* constants as 0.1540×10^{-1} 0.1540×10^{-1} N, while this parameter dramatically increases with the augmentation of cadmium oxide impurity. The CdO-5 material has the maximum *W* value of 0.4154×10^{-1} 0.4154×10^{-1} N, reflecting its heightened response to applied test loads because of the significant degradation in ceramic quality and intrinsic slip systems. Other CdO-added Bi-2223 structures exhibit moderate *W* values (0.1868×10^{-1} 0.1868×10^{-1} N, 0.2703×10^{-1} 0.2703×10^{-1} N, 0.2975×10^{-1} 0.2975×10^{-1} N, and 0.3729×10^{-1} 0.3729×10^{-1} N). Regardless, all studied products reveal both reversible and plastic deformations under external forces.

The change in the value of A_3HK coefficients within the Bi-2223 ceramic system with cadmium oxide impurity addition has also been determined. The numerical values in Table 1 reveal a systematic decrease in A_3HK parameters from 2.244×10^{-4} 2.244×10^{-4} N/μm² to 1.566×10^{-4} 1.566×10^{-4} N/μm² with an increase in cadmium oxide impurity. The unadded sample has the maximum A_3HK value, while the maximum cadmium oxide-added Bi-2223 (CdO-5) has the smallest A_3HK value. Other CdO-added Bi-2223 ceramics have moderate A_3HK values. The decrease in A_3HK values with the addition of cadmium oxide stems from the truncation in the mechanical strength and durability performance of Bi-2223 ceramics due to increased crystal structure problems in the main matrix.

Similar to other models (PSR, EPD, and MPSR), the Hays–Kendall model has been widely employed to examine the variation of main mechanical characteristic features and load-independent microindentation hardness parameters in the plateau limit regions. The examination is conducted using the following relation:

$$H_{HK} = 1854.4 A_{3HK}$$

All computations are detailed in Table 2, which also includes load-independent Vickers microhardness parameters for other model approaches. This section focuses solely on the HK model results. It is evident from the table that numeric values are closely aligned with real microhardness quantities in saturation limits. In conclusion, the HK model demonstrates reliable findings for both main mechanical identification quantities and original microindentation hardness features in plateau regions.

Table 2. Coefficients of experimental H_v in saturation limit regions, H_{EPD}, H_{PSR}, H_{HK}, H_{MPSR}, and H_{IIC} determined from PSR, EPD, MPSR, HK, and IIC theoretical methods (in GPa unit)

Samples	H_{PSR}	H_{MPSR}	H_{EPD}	H_{HK}	H_{IIC}	Hv
Pure	0.410	0.413	0.409	0.416	0.427	0.418-0.441
CdO-1	0.386	0.394	0.386	0.394	0.417	0.397-0.427
CdO-2	0.352	0.369	0.353	0.365	0.419	0.368-0.414
CdO-3	0.324	0.347	0.325	0.338	0.392	0.342-0.392
CdO-4	0.296	0.318	0.297	0.311	0.383	0.315-0.372
CdO-5	0.274	0.298	0.276	0.290	0.372	0.295-0.355

3.3. Usage of Indentation-induced cracking approach for examination of original hardness parameters in saturation sites

Furthermore (the final model explored in this study), we have examined the primary mechanical performance features and mechanical characterization (ISE or RISE) behavior of the ceramic products, along with analyzing load-independent microindentation hardness parameters along plateau sites using the IIC method (Li & Bradt, 1996). In this model, four primary mechanisms, including 1- indenter and indenter friction, 2- elastic deformation, 3- reversible deformation, and finally 4- crack mechanism in the ceramic matrix, have significantly influenced the mechanical behavior of the studied ceramic materials. This is precisely why the equation pertaining to the IIC semi-empirical mechanical modeling approach can be expressed as follows:

$$H_{IIC} = \lambda_1 K_1 \left(F/d^2\right) + K_2 \left(F^{5/3}/d^3\right)$$

in equation, the value of λ_1 constant is coincided with the product type. When the value of K_1 constant is tuned with the indenter geometry, the value of K_2 coefficient points out the externally applied test forces. Accordingly, the relation for the IIC semi-empirical mechanical modeling approach should be rewritten for the perfect brittle nature of ceramic structure, in this respect, the first coefficient, λ_1 in left side of equation goes to 0, and hereafter the new relation will be recalled as $K_2\,(F^{5/3}/d^3)$, and to sum up the last coefficient of the formulization is rewritten as below:

$$H_{IIC} = K\left(\frac{F^{5/3}}{d^3}\right)^m$$

in the relation, the values pertaining to the K and m coefficients point out true Vickers microhardness constants. The constants can be extracted from the extrapolation approach on the differentiation in the values of Vickers hardness parameters ln(Hv) over the externally applied indentation forces, ln($F^{5/3}/d^3$) plots as provided in Fig. 4.

One can see all the computations about K and m constants in Table 1. As observed from the table that the unadded and different CdO added bulk Bi-2223 ceramic structures has been obtained to present the standard ISE behavior. Here, the values of m parameter can be larger than 0.6 or smaller than 0.6. In more detail, when m<0.6, the ceramic structure has been obtained to show the typical ISE nature. On the other hand, when m>0.6 the ceramic material has been noticed to indicate the untypical RISE behavior. Moreover, the value of m parameters has been observed to reduce regularly with enhancing the cadmium oxide impurity amount. On this basis, the unadded material has been obtained to exhibit the maximum value of -0.160, on the other hand, the smallest value of m parameter has been noted to be about -0.560 for the bulk CdO-5 ceramic structure.

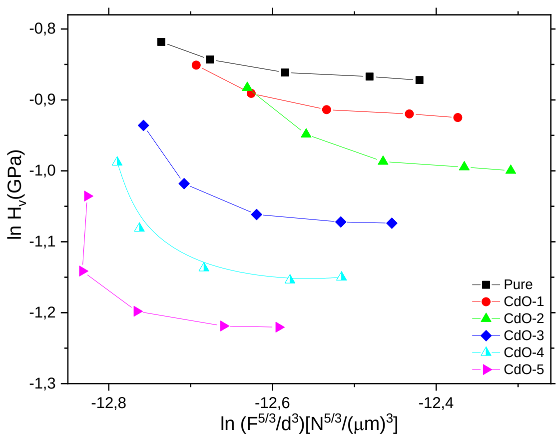

Figure 4. ln (Hv) curves versus external test forces, ln($F^{5/3}/d^3$) curves for pure and varied CdO added bulk Bi-2223 ceramic structures.

The other materials have been found to have moderate values between -0.210 and -0.490. The regression of m constants has stemmed from decrease of the mechanical strength and mechanical durability performance of the Bi-2223 ceramics due to the revived crystal structure problems based on augmentation of the stress consideration and related stress raiser sites in the main matrix. Similar to the results deduced from other mechanical modelling approaches, the CdO-5 ceramic sample exhibited the most response to the forces whereas unadded Bi-2223 compound showed the least response to the external forces applied. As for the role of CdO impurity on the value of K coefficients depicted in Table 1 for the pure and different CdO added bulk Bi-2223 ceramic structures, with the augmentation of cadmium particles amount in Bi-2223 ceramic lattice, the values of K coefficients have decrease dramatically depending on not only the enhancement in the crystal structure problems but also the decrease in the slip systems throughout the Bi-2223 ceramic system. Numerically, the unadded Bi-2223 sample has been found to present the maximum K value of 5.966 $x10^{-2}$. On the other hand, for the largest CdO impurity amount of x=0.01, the CdO-5 sample has had the smallest K value of 0.0025 $x10^{-2}$ $N^{(3-5mA)/3}/ \mu m^{(2-3m)}$. The other samples have shown the moderate values for the K parameters. That is exactly why the decrease in K constants has indicated the harsh reduction of crystal structure quality.

Additionally, we have analyzed the load-independent Vickers microhardness parameters in the saturation sites of pure and different CdO molar added Bi-2223 ceramics with the aid of IIC approach. The related data can be seen in Table 2. It has been based on the findings that the IIC model has exhibited the superior strength as compared to the findings deduced from other models to inspect the real Vickers hardness tests. Accordingly, of the semi-empirical mechanical modeling approaches the IIC method with the most reliable and closest results to the real Vickers hardness values has been obtained to be the best approach for investigating the load-independent microindentation hardness parameters in the plateau limit regions, mechanical performance features and mechanical characterization behavior belonging to the ceramic products.

4. CONCLUSION

We explored the variations in the primary mechanical characteristics and load-independent microindentation hardness parameters within solid $Bi_{2.1}Sr_{2.0}Ca_{2.1}Cu_{3.0}O_y(CdO)_x$ ceramic structures containing cadmium oxide impurity. This investigation was conducted through Vickers hardness experiments conducted under external forces. The experimental data were analyzed using various mechanical modeling methods, including elastic/plastic deformation, Meyer's law, MPRS, PRS, HK, and IIC models in the plateau limit regions. However, for the purpose of this study, we focused our discussions solely on ML, HK, and IIC methods, as they provided the most useful and reliable results for real Vickers hardness values in the plateau limit regions, while still presenting all modeling findings. The increase in cadmium oxide impurity in the Bi-2223 ceramic system resulted in a decline in crystal structure quality and intrinsic slip systems, driven by a consistent rise in stress consideration and related stress raiser sites throughout the Bi-2223 crystal system. Consequently, the presence of cadmium oxide impurity led to a degradation in mechanical strength and durability. Conversely, the unadded Bi-2223 compound exhibited the least response to applied external test forces, while the CdO-5 sample demonstrated the most significant response to these forces. Regarding the mechanical characteristic behavior of the bulk Bi-2223 ceramic structure, both pure and CdO-added Bi-2223 ceramics exhibited characteristic ISE behavior. Notably, the unadded sample demonstrated the highest ISE nature among all materials. Furthermore, the results from semi-empirical mechanical modeling indicated that among the studied models, the IIC semi-empirical mechanical model provided the closest results for true microindentation parameters in plateau sites. Consequently, the IIC mechanical model emerged as the most reliable for analyzing Bi-2223 systems containing cadmium oxide impurity.

REFERENCES

Altunpak, Y., & Akbulut, H. Effects of aging heat treatment on machinability of alumina short fiber reinforced LM 13 aluminum alloy, International Journal of Advanced Manufacturing Technology, 43 (2009) 449-454

Altunpak, Y., & Akbulut, H. Mechanical properties of a squeeze-cast 2124 Al composite reinforced with alumina short fibre, Metallurgical Research and Technology, 114 (2017) 509.

Altunpak, Y., Aslan, S., Guler, M.O., & Akbulut, H. Effect of alternative heat-treatment parameters on the aging behavior of short-fiber-reinforced 2124 Al composites, Materiali in Tehnologije, 50 (2016) 1011-1016

Awad, R., Abou Aly, A. I., Kamal, M., Anas, M. (2011). Mechanical properties of $(Cu_{0.5}Tl_{0.5})$-1223 substituted by Pr. Journal of superconductivity and novel magnetism, 24, 1956.

Awad, R., Abou-Aly, A. I., Abdel Gawad, M. M. H., & G-Eldeen, I. (2012). The influence of SnO_2 nano-particles addition on the vickers microhardness of (Bi, Pb)-2223 superconducting phase. Journal of superconductivity and novel magnetism, 25, 739-745.

Bilge, H., & Morgül, Ö. K. (2023). Analytical and Experimental Investigation of the Rotary Inertia Effects of Unequal End Masses on Transverse Vibration of Beams. Applied Sciences, 13(4), 2518.

Bilge, H., Doruk, E., Fındık, F., & Pakdil, M. (2019). Effect of fatigue crack propagation on natural frequencies of system in AISI 4140 Steel. Steel and Composite Structures, An International Journal, 32(3), 305-312.

Dogruer, M., Yildirim, G., Ozturk, O., Belenli, I., & Terzioglu, C. (2013). Variation of mechanical properties of Cr doped Bi-2212 superconductors. Journal of superconductivity and novel magnetism, 26, 2949-2954.

Elmustafa, A. A., & Stone, D. S. (2003). Nanoindentation and the indentation size effect: Kinetics of deformation and strain gradient plasticity. Journal of the Mechanics and Physics of Solids, 51(2), 357-381.

Güner, S. B., Abdioğlu, M., Öztürk, K., & Çelik, Ş. (2020). The comparison of levitation and lateral force of bulk and cut-pasted bulk GdBCO samples at different temperatures. Journal of Alloys and Compounds, 822, 153637.

Guner, S. B., Zalaoglu, Y., Turgay, T., Ozyurt, O., Ulgen, A. T., Dogruer, M., & Yildirim, G. (2019). A detailed research for determination of Bi/Ga partial substitution effect in Bi-2212 superconducting matrix on crucial characteristic features. Journal of Alloys and Compounds, 772, 388-398.

Hays, C., & Kendall, E. G. (1973). An analysis of Knoop microhardness. Metallography, 6(4), 275-282.

Jr. Callister, W.D., & Rethwisch, D.G. (2013). Materials Science and Engineering: An Introduction, 9th ed., Wiley Binder Version, USA.

Li, H., & Bradt, R. C. (1996). The effect of indentation-induced cracking on the apparent microhardness. Journal of materials science, 31, 1065-1070.

Ling, H. C., & Yan, M. F. (1988). Microhardness measurements on dopant modified superconducting $YBa_2Cu_3O_7$ ceramics. Journal of applied physics, 64(3), 1307-1311.

Mohammed, N. H., Abou-Aly, A. I., Ibrahim, I. H., Awad, R., & Rekaby, M. (2009). Mechanical properties of $(Cu_{0.5}Tl_{0.5})$-1223 added by nano-SnO_2. Journal of alloys and compounds, 486(1-2), 733-737.

Sangwal, K. (2000). On the reverse indentation size effect and microhardness measurement of solids. Materials Chemistry and Physics, 63(2), 145-152.

Saritekin, N. K., Terzioglu, C., Pakdil, M., Turgay, T., & Yildirim, G. (2016). Solubility limit of tetravalent Zr nanoparticles in Bi-2223 crystal lattice and evaluation of fundamental characteristic properties of new system. Journal of Materials Science: Materials in Electronics, 27, 1854-1865.

Savaskan, B., Guner, S. B., Yamamoto, A., & Ozturk, K. (2020). Trapped magnetic field and levitation force properties of multi-seeded YBCO superconductors with different seed distance. Journal of Alloys and Compounds, 829, 154400.

Takayama-Muromachi, E. (1998). High-pressure synthesis of homologous series of high critical temperature (Tc) superconductors. Chemistry of materials, 10(10), 2686-2698.

Ulgen, A. T., Okur, S., Erdem, U., Pakdil, M., Turgay, T., & Yildirim, G. (2022). Evaluation of load-independent microhardness values in Plateau regions of Vanadium substituted Bi-2212 ceramics. Physica Scripta, 97(8), 085703.

Yamauchi, H., & Karppinen, M. (2000). Application of high-pressure techniques: stabilization and oxidation-state control of novel superconductive and related multi-layered copper oxides. Superconductor Science and Technology, 13(4), R33.

Yasar, M., & Altunpak, Y. The effect of aging heat treatment on the sliding wear behaviour of Cu-Al-Fe alloys, Materials and Design, 30 (2009) 878-884.

Zalaoglu, Y., Bekiroglu, E., Dogruer, M., Yildirim, G., Ozturk, O., & Terzioglu, C. (2013). Comparative study on mechanical properties of undoped and Ce-doped Bi-2212 superconductors. Journal of Materials Science: Materials in Electronics, 24, 2339-2345.

OPTIMIZATION OF WOOD SURFACE ROUGHNESS IN CNC MILLING BY TAGUCHI METHOD

Abdullah Cemil İLÇE[1]

1. INTRODUCTION

Surface roughness plays a key role in determining the quality of furniture design and production. A smooth surface contributes to the elegant and high-quality appearance of furniture. It has a profound effect on the viewer's first impression and promotes a positive perception of the overall quality of the piece of furniture. Smooth surfaces also reflect light evenly, enhancing the coherence of the furniture with the general atmosphere of the room. Surface roughness is also a critical factor for the mechanical durability, strength, and life cycle of furniture (Kilic, Hiziroglu and Burdurlu, 2006; Malkoçoğlu, 2007; Ilçe, 2019). A smooth surface increases the furniture's resistance to wear and tear, providing protection against scratches, stains, and other forms of deformation over time. In addition, a smooth surface makes the furniture easier to clean and maintain, contributing to its long-term strength. Furniture manufacturers can therefore optimize surface roughness to extend the life of

[1] Assoc.Prof.Dr., Bolu Abant Izzet Baysal University, Faculty of Engineering, Department of Industrial Engineering, cemililce@ibu.edu.tr, https://orcid.org/0000-0001-5133-683X.

their products, ultimately increasing customer satisfaction through products that stand the test of time.

In a comprehensive analysis, it is imperative to consider numerous quantitative factors that impact surface roughness, denoted as the arithmetic average of surface irregularities concerning a mean line. These factors can be broadly classified into four main groups (Ratnam, 2017): Firstly, machining parameters, which encompass crucial elements like feed rate, cutting speed, and depth of cut. Secondly, cutting tool parameters, incorporating aspects such as wear, geometry, material, and coating of the tools employed. The third group involves considerations related to machining and machine tool conditions, taking into account factors similar to dry or wet turning, cutting fluid type, fluid applications, machine tool rigidity, and the presence of vibrations or chatter. Lastly, the fourth group revolves around the properties of the workpiece material, including hardness, microstructure, grain size, and the presence of inclusions on the specimen surface.

Understanding these diverse factors is crucial in gaining a comprehensive insight into the intricacies of surface roughness and its dependence on various aspects of the machining process. This nuanced understanding enables researchers and practitioners to tailor their approaches to achieve desired surface finishes based on specific requirements and material characteristics.

At the same time, there have been several studies in the literature to improve some critical features such as Surface roughness based on the machining, cutting tool, machine tool, hardness, microstructure, and grain size parameters of the plant-based wood materials (Altunpak, et. al, 2016; Altunpak, Y. and Akbulut, 2009). Pesticides are composed of the other critical problem for the wood materials to overcome. In other words, preventing pests strengthens wooden materials for use in furniture production. This is exactly why the interests of scientists in the last few decades have enormously been attracted by the inhibition effect of the magnetic field applications on some problematic features (Ulgen, et. al, 2021; Ulgen, et. al, 2017).

In recent years, as part of Industry 4.0, the furniture manufacturing process has seen a shift towards digital design and production technologies. Thus, CNC (Computer Numerical Control) machines integrated with Computer Aided Design (CAD) have gained the ability to produce complex furniture components with precision. These machines can effectively process wood materials through computer-controlled cutting and shaping processes to achieve smooth and homogeneous surfaces. The high precision of CNC technology allows detailed patterns and intricate designs to be easily applied to wood (Hazir, Erdinler and Koc, 2018; Hazir and Koc, 2019; Koc, Erdinler, Hazir and Öztürk, 2017; Pelit, Korkmaz and Budakçı, 2021; Zeqiri, Alkan, Kaya and Toros, 2018). This has given designers and manufacturers unprecedented creative freedom and flexibility, and increased productivity by reducing errors in the digital design and production process. However, wood surfaces are still shaped by a metal cutter and optimization of surface roughness parameters is still required in the new situation. Moreover, the systematic studies related to the magnetic fields have been endeavored to strengthen the material quality (Ulgen et. al, 2020; Ulgen et. al, 20203).

The Ra value of many tree species has been investigated in the recent years (Akbulut and Ayrilmis, 2006; Cota, Dritan, Habipi, Çota and Ajdinaj, 2017; Kilic, Hiziroglu and Burdurlu, 2006; Laina et al., 2017; Malkoçoğlu, 2007; Thoma, Peri and Lato, 2015; Yang, Ma, Liu, Ding and Qu, 2023). This value expresses the roughness of a treated or untreated material averaged over a surface. The Ra value indicates the amount of waviness and peaks and valleys on a surface (De Moura and Hernández, 2006; Hiziroglu, 1996; Sulaiman, Hashim, Subari and Liang, 2009). It is a widely used measurement for assessing the smoothness of a surface and the quality of machining (Sandak and Tanaka, 2003). In the woodworking industry, especially in furniture production, the Ra value is considered an important criterion for determining and optimizing the quality of machined wood surfaces (Budakçi, Ilçe, Gürleyen and Utar, 2013; Hazir et al., 2018; Kilic et al., 2006; Singer and Özşahin, 2022). Researchers and industry professionals use Ra data to adjust machining parameters and optimize the roughness of wood surfaces.

Taguchi Box Benkhen or Artificial Neural Network methods are commonly used to optimize this value (Ayanleye, Nasir, Avramidis and Cool, 2021; Gaitonde, Karnik and Paulo Davim, 2008; Gürgen, Çakmak, Yıldız and Malkoçoğlu, 2022; Hazir et al., 2018; Koc et al., 2017; Lin, Wu, Shih, Hsu and Hung, 2020; Loc and Hung, 2021; Prakash, Mercy and Goswami, 2014; Rabiei and Yaghoubi, 2023; Singer and Özşahin, 2022; Sofuoglu, 2015) Taguchi experimental design, developed by Genichi

Taguchi, is renowned for its efficiency in conducting experiments with minimal resources while simultaneously evaluating the influence of multiple factors on a response variable. In contrast, Box-Behnken design is characterized by its ability to fit response surfaces with a relatively small number of trials (Ilçe, 2019). This approach is favored for its ability to assess both linear and quadratic effects of factors on response, providing a balance between precision and practicality. Artificial Neural Networks (ANNs), on the other hand, represent a data-driven paradigm capable of modelling complex, non-linear relationships between input and output variables. ANNs are particularly adept at handling large data sets, capturing intricate patterns, and demonstrating versatility across different types of data (Demir, Cakiroglu and Aydin, 2022). In a comparative analysis, Taguchi and Box-Behnken share common ground as experimental design methods that focus on process optimization with minimal experimental runs. Taguchi's strength lies in resource efficiency and robustness, while Box-Behnken excels in response surface modelling. Taguchi and ANNs differ in their underlying principles, with Taguchi being a statistical approach suitable for well-defined factors and limited data, whereas data driven. ANNs are adept at modelling intricate relationships in complex environments. Similarly, Box-Behnken and ANNs differ in their focus, with Box-Behnken specializing in experimental design (Ilçe, 2019) and ANNs excelling at modelling complex relationships in data-rich contexts (Tiryaki, Malkoçoğlu and Özşahin, 2014)

The Taguchi method for predicting wood surface roughness was used in this study. The main reason for choosing the Taguchi method is its effectiveness and practical applicability in the context of multifactorial experimental designs (Gaitonde et al., 2008). In complex production processes such as woodworking, it is essential to understand and optimize the effects of different factors on surface roughness (Hazir and Koc, 2019). The use of the Taguchi method in this context addresses the need to optimize resources and conduct cost-effective experiments (Prakash et al., 2014). Another advantage of the Taguchi method is its robustness to experimental results. This method can deal with different sources of noise and variation, taking into account the uncertainties encountered in real production conditions. Therefore, the aim of this study is to optimize the factors that cause the roughness of wood surfaces machined on CNC machines by using Taguchi method with a small number of experiments. This method makes a significant contribution to understanding and optimizing the interactions of factors in complex woodworking processes.

2. EXPERIMENTAL

2.1. Materials

Oriental beech was chosen because it is widely used in the furniture industry in Turkey, is readily supplied, has an economical price and its processing methods are well-known. A total of 16 dried oriental beech samples, measuring 18 mm x 110 mm x 350 mm, were constructed according to TS 2470 (2005).

Their annual rings were arranged vertically on the surfaces. In addition, the samples were of high quality, fine grain, free of knots, cracks and had no differences in colour or density. It was then stored in a climatic chamber at 20°C ± 2°C and 65% ± 5% relative humidity until it reached a constant weight. Experimental materials (0.7±0.03 air dry density and 9±1% moisture content) were patterned by milling on a CNC machine in a factory in Ankara, and roughness measurements were made in the laboratory of this manufacturer.

CNC milling of wood surfaces was performed using the following milling parameters (Table 1). The feed rate is the speed at which the CNC router moves across the workpiece while performing the routing operation. This parameter can affect surface roughness, cutting efficiency and overall machining speed.

Table 1. Surface roughness parameters for the CNC milling process.

Parameter	Level 1	Level 2	Level 3	Level 4
Feed rate (A) (m/min)	3	5	7	9
Spindle speed (B) (rpm)	14000	18000		
Depth of cut (C) (mm)	2	3		

The depth of cut determines how deeply the router will cut into the wood material. This parameter is adjusted based on the thickness of the workpiece and the desired result during the milling process. The spindle speed refers to the rotational speed of the cutting tools used during the milling process. This speed is determined by the material properties of the workpiece, the type of cutting tools used and the overall requirements of the process.

Spindle speed has a significant effect on surface finish, cutting accuracy and tool life. Accurate adjustment of these parameters helps to achieve the desired quality, efficiency, and machining speed during CNC milling. The characteristics of the workpiece, the type of cutting tools used and the overall purpose of the process play a crucial role in optimizing these parameters.

2.2. Taguchi method

This study focused on the optimization of the surface roughness parameters (feed rate, cutting depth and spindle spin) of beech wood in the CNC (Computer Numerical Control) milling process by using the Taguchi method. The utilization of the Taguchi method represents a strategic approach for optimizing multiple factors in intricate scenarios. This method involves an initial step of aggregating the degrees of freedom for each parameter, followed by the selection of an orthogonal array tailored to the total degrees of freedom acquired. In the context of this study, the application of the Taguchi method encompasses four cutting feed, two cutting depth, and two spindle spin parameters.

The experimental design is carefully organized, with the number of samples matched to the roughness parameter levels and the Taguchi L16 orthogonal array chosen. Steps to perform parameter design are shown schematically in Figure 1. The S/N ratio was calculated by equation 1.

The signal to noise ratio (S/N) is used as a key metric to effectively control the response and reduce the associated variability. Its ratio encompasses three distinct performance criteria: minimum (smaller-the better), maximum (larger-the better), and average (nominal-the best). Notably, in this study, the primary objective function is the achievement of minimum surface roughness.

The Taguchi method provides a systematic and structured approach to optimizing machining parameters and improving overall surface quality (Nas and Altan Özbek, 2020). This methodological framework proves particularly valuable in addressing complex optimization challenges involving a multitude of interconnected factors.

$$\frac{S}{N} = -10\log\left(\frac{1}{n}\sum_{i=1}^{n} y_i^2\right) \quad 1$$

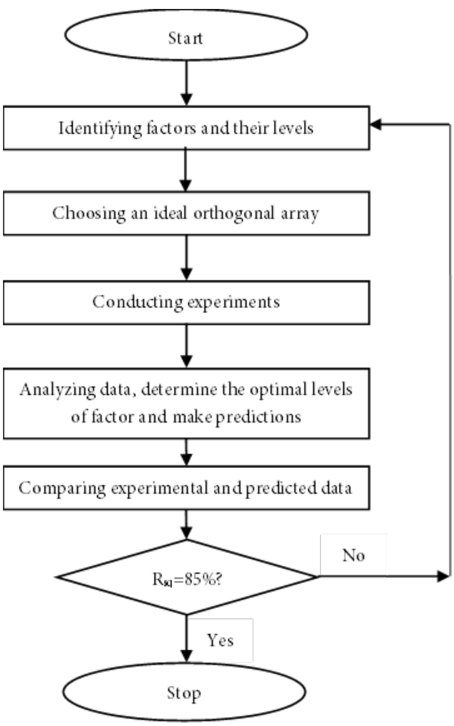

Figure 1. Flowchart of the Taguchi method for surface roughness

3. RESULTS

Table 2 shows the results of the surface roughness experiments carried out according to the Taguchi L16 experimental design. The optimum values of the parameters are always obtained at the levels with maximum signal to noise ratio.

Table 2. Results of L16 design experiments.

No	Feed rate (m/min)	Spindle speed (rpm)	Depth of cut (mm)	Surface roughness
1	3	14000	2	3,92
2	3	14000	2	3,98
3	3	18000	3	4,65
4	3	18000	3	4,42
5	5	14000	2	4,86
6	5	14000	2	4,50
7	5	18000	3	5,36
8	5	18000	3	5,74
9	7	14000	3	5,96
10	7	14000	3	5,80
11	7	18000	2	4,64
12	7	18000	2	4,72
13	9	14000	3	6,12
14	9	14000	3	6,28
15	9	18000	2	4,86
16	9	18000	2	4,66

The signal to noise ratio for surface roughness (smaller is better) is presented in Table 3. In addition, Figure 2 clearly indicates optimal design parameters for this experimental design are 3 m/min for the first level of feed rate (A), 18000 rpm for the second level of spindle speed (B) and 2 mm for the first level of depth of cut (C). Accordingly, the optimum values were obtained at the A1B2C1 levels of surface roughness.

Table 3. Response table for signal to noise ratios of surface roughness (smaller is better)

Level	Feed rate (m/min)	Spindle speed (rpm)	Depth of cut (mm)
1	-12,53	-14,15	-13,08
2	-14,15	-13,75	-14,82
3	-14,40		
4	-14,70		
Delta	2,17	0,40	1,74
Rank	1	3	2

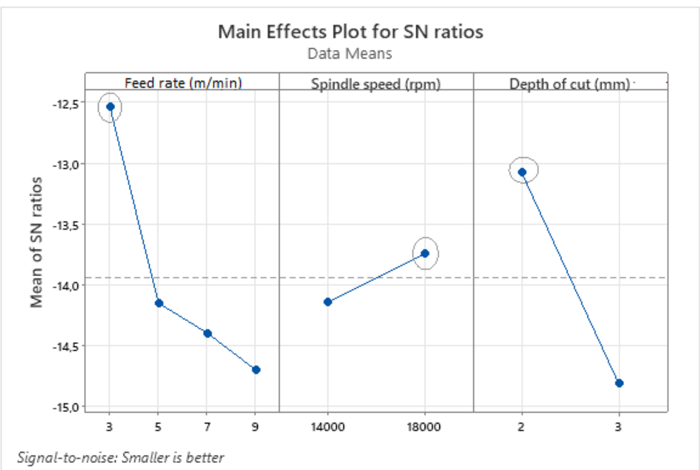

Figure 2. Main effects plot for S/N surface roughness ratio

The detailed analysis of the experimental results, carried out by means of variance analyses using signal-to-noise ratios, has revealed in detail the effects of the studied parameters on the surface roughness of wood (Table 4). This variance analysis was carried out at a 5% significance level and a 95% confidence level, with the aim of assessing the extent to which the selected output value is influenced by the factors studied and the variability induced by the different levels. In ANOVA, the significance of the control factors is determined by comparing the F-values of each control factor (Nas, Samtas and Demir, 2012).

Table 4. ANOVA results for surface roughness

Source	DF	Seq SS	Contribution	Adj SS	Adj MS	F-Value	P-Value
Feed rate (m/min)	3	3,5695	42,51%	3,5695	1,1898	41,98	0,000
Spindle speed (rpm)	1	0,3510	4,18%	0,3510	0,3510	12,38	0,006
Depth of cut (mm)	1	4,1922	49,93%	4,1922	4,1922	147,89	0,000
Error	10	0,2834	3,38%	0,2834	0,0283		
Lack-of-Fit	2	0,0694	0,83%	0,0694	0,0347	1,30	0,325
Pure Error	8	0,2140	2,55%	0,2140	0,0267		
Total	15	8,39629	100,00%				
R-sq= 96,62% R-sq(adj)= 94,94% Surface roughness = 5,0294-0,7869 Feed rate_3+ 0,0856 Feed rate_5+ 0,2506 Feed rate_7 + 0,4506 Feed rate (mm/s)_9+ 0,1481 Spindle speed_14000 - 0,1481 Spindle speed_18000- 0,5119 Depth of cut_2 + 0,5119 Depth of cut _3							

The results of the analysis show that all the parameters, namely feed rate (A), spindle speed (B) and depth of cut (C), have a significant influence on the surface roughness of the wood ($P>0.05$). The depth of cut parameter stands out as the most significant factor with a 49.93% effect on surface roughness. This is followed by feed rate with a 42.51% effect and spindle speed with a 4.18% effect. These results provide valuable insights into understanding and optimizing the effect of the parameters used in the experiment on wood surface roughness. In addition, the statistical reliability of the results obtained has been tested and an Rsq value of 96.62% has been obtained, indicating a high level of reliability in the modelling process of the data collected.

The Normal Probability plot visually illustrates the deviation of the measured values compared to the regression model equation (Fig. 3). Clustering around the line indicates low deviation values, which means minimal deviation in surface roughness values on this plot. This graphical analysis is an important tool for assessing the consistency and accuracy between the values predicted by the regression model and the actual measurements. The density around the line indicates the degree of agreement between the predicted and measured values, emphasizing the reliability of the model. Visually, this alignment indicates that the model is successfully predicting measurements, resulting in minimal variation in surface roughness values.

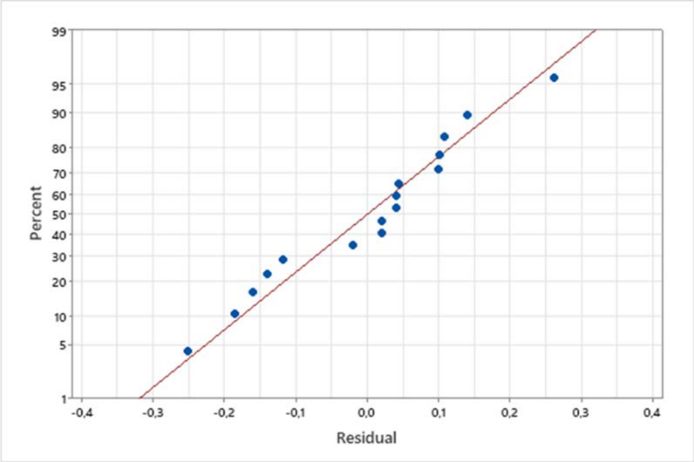

Figure 3. Normal probability plot for surface roughness

The normal probability plot is essential in assessing the performance of the regression model and provides insight into its effectiveness. Examining the clustering pattern helps to understand the level of agreement between predicted and observed values, particularly in the context of surface roughness. The plot effectively conveys the model's ability to make accurate predictions and its ability to minimize variation in surface roughness values. Overall, the normal probability plot provides valuable insight into the predictive accuracy of the model and the agreement between predicted and measured results (Nas and Altan Özbek, 2020).

Although a reduced depth of cut is generally expected to lead to a reduction in surface roughness, in certain cases a 3 mm depth of cut may be required. Thus, separate regression models were developed for 2mm and 3mm cuts (Table 5).

Table 5. Regression equations for different cutting depth

Depth of cut (mm)	Regression Equation
2	Surface roughness= 4,539 + 0,1939 Feed rate- 0,000074 Spindle speed
3	Surface roughness= 5,563 + 0,1939 Feed rate - 0,000074 Spindle speed
R-sq=89,92% R-sq(adj)= 87,41%	

These equations can be used to make more accurate predictions of surface roughness when calculating it for 2 mm and 3 mm depths of cut compared to the general equation. Therefore, the use of specific models for specific depths of cut can be of great value when trying to optimize or tailor surface roughness to specific requirements. Future studies could aim to investigate the effects of depth of cut variability on surface roughness in more detail, to understand the underlying reasons for these specific cases and to provide more information for optimized production processes. Evaluation of the effectiveness of regression models developed specifically for certain depths of cut in practical applications may be necessary for experimental studies. In addition, a comprehensive analysis addressing issues such as the generalizability of these models and their compatibility with different materials could improve knowledge in this area. Thus, this study, focusing on specific depths of cut, provides important insights that can guide future researchers.

It was then necessary to assess whether the system was performing the optimization accurately enough. The best results were obtained by using the Taguchi method to determine the confidence interval (CI) for the estimated Ra. This experiment was carried out to determine the relationship between the values estimated by the Taguchi method and the experimental results. The results showed that the predicted values in the regression analysis were within the CI limits (95%) (Figure 4).

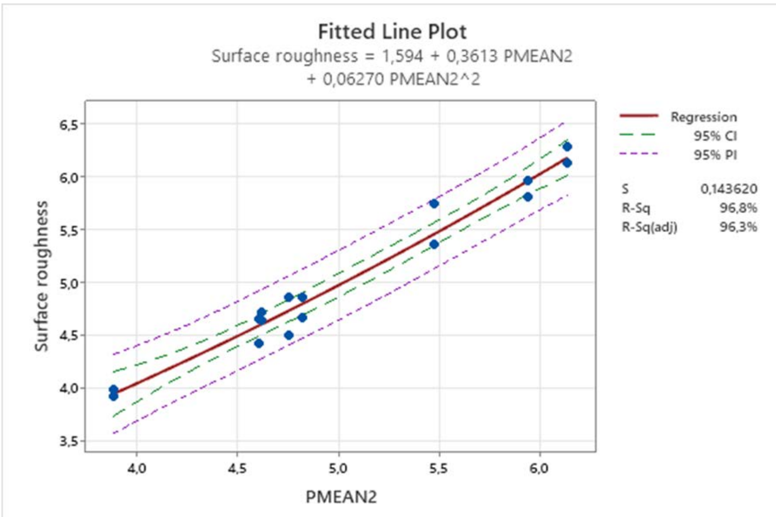

Figure 4. Comparison of experimental and predicted results.

4. CONCLUSION

The surface roughness value deduced from CNC machining of solid beech surfaces was found to be related to feed rate, spindle speed and depth of cut and was successfully modelled using the Taguchi experimental design method. The Taguchi experimental design model predicted the surface roughness values with 96.62% success with only 16 experiments. When the obtained equation was compared with the experimental and predicted values, the values were found to be in agreement with a success rate of 96.80%.

Cutting depth was found to have a greater effect on surface roughness than other factors with a rate of 49.93% and equations were developed to predict surface roughness for different cutting depths with a successful rate of 89.92%.

According to the results derived from the model, the combination of 3 m/min feed rate, 18000 rpm and 2 mm depth of cut is corrected by both experimental evidence and theoretical results for the lowest surface roughness in CNC machining of solid beech surfaces. In conclusion, the present results confirm that effective optimization can be achieved using a Taguchi experimental design model with a small number of experimental measurement points.

To sum up, it can be declared that the theoretical model correctly selected for this study allows researchers to easily and economically determine the optimum operating parameters for the most uniform surface roughness.

REFERENCES

Akbulut, T. and Ayrilmis, N. (2006). Effect of compression wood on surface roughness and surface absorption of medium density fiberboard. Silva Fennica, 40(1). doi:10.14214/sf.358

Altunpak, Y. and Akbulut, H. (2009) Effects of aging heat treatment on machinability of alumina short fiber reinforced LM 13 aluminum alloy, International Journal of Advanced Manufacturing Technology, 43, 449-454.

Altunpak, A., Aslan, S., Guler, M.O. and Akbulut, H. (2016) Effect of alternative heat-treatment parameters on the aging behavior of short-fiber-reinforced 2124 Al composites, Materiali in Tehnologije, 50, 1011-1016

Ayanleye, S., Nasir, V., Avramidis, S. and Cool, J. (2021). Effect of wood surface roughness on prediction of structural timber properties by infrared spectroscopy using ANFIS, ANN and PLS regression. European Journal of Wood and Wood Products, 79(1). doi:10.1007/s00107-020-01621-x

Budakçi, M., Ilçe, A. C., Gürleyen, T. and Utar, M. (2013). Determination of the surface roughness of heat-treated wood materials planed by the cutters of a horizontal milling machine. BioResources, 8(3). doi:10.15376/biores.8.3.3189-3199

Cota, H., Dritan, A., Habipi, B., Çota, H. and Ajdinaj, D. (2017). The influence of machining process on wood surface roughness. Albanian Journal of Agricultural Sciences.

De Moura, L. F. and Hernández, R. E. (2006). Effects of abrasiand mineral, grit size and feed speed on the quality of sanded surfaces of sugar maple wood. Wood Science and Technology, 40(6). doi:10.1007/s00226-006-0070-0

Demir, A., Cakiroglu, E. O. and Aydin, I. (2022). Determination of CNC processing parameters for the best wood surface quality via artificial neural network. Wood Material Science and Engineering, 17(6). doi:10.1080/17480272.2021.1929466

Gaitonde, V. N., Karnik, S. R. and Paulo Davim, J. (2008). Taguchi multiple-performance characteristics optimization in drilling of medium density fibreboard (MDF) to minimize delamination using utility concept. Journal of Materials Processing Technology, 196(1-3), 73-78. doi:10.1016/J.JMATPROTEC.2007.05.003

Gürgen, A., Çakmak, A., Yıldız, S. and Malkoçoğlu, A. (2022). Optimization of cnc operating parameters to minimize surface roughness of pinus sylandstris using integrated artificial neural network and genetic algorithm. Maderas: Ciencia y Tecnologia, 24. doi:10.4067/S0718-221X2022000100401

Hazir, E., Erdinler, E. S. and Koc, K. H. (2018). Optimization of CNC cutting parameters using design of experiment (DOE) and desirability function. Journal of Forestry Research, 29(5). doi:10.1007/s11676-017-0555-8

Hazir, E. and Koc, K. H. (2019). Optimization of wood machining parameters in CNC routers: Taguchi orthogonal array based simulated angling algorithm. Maderas: Ciencia y Tecnologia, 21(4). doi:10.4067/s0718-221x2019005000406

Hiziroglu, S. (1996). Surface roughness analysis of wood composites: A stylus method. Forest Products Journal, 46(7-8).

Ilçe, A. C. (2019). Determination of surface roughness based on the sanding parameters of oriental beech wood. BioResources, 13(3). doi:10.15376/biores.13.3.5942-5952

Kilic, M., Hiziroglu, S. and Burdurlu, E. (2006). Effect of machining on surface roughness of wood. Building and Environment, 41(8), 1074-1078. doi:10.1016/j.buildenv.2005.05.008

Koc, K. H., Erdinler, E. S., Hazir, E. and Öztürk, E. (2017). Effect of CNC application parameters on wooden surface quality. Measurement, 107, 12-18. doi:10.1016/j.measurement.2017.05.001

Laina, R., Sanz-Lobera, A., Villasante, A., López-Espí, P., Martínez-Rojas, J. A., Alpuente, J., … Vignote, S. (2017). Effect of the anatomical structure, wood properties and machining conditions on surface roughness of wood. Maderas: Ciencia y Tecnologia, 19(2). doi:10.4067/S0718-221X2017005000018

Lin, Y. C., Wu, K. Da, Shih, W. C., Hsu, P. K. and Hung, J. P. (2020). Prediction of surface roughness based on cutting parameters and machining vibration in end milling using regression method and artificial neural network. Applied Sciences (Switzerland), 10(11). doi:10.3390/app10113941

Loc, N. and Hung, T. Q. (2021). Optimization of Cutting Parameters on Surface Roughness and Productivity when Milling Wood Materials. Journal of Machine Engineering, 21(4), 72-89. doi:10.36897/jme/144426

Malkoçoğlu, A. (2007). Machining properties and surface roughness of various wood species planed in different conditions. Building and Environment, 42(7), 2562-2567. doi:10.1016/J.BUILDENV.2006.08.028

Nas, E. and Altan Özbek, N. (2020). Optimization of the machining parameters in turning of hardened hot work tool steel using cryogenically treated tools. Surface Review and Letters, 27(5). doi:10.1142/S0218625X19501774

Nas, E., Samtas, G. and Demir, H. (2012). Mathematically Modeling Parameters Influencing Surface Roughness in CNC Milling. Pamukkale Uniandrsity Journal of Engineering Sciences, 18(1). doi:10.5505/pajes.2012.58077

Pelit, H., Korkmaz, M. and Budakçı, M. (2021). Surface Roughness of Thermally Treated Wood Cut with Different Parameters in CNC Router Machine. BioResources, 16(3). doi:10.15376/biores.16.3.5133-5147

Prakash, S., Mercy, J. L. and Goswami, K. (2014). A systemic approach for evaluating surface roughness parameters during drilling of medium density fiberboard using Taguchi method. Indian Journal of Science and Technology, 7(11). doi:10.17485/ijst/2014/v7i11.21

Rabiei, F. and Yaghoubi, S. (2023). A comprehensiand inandstigation on the influences of optimal CNC wood machining variables on surface quality and process time using GMDH neural network and bees optimization algorithm. Materials Today Communications, 36. doi:10.1016/j.mtcomm.2023.106482

Ratnam, M. M. (2017). Factors Affecting Surface Roughness in Finish Turning. Comprehensiand Materials Finishing içinde (C. 1-3). doi:10.1016/B978-0-12-803581-8.09147-5

Sandak, J. and Tanaka, C. (2003). Evaluation of surface smoothness by laser displacement sensor 1: Effect of wood species. Journal of Wood Science, 49(4). doi:10.1007/s10086-002-0486-6

Singer, H. and Özşahin, Ş. (2022). Prioritization of factors affecting surface roughness of wood and wood-based materials in CNC machining: a fuzzy analytic hierarchy process model. Wood Material Science and Engineering, 17(2). doi:10.1080/17480272.2020.1778079

Sofuoglu, S. D. (2015). Determination of Optimal Machining Parameters of Massiand Wooden Edge-Glued Panels Made of European larch (Larix decidua Mill.) using Taguchi Design Method. BioResources, 10(4). doi:10.15376/biores.10.4.7772-7781

Sulaiman, O., Hashim, R., Subari, K. and Liang, C. K. (2009). Effect of sanding on surface roughness of rubberwood. Journal of Materials Processing Technology, 209(8). doi:10.1016/j.jmatprotec.2008.09.009

Thoma, H., Peri, L. and Lato, E. (2015). Evaluation of wood surface roughness depending on species characteristics. Maderas: Ciencia y Tecnologia, 17(2). doi:10.4067/S0718-221X2015005000027

Tiryaki, S., Malkoçoğlu, A. and Özşahin, Ş. (2014). Using artificial neural networks for modeling surface roughness of wood in machining process. Construction and Building Materials, 66. doi:10.1016/j.conbuildmat.2014.05.098

Ulgen, C., Yildirim, A. B., Sahin, G. And Turker, A. U. (2021). Do magnetic field applications affect in vitro regeneration, growth, phenolic profiles, antioxidant potential and defense enzyme activities (SOD, CAT and PAL) in lemon balm (Melissa officinalis L.)? Industrial Crops and Products, 169, 113624.

Ulgen, C., Yıldırım, A.B. and Turker, A.U. (2017). Effect of magnetic field treatments on seed germination of melissa officinalis L. International Journal of Secondary Metabolite, 4(3, Special Issue 1), 43-49.

Ulgen, C., Yildirim, A. and Turker, A. (2020). Enhancement of plant regeneration in lemon balm (Melissa officinalis L.) with different magnetic field applications. International Journal of Secondary Metabolite, 7(2), 99-108.

Ulgen, C., Yildirim, A. and Turker, A. (2023). Melissa officinalis: Antibacterial and Antioxidant Potential, Phenolic Profile and Enzyme Activities. Kahramanmaraş Sütçü İmam Üniversitesi Tarım ve Doğa Dergisi, 26(5), 1075-1085.

Yang, C., Ma, Y., Liu, T., Ding, Y. and Qu, W. (2023). Experimental Study of Surface Roughness of Pine Wood by High-Speed Milling. Forests, 14(6). doi:10.3390/f14061275

Zeqiri, F., Alkan, M., Kaya, B. and Toros, S. (2018). Experimental Research and Mathematical Modeling of Parameters Effecting on Cutting Force and Surface Roughness in CNC Turning Process. IOP Conference Series: Materials

Science and Engineering içinde (C. 295). doi:10.1088/1757-899X/295/1/012011

DEVELOPMENTS IN ROBOTIC SYSTEMS AND IMAGE PROCESSING APPLICATIONS IN ROBOTIC SYSTEMS

Mehmet GÜL[1]

1. INTRODUCTION

The variety of applications based on artificial intelligence (AI) is increasing by the day. Especially, applications carried out by robotic automation systems have a distinct place among the most striking concrete applications among AI applications. In this study, firstly, general information regarding the components and working principles used in robotic automation systems and the usage areas of AI in robotic automation systems will be given.

2. FOUNDER OF ROBOTICS (CYBERNETICS)

The Muslim scientist, whose short name is Al-Jazari, was born in Cizre around 900 years ago. The Muslim scholar who is regarded as the creator of cybernetics worked in the Mesudiye madrasah in Diyarbakır under the patronage of the Artuqid Sultan of the period, El-Salîh Nâsîrüddîn Ebû'l-Feth Mahmûd bin Muhammed bin Karaaslan bin Davûd ibn Sukmân bin Artuk (1200–1222). El-Cezeri's given name is "Ebû'l İz İbni İsmail İbni

[1] Assist. Prof. Dr., Şırnak University, Faculty of Engineering, Computer Engineering, Şırnak-Türkiye, 73100, email: mgul@sirnak.edu.tr; mehmetgul@ymail.com ; ORCID: 0000-0002-4819-4743

Rezzaz El Cezerî". It is widely acknowledged that Al-Jazari's automatic devices are the foundations of today's mechanical and cybernetic sciences. The works of the Muslim scientist, the founder of the science of cybernetics, were published in a book called Kütab-ül Hiyel. Mechanical clocks are among the most notable works he created, far ahead of his time. These clocks are developed using the method of establishing balance with hydro-mechanical effects. He designed extremely complex mechanical systems that are astonishing even today, and his work appealed far beyond his time. The Elephant Water Clock is the most prominent example of a mechanical watch among his masterpieces (Figure 1). Detailed drawings, calculations, and visuals of the robotic automation machines he developed are included in the book Kütab-ül Hüel. Today, his book is exhibited in the Topkapı Palace Museum. This study is attributed to Al-Jazari, the founder of cybernetic science (El Cezeri, n.d.).

Figure 1: Elephant Water Clock (Cezeri, n.d.)

3. ROBOT

Robotic systems, which are increasingly being used in practically every field in the developing world, are now becoming more cost-effective and widely available. Their use is expanding in many fields, including health, industrial, educational, and agricultural applications, among others. Especially, the use of robots in the plant regeneration, industrial crops and products to regulate, follow, and improve the enzyme activities is thought to make the main duties of scientists easier. It is well known that several researchers have endeavored to overcome the problems mentioned above by using different techniques such as exposure of the plants to different magnetic field strengths (Ulgen et. al, 2020; Ulgen, et. al, 2017). Namely, the use of robotics in many application areas makes the works and lives of humanity easier in every sense. To briefly define a robot, it is a mechanical structure in which programmable moving elements are used to perform a specific purpose. Almost all robotic systems consist of three basic components: an actuator, a driver, and a control unit.

4. ACTUATORS

If the robot is considered to be a moving mechanical vehicle, the general structures that move the robot are actuators. There are two kinds of actuators used to operate robotic systems: structures that move with fluid power control and structures that move with electric power control. For example, the movement of a robotic arm, the movement of robot fingers, aerial vehicle movement, etc. Actuators need a power source and signal for control purposes. The fact that the sent signal is programmable can be considered as controlling the robot. Mechanical parameters such as speed, torque, position, and acceleration can be controlled with signals sent to actuators ("Actuator Principles and Classification," n.d.).

There are two types of fluid power controls: hydraulic systems and pneumatic systems.

4.1. Hydraulic Systems

These are moving constructions that are mostly constructed predominantly using liquid fluids. Among the fluids used, petroleum-derived oils, synthetic oils, water and many other liquids can be used.

4.2. Pneumatic systems

These are moving constructions realized by air control. Systems can be programmed by using valves in pneumatic systems.

5. ELECTRICAL POWER CONTROLS

Electrical power controls are also known as motors. When compared to fluid power control systems, electric motion elements have some advantages. These advantages are respectively:

- Can be used in more sensitive studies.
- The mechanical device used to provide movement is smaller and lighter.

- Since there is no use of liquid or gas, the environment is least polluted in case of possible accidents.
- Easy assembly and repair are possible.

On the other hand, situations such as electric shock due to possible electrical leakage and overheating during long periods of operation can be listed as conspicuous disadvantages of electric power units. Structures known as electric power units are also known as motor units. There are several types of motors used in the joints of robots, enabling the movement of the robot (Dev Shrestha, 2019).

6. DC MOTOR

It is the most common form of motor, converting direct current electrical energy into mechanical energy. There are two magnets with opposite magnetic poles inside the motor. Movement is achieved through the impact of the fixed position rotor and stator pushing or pulling on each other. DC motors are classified as follows based on the additional components they contain: brushed DC motors and brushless DC motors are two types of DC motors.

6.1. Brushed Dc Motor

It is known as the most basic DC motor type. This motor model, designed to be operated with direct current, has been in use for over a century. Changing the strength of the driving voltage or magnetic field controls the motor’s speed. It has complex features due to its brush and commutator structure. Especially the brush that needs to be replaced makes regular maintenance essential. It is extremely easy to control. For this reason it is very common.

6.2. Brushless DC Motor

It is made up of two main components: stator and rotor. The rotor is a bipolar permanent magnet, while the stator consists of coil winding. This motor structure includes permanent magnets, windings, magnetic pole sensors and driver circuits. It is extremely successful in terms of controllability of engine speed and energy saving.

6.3. Difference Between Brushed and Brushless DC Motors

Friction in brushless motors is minimal compared to brushed motors. As a result, efficiency is at the highest level. On the other hand, since brushless motors do not have any brushes, there is no need for regular maintenance. The most significant disadvantage of the brushless motor compared to the brushed motor is the need for the driver during operation (https://nit-edu.org/wp-content/uploads/2021/09/ch-29-Dc-motor.pdf, n.d.).

7. STEP MOTOR

A stepper motor is an electromechanical device that converts electrical energy into rotational motion and physical energy. It is a brushless motor with a programmable rotating movement. The number of steps required for one full cycle must be reached. The step numbers of stepper motors are not fixed. If

200 steps are required for a 360-degree rotation effect, each step corresponds to 360/200 = 1.8 degrees. When its mechanical structure is examined, it includes a rotor, stator, and bearing. The bearings allow the shaft linked to the rotor to move freely. The polarity of the stator, which has more than one pole, is constantly changing via electronic switches. The rotation direction of the stepper motor, which is also considered a stepper motor, can be changed clockwise or counterclockwise by changing the order of applied signals. As a result, stepper motors are useful motors used in robotic automation systems as a type of motor whose speed, direction of rotation, step degree, and position can always be determined (https://www.megep.meb.gov.tr/mte_program_modul/moduller_pdf/Step-servo%20Motorlar.pdf, 2011).

8. SERVO MOTOR

The servo motor is an exceptionally effective motor with variable rotation angles. The servo motor is designed to reach a desired position between 0 and 180 degrees. The servo motor's interior structure contains a DC or AC servo motor. To increase the sensitivity of the servo motor, the position of the shaft is determined by a control circuit as well as a potentiometer or encoder in the internal structure of the servo motor. In this manner, the steps of the servo motor can be controlled. Servo motors mainly have three output connections. While two outputs of connections are used to energize the motor, the last one reports the position of the motor shaft. The servo motor driver circuit is an electronic amplifier that provides coded signals to the motor mechanism, allowing the ability to rotate the motor shaft in its angular position. Servo motors operate in a sensitive structure because they reduce the angular shaft movement and vibration level during operation. Although servo motors include an internal driver circuit that allows for angular movement, an external driver circuit is also required. The disadvantage of servo motors is that they require a microcontroller or RC control receiver to move them (https://www.megep.meb.gov.tr/mte_program_modul/moduller_pdf/Step-servo%20Motorlar.pdf, 2011; Servo Motor, n.d.).

Features of servo motors:

- It is more preferred in mechanical works that require precision,
- It gains angular rotation feature thanks to the encoder inside,
- Can be controlled by the driver,
- It is programmable

Servo motors are divided into two types according to the type of motor they use in their internal structure; DC Servo motor and AC Servo motor.

8.1. Dc Servo Motor

The potentiometer used in the internal structure of the DC servo motor creates resistance equal to the amount of angular rotation. In this manner, the angular value is sent to the control circuit inside the servo motor, and the motor is controlled at a more precise angle. The task of the control circuit is to maintain the position of the servo motor at the specified angle. If the servo motor is at the specified angle value, the motor does not run; if not, it runs the motor until it reaches the specified angle value. When the servo motor approaches the desired position, the operating speed of the motor is slowed down, thus increasing the sensitivity of the motor.

8.2. AC Servo Motor

It is called an AC servo motor because it has a motor that uses alternating current (AC). Since the angular value of servo motors is controllable, unlike other motor types, motion control is carried out with an encoder. In this manner, the rotation action that provides angular sensitivity is performed. The main aspect that separates DC motors is that they are employed in jobs that require a lot of power. On the other hand, as much torque as DC servo motors is not obtained. There are also some that have the capacity to operate at high frequency values. It is particularly preferred in applications such as CNC machines and heavy industry machines. The rotors in AC servo motors with two or three phase inputs have a short-circuit rod or natural magnet structure.

9. DRIVER

Motor drivers generally refer to devices that help start motors. To use the motor driver, there must be a motor driver chip on the motor to be used. The driver serves as a link between the motor and the microcontroller. The main reason for this is that the microcontroller and the motor work at different voltage levels. In terms of power requirements, motors always require a higher current than microcontrollers. In general, different motor drivers are used according to the different motor types used. Although the application purposes of low-power model servo motor drivers for engineering students and servo motor drivers used in heavy industrial machines are the same, their circuit diagrams are substantially different. The most important feature sought in motor drivers is voltage-current compatibility. The voltage and current required in any robotic automation system to be developed must be determined in advance.

10. MOTOR DRIVER TYPES

There are differences between drivers depending on the engine types they are used in, automation systems that provide off-speed control, automation systems that provide high-speed control, and so on. While it is possible to control a motor with more than one different motor driver, there are also single motor drivers developed for the use of only a motor (Table 1).

Table 1: Some types of motors and drivers they used.

Motor kinds	Driver kinds
Step motor	L293D, A4988, A3967, L9110, TB6600, Ma860, TB6560
Servo motor	PCA9685, PL-1350,
DC Motor	L298N, BTS7960B, L9110,

Thanks to the microcontroller on the motor driver, the motor is controlled by sending a signal to the motor. Control signals coming from the microcontroller are analyzed and controlled based on the power required by the motor. In other words, direct motor control cannot be achieved with a microcontroller. Because the motor necessitates a high voltage. Motor control is accomplished by adjusting the microcontroller's current value to match the current required by the motor (Motor Drivers, n.d.).

11. THE USED CONTROL UNIT IN ROBOTIC AUTOMATION SYSTEMS

Robotic automation systems are the most essential players in Industry 4.0's fast-growing industrial control systems. It is possible to transform any industrial unit into a smart system with the developed robotic automation system. Thanks to developing industrial infrastructures, there are now many I/O connection points even in the ordinary production stage, and it continues to grow day by day. To overcome such situations, especially 5G and AI-supported industrial automation systems are used. With automation systems established with real-time and high-speed data transfer, highly sensitive processes can be watched, monitored, and controlled. Different control units are used in developed automation systems. For instance, while a single mainboard such as Arduino or Rasberry Pi can be used in the automation system developed by an engineering student, the control units required in industrial factories can be used with a server-based advanced computer with high processing capacity.

12. ARTIFICIAL INTELLIGENCE APPLICATIONS IN ROBOTIC AUTOMATION SYSTEMS

Image processing applications are being used in many industrial organizations at various phases, from the manufacturing process to the final stage, the packaging process. Especially in the automation system, some applications are of extremely critical importance in the control stages. Image processing applications in robotic automation systems are extremely diverse.

13. ROBOTIC AUTOMATION

The first thing that springs to mind when discussing robotic automation systems is industrial automation systems. The first thing that comes to mind when discussing robotic automation systems is industrial automation systems. It is extremely important to increase production capacity in industrial production centers to keep up with the ever-increasing production supply and supply with Industry 4.0. There are robotic automation systems that can be developed for almost every production center. In this respect, the use of robotic automation on both the investigation of antibacterial and antioxidant potential and regulation of enzyme activities belonging to the plants (Wang, et. al, 2023; Ulgen, et. al, 2021; Zhou et. al, 2023; Ulgen et. al, 2023) as well as the mass production of materials is of important. The production center where an example robotic automation system is used is shown in Figure 2.

Figure 2: Robotic automation system used in the food industry

Today, robotic automation is not used only in centers that carry out industrial production. Robotic systems are used in open or closed agricultural areas for greenhouse production and agricultural production. Many different areas of use have attracted attention among agricultural robotic systems in recent years. It is possible to demonstrate the destruction of dangerous plants on agricultural land using autonomous robotic vehicles rather than drones (Figure 3).

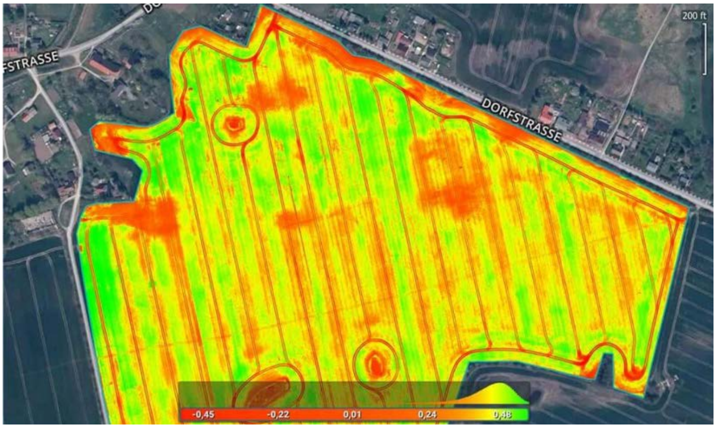

Figure 3: The weed detection with agricultural drone

Harmful plants can be detected in the images obtained with the camera system on the drone, thus reducing the use of pesticides. When dangerous weeds are detected, they are eradicated by burning before they grow to a size that can harm plants (Figure 4).

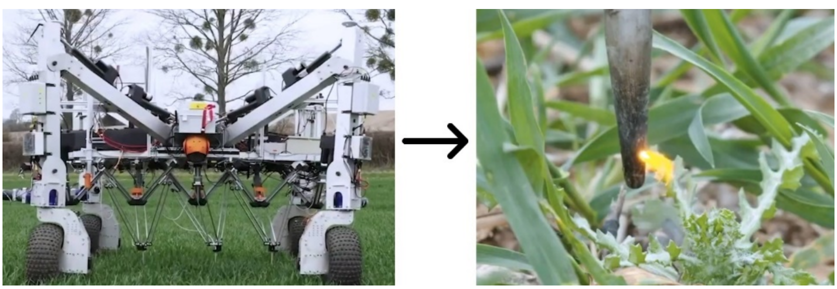

Figure 4: The elimination of detected weeds by burning method

Robotic systems, on the other hand, can be used to harvest crops, particularly in settings such as greenhouses, and they can even be utilized to harvest crops in open agricultural lands. Some of the most common examples in this field are the harvesting of products such as tomatoes, strawberries, etc. in the greenhouse, etc. by autonomous movement via a robot arm on a platform (Figure 5).

Figure 5: Berry robot harvesting strawberries in greenhouse.

14. DRONE SYSTEMS

Another notable example of essentially robotic automation applications is drone systems. Agricultural drone applications are among the most common image-processing applications in drone systems. When agricultural drones are mentioned, the first association that comes to mind is agricultural fertilization and pesticide applications. Some useful plants are damaged during the traditional agricultural spraying process due to the movement of agricultural spraying vehicles. On the other hand, there is no such product loss with pesticide application using agricultural drones. If image analysis is performed on drone systems used for agricultural purposes, this efficiency will be extremely high. During the agricultural spraying process, the entire agricultural land is sprayed, damaging the ecosystem with excessive use of pesticides and the residues of the pesticides used to reach the end customer, humans. The pesticides, however, also cause some damage to useful plants (Osman TİRYAKİ et al., 2010). Image processing can be used to conduct a highly successful investigation with pesticide methods. Some of the prominent benefits obtained from this type of transaction can be listed as follows: fewer pesticides are used, pesticides are applied in a shorter time, the ecosystem is protected at an optimum level, and damage to useful plants due to agricultural pesticides is avoided.

Agricultural drone applications are exclusively used in spraying or fertilization processes. Agricultural drones can also be used to pollinate plants. As it is known, bumblebees are used in the most common plant pollination process used in greenhouses. Pollination can be accomplished with a high-tech drone (Figure 6).

Figure 6: Bumblebees used for plant pollination in the greenhouse

Thanks to the developed micro drone, the pollination process of plants is tried to be carried out in this way. Figure 7 can be shown as an example of this type of micro drone, which is in the development process today.

Figure 7: Micro drone that undertakes the pollination process of plants

The last work to be given in this section among agricultural drone applications is the harvesting of crops. In the greenhouse, it may, for example, be possible to harvest products such as peppers, tomatoes, strawberries, and so on. Moreover, it may be possible to harvest products such as apples, pears, and etc. on open agricultural lands. Harvesting such products can also be done with a drone (Figure 8).

Figure 8: Agricultural drone harvesting apples

15. CONCLUSION

Bundan yaklaşık 900 yıl önce ilk kez sibernetik biliminin insanlar ile tanışması ve günümüzde sanayi devrimi ile beraber ortaya çıkan fabrikalar ve arz-talep dengesinde sibernetik biliminin son derece yararlı örnekleri kullanıldı. Sanayi devriminden özellikle Endüstri 4.0 ile sibernetik bilimindeki gelişmeler giderek hızlanmakta ve ortaya son derece dikkat çekici örnek geliştirilmeye devam edilmektedir. Çalışma kapsamında sibernetik biliminin kısa bir tanıtımı yapılmak ile beraber özellikle yakın zamanda kullanılan en son gelişmelerden göze çarpan örnekler hakkında bilgi verildi. Bu çalışmanın sibernetik (robotik) bilimi ilgili araştırma yapan araştırmacılara, bu alanda gerçekleşen yenilikler hakkında ışık tutması düşünülmektedir.

ACKNOWLEDGEMENT

This study is attributed to Al-Jazari, the founder of cybernetics-robotics science.

Approximately 900 years ago, cybernetic science was introduced to humanity for the first time, and today, incredibly important examples of cybernetic science were used in the factories and supply-demand balance that emerged with the industrial revolution. With the industrial revolution, particularly Industry 4.0, advances in cybernetic research are accelerating, and extremely remarkable examples continue to be developed. Within the scope of the study, a brief introduction to the science of cybernetics was provided, as well as information on prominent examples of current advances that have been applied. This study is expected to give light on the developments in this field for researchers working on cybernetics (robotics).

REFERENCE

Actuator Principles and Classification. (n.d.). In *Design Rules for Actuators in Active Mechanical Systems* (pp. 3–28).

Cezeri. (n.d.). Https://Cezeri.Meb.K12.Tr/Meb_iys_dosyalar/06/27/763695/Dosyalar/2019_02/03163849_Filli_su_saati.Pdf?CHK=c156e05dc9243a3c4e7ed249fdace327.

Dev Shrestha. (2019). Electric power controls.

El Cezeri. (n.d.). Https://Tr.Wikipedia.Org/Wiki/Cezer%C3%AE.

https://nit-edu.org/wp-content/uploads/2021/09/ch-29-Dc-motor.pdf. (n.d.). DC Motor (pp. 996–1030).

https://www.megep.meb.gov.tr/mte_program_modul/moduller_pdf/Step-servo%20Motorlar.pdf. (2011). Step ve Servo Motorlar.

Motor Drivers. (n.d.). Https://Www.Ourpcb.Com/What-Is-Motor-Driver.Html.

Osman TİRYAKİ, Ramazan CANHİLAL, & Sümer HORUZ. (2010). Tarım ilaçları kullanımı ve riskleri . Erciyes Üniversitesi Fen Bilimleri Enstitüsü Dergisi, 26(2), 154–169.

Servo Motor. (n.d.). Https://Www.Aksaotomasyon.Com/Servo-Motor-Nedir-Cesitleri-Nelerdir/.

Ulgen, C., Yıldırım, A.B. and Turker, A.U. (2017). Effect of magnetic field treatments on seed germination of melissa officinalis L. International Journal of Secondary Metabolite, 4(3, Special Issue 1), 43-49.

Ulgen, C., Yildirim, A. and Turker, A. (2020). Enhancement of plant regeneration in lemon balm (Melissa officinalis L.) with different magnetic field applications. International Journal of Secondary Metabolite, 7(2), 99-108.

Ulgen, C., Yildirim, A. B., Sahin, G. and Turker, A. U. (2021). Do magnetic field applications affect in vitro regeneration, growth, phenolic profiles, antioxidant potential and defense enzyme activities (SOD, CAT and PAL) in lemon balm (Melissa officinalis L.)? Industrial Crops and Products, 169, 113624.

Ulgen, C., Yildirim, A. and Turker, A. (2023). Melissa officinalis: Antibacterial and Antioxidant Potential, Phenolic Profile and Enzyme Activities. Kahramanmaraş Sütçü İmam Üniversitesi Tarım ve Doğa Dergisi, 26(5), 1075-1085.

Wang, X. Y.,Meng, Z. Q., and Chen, C. Q. (2023). Robotic Materials Transformable Between Elasticity and Plasticity, Advances Science, 10(13), 2206637

Zhou, X. Y., and Cao, W. H. (2023). Flexible and Stretchable Carbon-Based Sensors and Actuators for Soft Robots, Nanomaterials, 13(2), 316

INCREASING THE ELECTRODE LIFE AND WELDING QUALITY USED IN RESISTANCE WELDING OF KITCHEN OVEN GRILL WIRES

Fatih TAŞKIN[1,2], Yahya ALTUNPAK[3]

1. INTRODUCTION

Electric resistance spot welding (RSW) is used to join two or more work pieces (Gugel, 1995). Some mechanical or electrical mechanisms and control units are required to prevent an arc from occurring when combining and separating the electrodes. Determining and controlling current, pressure and dead times throughout the electrical resistance plays an important role for welding process (Peşint, 2000; Gourd, 1995; Keleş, 2008; Kurşungöz, 1986). The pressure force required for RSW can be provided form the different sources such as pneumatically, hydraulically or mechanically. Besides, the theoretical vibrational analysis can increase the lifespan of welding process (Bilge and Morgul, 2023). Of the process, the pneumatic systems are more preferred due to their faster and more economical. All systems

[1] This study was produced from the master's thesis titled "Increasing Resistance Weld Strength in Cross-Wire Steel Gratings Used in Kitchen Ovens", completed by F. Taşkın in 2022, at Bolu Abant İzzet Baysal University, Institute of Science, Department of Mechanical Engineering.

[2] Mefa Group, fatih_taskin14@hotmail.com, ORCID NO: 0000-0001-9207-360X,

[3] Prof Dr, Bolu Abant İzzet Baysal University, Department of Mechanical Engineering), altunpak_y@ibu.edu.tr, ORCID NO: 0000-0001-8676-4789.

generally work with the lower electrode fixed and the upper electrode mobile (Altun, 2012; Esendir, 2008). This method, being mostly used in joining low carbon steel sheets and wires, has also begun to be widely used in joining stainless steels (Onsekiz and Altunpak, 2018; Bilge et al, 2019; Gavas et al., 2013; Akyol, 2001). The method of RSW has widely been used in the welding of different materials used in many fields such as electrotechnics and pipe and profile production, especially in the automotive, steel constructions and white goods industry. Compared to other welding methods; it has many advantages such as being suitable for mass production, no need for qualified welders, short production time, suitability for automation and high welding strength. An average of 5000 spot welds is applied to sedan car bodies produced today (Doruk 2015, Donders 2005, Geißler 2011, Sonat 1999). Approximately 85% of the welded joints on a vehicle body are resistance spot welding (Doruk 2015). Wire grates used in kitchen ovens possess 40-50 resistance spot welds in an average product for only Mefa A.Ş. within Arçelik A.Ş. Cooking Appliances Business, Bsh, Candy Haier, Defy and Electrolux etc. Approximately 18,000 oven inner grills are produced daily for companies. This shows that approximately 720,000-900,000 resistance spot welds are used in Mefa A.Ş.'s daily oven inner grill production. It is clear that this number will be much higher when other companies producing for white goods manufacturers in Turkey are also considered. In the light of these data, it is clearly seen how important the determination and research of optimum welding parameters is in terms of both weld strength and electrode life in welding studies to be carried out in the field of white goods industry.

Depending on the developing technology, welding techniques that can apply high pressure and current in a shorter time and with less energy have been developed (Almus, 2006). Most of the automatic resistance welding machines use a current and time controlled resistance spot welding machine (Anık 1991, Akkuş 2006, Megep 2014).

In order to determine the optimum welding parameters (such as welding time and pressure) for resistance spot welded structures, there are many studies conducted with the finite element method as well as mechanical experiments (Onsekiz and Altunpak 2019, Shanmugam 2010, Zhang 2000, Salvini 2000).

The majority of studies on spot resistance welding of low-carbon steels are on the welding of flat products (such as automotive body sheet metal) (Doruk 2015). Studies on resistance welding of cross-wire steels are generally related to the resistance welding of cross-bar construction steels (mesh) with a thickness of approximately 8-10 mm to be used in civil engineering fields (Nielsen 2021).

Cross wire welding is one of the most common non-automotive applications of resistance welding. The primary use of cross wire welding is in the electronics industry and wire mesh manufacturing. In electronics, wires are welded together in light bulbs, as presented by Goodman (1950), who discussed the loads that the joints would experience over the life of the bulb, together with their ultimate failure mode. Knowlson (1967) gives other examples of cross-wire welding in electronics; that is, welding various components such as resistors, capacitors, diodes and transistors into small devices close together, are examples. It is used in various products such as wire mesh, kitchen clothes, shopping carts and strengthening concrete structures. Jones (1948), Wängsjö and Palmqvist (1958), Fukumoto et al. (2008) examined the cross-wire welding of microwires and the resulting microstructures and strengths.

In order to keep the heating of the electrodes to a minimum, the electrodes must have high electrical conductivity, low contact resistance and high thermal conductivity to remove heat from the electrode tip. In addition, it must have high heat resistance to withstand the high pressure applied. When welding parts of the same composition and thickness, the tip diameters of the electrodes must be the same. Especially as the tip of the electrode wears out or due to fungus, the diameter of the weld core increases, leading to the reduction of the current density. On this basis, the weld quality will negatively be affected since the heat released will not be sufficient (Kaya 2010, Anık 1993).

In resistance welding applications, pure copper electrodes were previously generally used because they were very good conductors. However, many different hard copper alloys with sufficient high mechanical (such as hardness and temperature resistance) and physical properties (sufficient electrical and thermal conductivity) have begun to be used as electrode materials in automation systems where higher current intensity, electrode force and welding speed are used. The electrode alloy with the most suitable properties for the workpiece material to be welded should be used. For example, electrode materials with high conductivity are preferred in resistance welding of aluminium parts, and electrode materials with high hardness and compressive strength are preferred in welding stainless steels. Generally, as hardness and strength increase, the electrical conductivity of alloys decreases (ASM Metals Handbook 1983, Almus 2006). Electrode materials must have high thermal and electrical conductivity and creep resistance. These properties should not deteriorate at high temperatures (Ünlükal 2007). Electrodes must be able to resist the applied forces without excessive deformation (Kaya 2010, Keleş 2008).

The aim of this study is to use an alternative electrode material in resistance spot welding of grill wires of kitchen ovens. For this purpose, Ø6.5 mm and Ø2.3 mm low carbon and low silicon SAE 1006 quality wires were welded with resistance spot welding using 2 different electrode materials (CuCoBe(CBN) and $CuNi_3Si$(CuproNSH)) and different welding parameters. The maximum tensile strength of the welding joints was determined, the microstructures were examined and the lifetimes of the electrodes were compared with each other by welding with the optimum parameters. The welds are made using a current controlled and timed industrial resistance spot welding machine (HKTM) operating at 1000 Hz with a capacity of 40 kA and controlled by a programmable logic controller (PLC). Optical examination of welded products was carried out using Nikon brand microscope. Chatillon brand dynamometer was used to measure the maximum tensile strength. Mitutoyo brand gauge was used to measure the deformation of the electrodes.

2. EXPERIMENTAL DETAILS

In this study; SAE 1006 quality low carbon steel of Ø6.5 mm and Ø2.3 mm, used in the white goods industry, was selected. The chemical composition and mechanical properties of the SAE 1006 low carbon steel used in this study, specified in the company catalogue, are given in Table 1. The spectral analysis values of the electrode materials used in welding works in the catalog of the relevant companies (Sağlam metal, Arslan welding metal) are given in Table 2. Measurements of the chemical composition, hardness and electrical conductivity values of the electrodes in question were also carried out by TSE through the Mefa company, and the results obtained were compared with the catalog values of the electrode manufacturer companies.

Table 1. Chemical composition and mechanical properties of SAE 1006 low carbon steel used in the experiments.

Chemical composition						Mechanical Properties	
C	Si	Mn	P	S	Cu	YP(MPa)	TS(MPa)
0,05	0,05	0,35	0,01	0,01	0,19	242	353

YP (Yield strength); TS (Tensile strength)

A water-cooled, 40 kA capacity, operating at 1000 Hz, current and time controlled spot resistance welding machine from Mefa company was used in the welding works (See Fig. 1). In the welding work of the products, CuCoBe (CB4) electrodes with dimensions of 20x40x80 mm, obtained from Arslan Kaynak Metal, and $CuNi_3Si$ (Cupro NSH) electrodes, purchased from Sağlam Metal, were used. In welding studies, a constant electrode pressure force of 480 N was used and different welding parameters were tested using welding times of 8, 12 and 16 ms and welding current values of 8, 9, 10 and 12 kA, respectively.

Table 2. Spectral analysis of electrode materials used in experiments

Alloy standard	Chemical composition	Hardness (HB)	Electrical conductivity
CuCoBe (CB4) C17500	Co 2.3, Be 0.5, the rest Cu	220-266	≥43
$CuNi_3Si$ (Cupro NSH)	Ni3, Si 0.9, Cr0.4, others max 0.2, the rest Cu	220-240	≥40-43

In the figures given below, the mesh welding fixture designed and used to ensure standardization in joining wires with resistance spot welding are depicted in Fig. 2a, the way the wires are arranged in the fixture before welding as shown in Fig. 2b, the different positions of the fixture on the machine for welding are displayed in Fig. 2c and Fig. 2d, respectively. After the welding operation is completed, the fixture returns to its starting position (See Fig. 2e). Figure 2f shows a photo of an oven interior grill whose resistance spot welding operation has been completed before chrome plating.

Photo 2.1. Resistance spot welding machine used in welding works

In Fig. 3a, the photo of the CuCoBe electrode before welding is shown, and in Fig. 3 b, the photo of the CuCoBe electrode after the welding process is shown. In Fig. 3c, the photo of the $CuNi_3Si$ electrode before welding is shown, and in Fig. 3d, the photo of the $CuNi_3Si$ electrode after the welding process is shown.

For metallographic examination, samples were prepared using standard metallography procedure and the samples were etched (with nitric acid) in a prepared solution. Then, the weld core of the welded low carbon steel samples was examined using a Nikon brand optical microscope. The tensile strength of the welded parts was measured using the Chatillon brand tensile device.

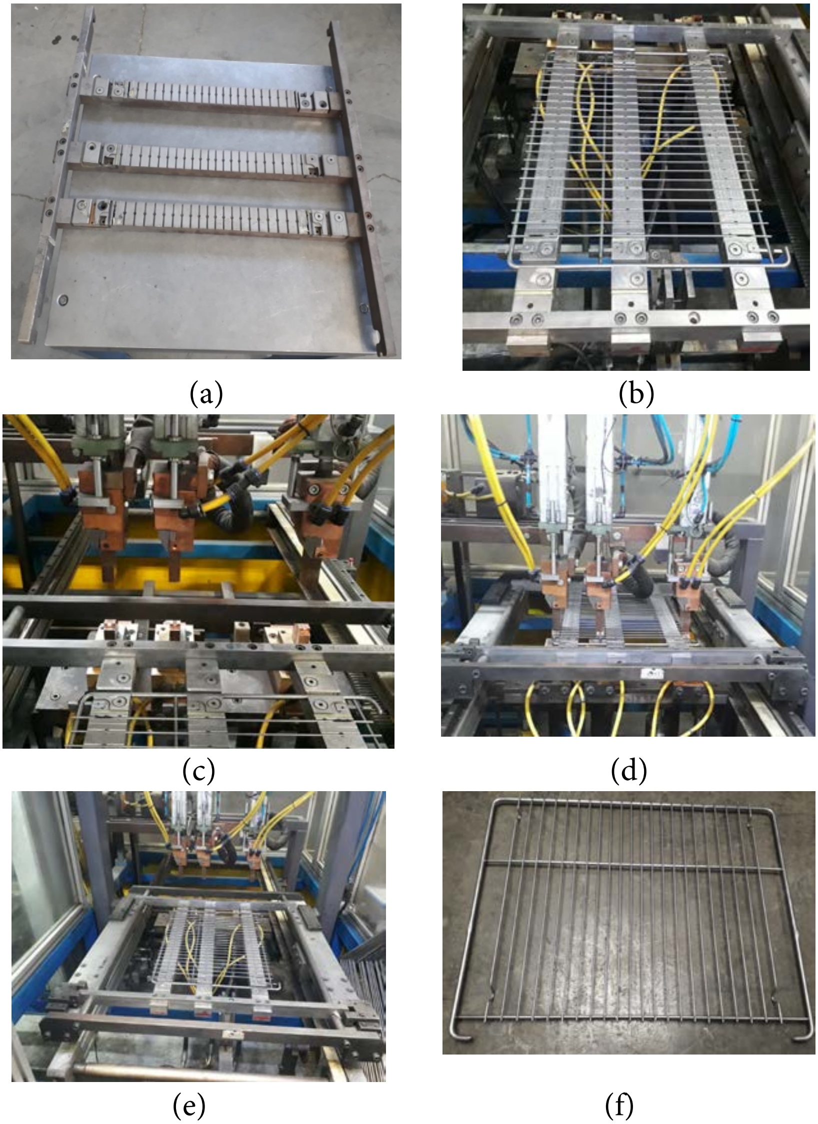

Figure 2. Fixture designed for resistance spot welding and different positions of the fixture in the machine during the welding process a) Mesh welding fixture b) The way the wires are arranged in the fixture before welding c) and d) Different positions of the fixture in the welding operation e) Initial position of the fixture after the welding process f) An oven interior grate assembled by resistance spot welding.

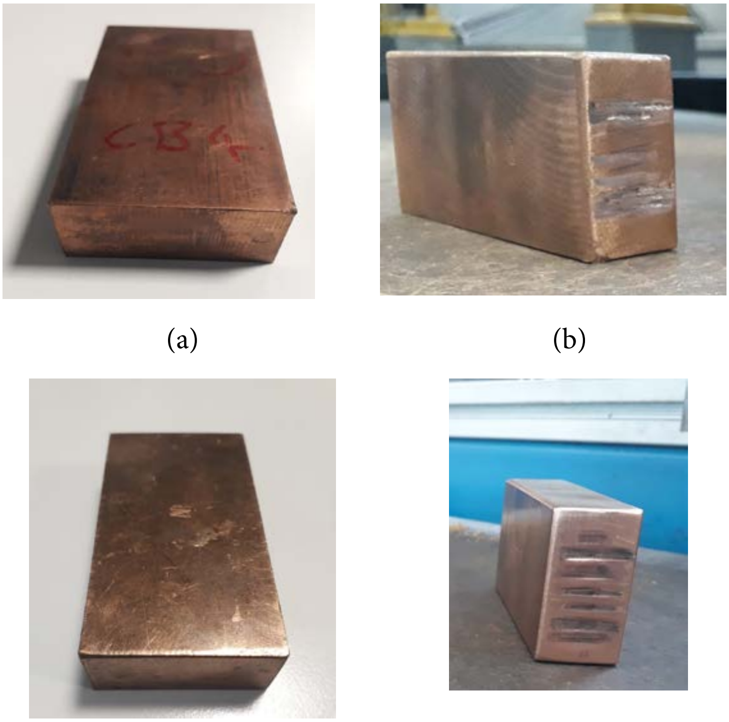

(a) (b)

(c) (d)

Figure 3. Pictures of a) CuCoBe electrode c) $CuNi_3Si$ electrode before welding, b) CuCoBe electrode d) Post welding photographs of $CuNi_3Si$ electrode.

3. RESULTS AND DISCUSSION

3.1. Mechanical Properties

In the welding studies, as in the previous study, the maximum tensile loads of the oven grill wires combined with resistance welding were investigated by trying different welding parameters. For this purpose, 8, 9, 10 and 12 kA welding current values and 8, 12 and 16 ms welding times were used for each welding current, respectively. In all these welding studies, the electrode pressure force of 480 N was kept constant. In a previous study using CuCoBe electrode and different welding parameters, it has been reported that 8 kA welding current value is insufficient in all cases and reduces the welding strength, and the welding parameter that gives the best tensile strength (1265.3N) should be 12 ms welding time under 9 kA current (Taşkın and Altunpak 2023).

Figure 4 shows the maximum tensile load values obtained in resistance spot welding studies using $CuNi_3Si$ electrodes and different welding parameters. The effect of welding current values on the tensile strength of the welded parts made by keeping the welding time values constant is observed. As can be clearly seen in the graphs, when 8kA welding current was used, it was insufficient, similar to previous welding studies with CuCoBe electrodes, and the tensile strength of the welded parts decreased. In all experiments, it is clearly seen that 9 kA welding current value should be used for maximum welding strength. The graphics show that the welding current value that gives the highest tensile strength (1111N) should be 16 ms welding time under 9 kA current.

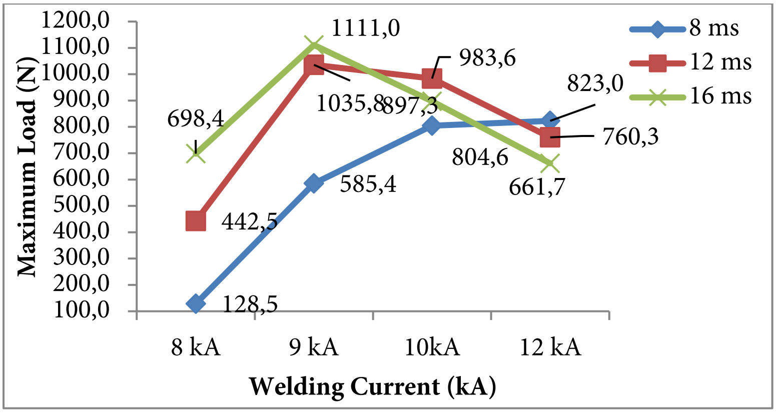

Figure 4. Effect of welding current on the tensile strength of samples welded using $CuNi_3Si$ electrodes and different welding times

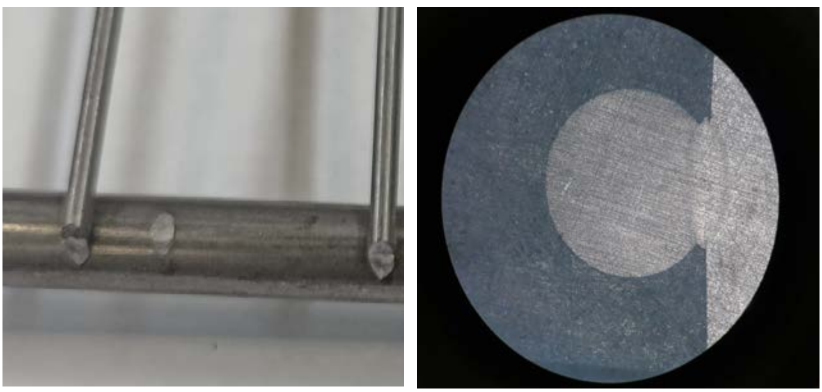

(a) (b)

Figure 5. a) Welded product photo of the weld made with $CuNi_3Si$ electrode with 8 kA and 8 ms welding parameters b) Weld core photo at 50 magnification

Figure 5 indicates the weld core views of the welded product made with $CuNi_3Si$ electrode with 8 kA and 8 ms welding parameters under an optical microscope at 50 magnification. As can be seen from the images, a sufficient welding core has not been formed. The tensile load value (128.5 N) measured in Figure 3.1 was also quite low as expected. Figure 6 reveals the weld core views at 50 magnification of the weld made with the CuNi3Si electrode with 9 kA and 16 ms welding parameters. As can be clearly seen from the images, a sufficient and distinct weld core has been formed. It can be seen that the measured tensile load value is 1111.0 N. Considering that the customer demands from the manufacturer are at least 750 N for the welding tensile strength of the oven grill wires, these tensile strength values can easily meet the need.

One of the most important factors required during resistance welding is the welding current. As can be seen in the heat formula, it creates a multiplier effect equal to the square of the current. Therefore, it is necessary to be very careful when choosing the welding current value. If the welding time is less than necessary, the weld core diameter will be small and the weld strength will decrease. If the welding time is kept longer than necessary, the molten area grows and gushes out due to the effect of the electrode pressure, and both the strength decreases and the weld core deteriorates in terms of appearance. Considering the heat (energy) formula ($Q = K \cdot I^2 \cdot R \cdot t$); Provided that the total resistance is constant, heat transfer is a function of time. The time required to develop a sufficient core diameter will not change much even if the welding current is increased (Yener, 1999).

(a)

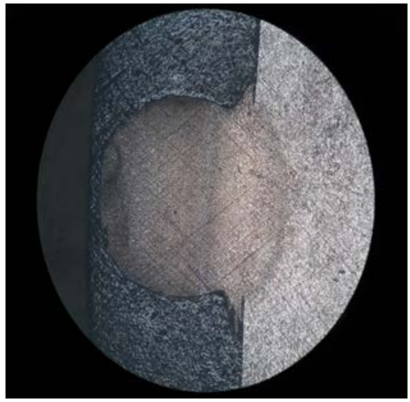

(b)

Figure 6. a) Welded product photo of the weld made with $CuNi_3Si$ electrode with 9 kA and 16 ms welding parameters b) Weld core photo at 50 magnification

During the welding process, the desired weld core size is achieved by appropriately adjusting the current intensity and time. If the welding time is kept short, the weld diameter will be insufficient. If it is kept longer than necessary, the molten area grows and the melt gushes out. Electrode composition and shape, welding current, welding time, welding force, type of material to be welded, the surfaces of the workpieces to be welded and the distance between the welded points are important factors that have an effect on heating and affect the welding quality (Kaya, 2010; Hayat, 2005).

3.2. Comparison of Welding Counts of Electrodes

In order to compare the lifespan of the electrodes, welding studies were carried out with CuCoBe and $CuNi_3Si$ electrodes using the optimum welding parameters that give maximum tensile strength in previous studies. The deformation (track depth) occurring in the electrodes when certain welding pressure numbers were reached (after 15000 welds) was measured and compared with the help of Mitutoyo brand gauge.

Photographs of CuCoBe and CuNi3Si electrodes before welding and after 15000 welds (Fig. 7 and Fig. 8) and measurement of deformation (track depth) with the help of a gauge are shown below (See Fig. 9).

(a) (b)

Figure 7. Pre-welding photos of (a) CuCoBe electrode (b) $CuNi_3Si$ electrode

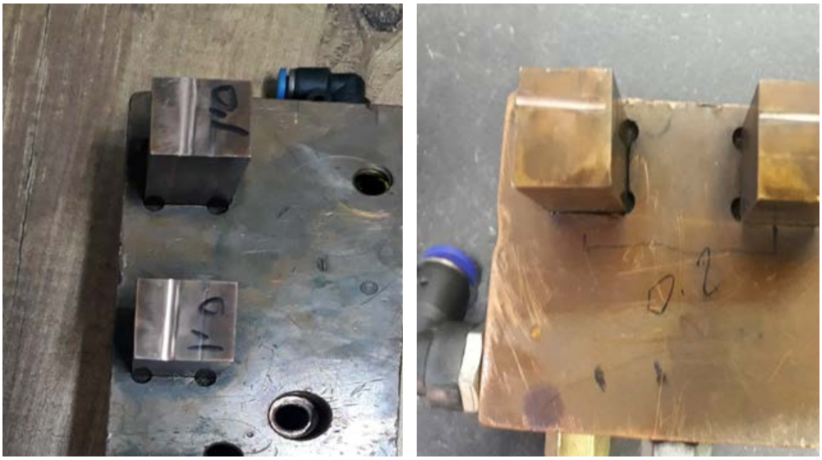

(a) (b)

Figure 8 Photographs of (a) CuCoBe electrode (b) $CuNi_3Si$ electrode after 15000 welds

Figure 9. Measuring the deformation (track depth) after welding on CuCoBe and $CuNi_3Si$ electrodes with the help of a gauge

As can be seen from Fig. 10, after 15000 welds, the deformation (track depth) rate in $CuNi_3Si$ electrodes was approximately 33% higher compared to CuCoBe electrodes. However, this did not cause any significant negative effects on the tensile strength, quality and electrode lifespan of the welded parts. Considering the negative effects of the Be element contained in CuCoBe electrodes on human health and the lower prices of $CuNi_3Si$ electrodes, and therefore the lower cost of welded part production, it can be said that it is more appropriate to use $CuNi_3Si$ electrodes in wire grid resistance welding processes.

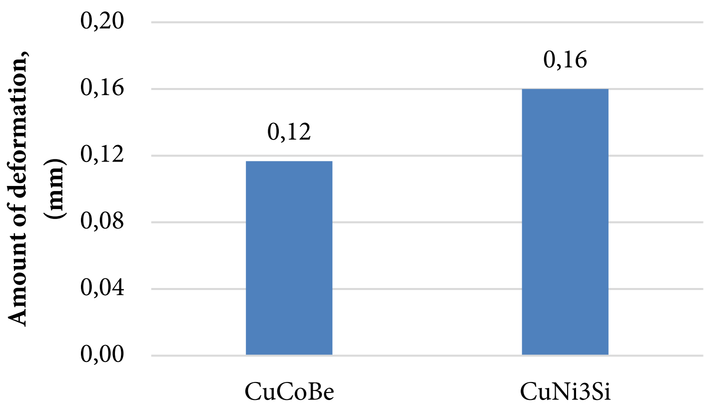

Figure 10. Comparison of deformation of CuCoBe and $CuNi_3Si$ electrodes after 15000 prints

4. CONCLUSION

In this study, the welding work of Ø6.5 mm and Ø2.3 mm SAE 1006 quality oven grate wires made of low carbon steel used in the white goods industry was carried out using a programmable resistance spot welding machine with current and time control. CuCoBe and $CuNi_3Si$ electrodes with dimensions of 20x40x80 mm were used in welding the products. In welding studies, different welding parameters were tested using a constant electrode pressure force of 480 N, welding times of 8, 12 and 16ms and welding current values of 8, 9, 10 and 12 kA, respectively. The microstructures of the weld cores of oven grate wires made of low carbon steel were examined. The maximum tensile load values of the welded samples were measured using a Chatillon brand testing device manually. The mechanical properties of welded parts are defined in terms of maximum tensile load. In addition, the deformations of two different electrodes (CuCoBe and $CuNi_3Si$) at equal pressure numbers were measured with the help of a gauge. In the experimental results of the welded parts used in this study are as follows;

The best welding parameters (the combination of welding current and time) was determined to be 9 kA and 12 ms for the CuCoBe electrode, and 9 kA and 16 ms for the $CuNi_3Si$ electrode.

Less deformation occurred in the CuCoBe electrode compared to the $CuNi_3Si$ electrode at the same pressure number. However, this amount of deformation did not harm the weld seam quality (such as appearance and strength) of the welded samples.

Considering the harms of beryllium element to human health as well as the cost of CuCoBe electrode, it can be confirmed that the use of $CuNi_3Si$ electrode in resistance spot welding applications is much more advantageous for the relevant companies.

REFERENCES

Akkuş, A. (2006). Investigation of Fatigue Strength of Spot Welded Connections of Galvanized and Austenitic Stainless Steel Sheets. ITU Institute of Science and Technology PhD Thesis, Istanbul.

Akyol, M. (2001). Resistance Spot Welding Applications Used in the Automotive Industry and Problems Encountered. I.T.U. Institute of Science and Technology Master's Thesis, Istanbul.

Almus, Z. (2006). Investigation of the effects of interconnector on joint properties in spot resistance welding. Gazi University Institute of Science and Technology Master's Thesis, Ankara.

Altun, Y. (2012). Control of Point Resistance Welding Manipulator used in ironing board manufacturing. Selçuk University Institute of Science and Technology Department of Electrical and Electronics Engineering Master's Thesis, Konya.

Anık, S. (1991). Welding Technique Handbook, Gedik Holding Publication, Istanbul.

Anık, S. (1993). Welding Technology Handbook in 1000 Questions, Birsen Publishing House, Istanbul.

Bilge, H., Doruk, E., Fındık, F., & Pakdil, M. (2019). Effect of fatigue crack propagation on natural frequencies of system in AISI 4140 Steel. Steel and Composite Structures, An International Journal, 32(3), 305-312.

Bilge, H., & Morgül, Ö. K. (2023). Analytical and Experimental Investigation of the Rotary Inertia Effects of Unequal End Masses on Transverse Vibration of Beams. Applied

Sciences, 13(4), 2518.

Donders, S.,Brughmans, M., Hermans, L., Tzannetakis, N., “The Effect of Spot WeldFailure on Dynamic Vehicle Performance”, IMAC-XXIII, the 23rd International Modal Analysis Conference, Orlando, February, 2005.

Doruk, E. (2015). Tofaş applications are the point of resistance in the automotive industry. Welding congress IX. National congress and exhibition proceedings book.

Esendir, E. (2008) Joining Different Metals with Spot Resistance Welding. Yıldız Technical University Institute of Science and Technology Master's Thesis, Istanbul.

Gavas, M., Yaşar, M., Aydın, M., & Altunpak, Y. (2013). Production methods and manufacturing technologies. Third edition, Seçkin Publishing, Ankara.

Geißler, G.,Hahn, T., “Process Development For Multi-Disciplinary Spot WeldOptimizationWithCAX-LOCO, LS-OPT and ANSA”, 8th EuropeanUsers Conference, Strasbourg, France, May 2011

Gugel M.D. (1995). Electrode Wear Mechanisms During the Resistance Spot Welding of Hot-Dipped Galvanized Steel, PhD Thesis, MTU,Michigan.

Hayat, F. (2005). Effect of mho and welding time on mechanical properties in spot resistance welding of double-phase steels. Zonguldak Karaelmas University Institute of Science and Technology Master's Thesis, Karabük.

Kaya, Y. (2010). Investigation of the weldability of titanium sheets with spot resistance welding. Karabük University Institute of Science and Technology, Department of Metal Education, Master's Thesis, Karabük.

Keleş, S. (2008) Application of Object-Oriented Process Planning System in Designed and Manufactured Spot Welding Machine. Dumlupınar University Institute of Science and Technology Master's Thesis, Kütahya.

Kurşungöz, N. (1986). Examination of Contact Resistance in Electrical Resistance Spot Welding of Aluminum Based Material. Anadolu University Institute of Science and Technology Doctoral Thesis, Eskişehir.

MEGEP (2014).“Electric Resistance Welding”, http://megep.meb.gov.tr/mte program modul/moduller pdf/%20Diren%C3%A7%20Kayna%C4%9F%C4 %B1pdf.

Nielsen, C.V. & W. Zhang, & N. Bay & P.A.F. Martins. (2021). “Cross-wire welding analyzed by experiments and simulations” Journal of Advanced Joining Processes, Volume 3.

Onsekiz, M.. (2018). The effect of resistance electrode material type on the resistance welding strength of ferritic stainless steels used in the white goods industry. Abant İzzet Baysal University, Institute of Science and Technology, Department of Mechanical Engineering, Master's Thesis, Bolu.

Peşint, M. A., & Ürkmez, A. (2000). Electrical Machines II-Transformers, MEB Publications, Fifteenth Edition, Ilıcak Printing House.

Salvini P., Francesco V., and Vullo V. (2000). “A spot weld finite element for structural modelling”, International Journal of Fatique, 22: 645-656,

Shanmugam, N. Buvanashekaran, G. Sankaranarayanasamy, and K. Kumar, S. (2010). “A transient finite element simulation of the temperature and bead profiles of T-joint laser welds", Materials and Design, 31: 4528-45427,

Sonat M., & Doyum A.B. (1999). Ultrasonic Examination of Resistance Spot Welds, Welding Technology II. National Congress, pp.97-106, Ankara.

Taşkin, F. (2023) "Increasing resistance welding strength ın cross-wire steel grills used in kitchen ovens" Abant İzzet Baysal University Graduate Education Institute, Department of Mechanical Engineering, Master's Thesis, Bolu.

Taşkın, F., & Altunpak, Y. (2023, september). Increasing resistance welding strength in cross-wire steel grills used in kitchen ovens. In latin american internatıonal congress on natural and applied sciences-v (p. 35).

Unlukal, E. (2007). Increasing the Quality of Resistance Spot Welding Used in the Automotive Industry. ITU Institute of Science and Technology Master's Thesis, Istanbul.

ASM Metals Handbook, U.S.A., (1983), 9th edition, "Welding brazing, and soldering, resistance spot welding", 469-493

Yener, S. (1999). Experimental analysis of resistance spot welding electrode life used in the automotive industry. Istanbul Technical University Institute of Science and Technology Master's Thesis, Istanbul.

Zhang, Y., & Taylor D. (2000). Sheet thickness effect of spot welds based on crack propagation, Engineering F.

DEVELOPMENTS IN THE FIELD OF ENGINEERING 2023

yaz
yayınları

YAZ Yayınları
M.İhtisas OSB Mah. 4A Cad. No:3/3
İscehisar / AFYONKARAHİSAR
Tel : (0 531) 880 92 99
yazyayinlari@gmail.com • www.yazyayinlari.com

ISBN: 978-625-6524-70-5